International Erasmus Mundus Master in
QUATERNARY AND PREHISTORY

ISOTOPIC INSIGHT INTO THE ECOLOGY OF THE RED DEER FROM RIPARO TAGLIENTE (ITALIAN PRE-ALPS) DURING THE LATE EPIGRAVETTIAN

Mahym Amanova

Supervisor: Prof. Federica FONTANA

Supervisor: Dr. Dorothée DRUCKER

Academic year 2023/2024

Abstract

The end of the Last Glacial Maximum (LGM) reveals a climatic progression from the cold conditions of the Greenland Stadial-2 (GS-2) to the abrupt sequence of warming conditions of the Greenland Interstadial-1 (GI-1), during which new ecological habitats flourished allowing hunter-gatherers to re-occupy the Alpine altitudes. In this context, Riparo Tagliente, a rock-shelter in northeast Italy, testifies to the earliest re-colonization in the south-eastern pre-Alps by the Late Epigravettian hunter-gatherers.

Exploring the ecology of red deer (*Cervus elaphus*) from the archaeological site of Riparo Tagliente provides insights into the significant impacts of the Late Glacial climatic fluctuations on human habitats. For this purpose, we measured the carbon and oxygen stable isotope ratios ($\delta^{13}C$, $\delta^{18}O$) of enamel carbonate through a sequential sampling of the second and third molar crowns of red deer from this major Alpine site, preserving the most expanded stratigraphic sequence of the region. The red deer molars were selected among the remains collected in the stratigraphic units 13 to 5, spanning from GS-2.1a to GI-1 phases.

Obtained $\delta^{13}C$ values on red deer show a diet based on terrestrial C_3 plants from a habitat characterized by the presence of an open canopy woodland during the Late Glacial. The $\delta^{18}O$ values yield the seasonal climatic conditions captured during the enamel formation, mainly summer for the second molars and winter for the third molars. In addition, seasonal conditions recorded in the $\delta^{18}O$ values were estimated based on known equations relating the $\delta^{18}O$ values of carbonate to those of consumed water and the $\delta^{18}O$ values of the meteoric water to the mean monthly air temperature (MMT) and the mean annual air temperature (MAT). The resulting reconstruction indicates the MMT temperature around –6.5 °C in winter for layer 13 for the period 16,634–15,286 cal. BP, when glaciers were melting in the Alpine region. In layer 10, is the transition between GS-2.1a and GI-1, the MMT temperatures drop down to –8.9 °C in winter and reach around 9.9 °C in summer. Temperatures increase in summer reaching values around 15.4 °C in layer 9 and 14.5 °C in layer 7 for the period 14,572–13,430 cal. BP, associated with the temperate Interstadial GI-1. Together these results suggest no significant changes in the diet of this key game and the presence of relatively open forest landscape through the entire sequence despite the environment influenced by paleoclimatic variations over the seasons.

Keywords: Riparo Tagliente, red deer (*Cervus elaphus*), Late Glacial, Late Epigravettian, stable isotopes, paleoclimate, paleoenvironment, temperature.

To the Memory of My Father

Myrat Amanov Babayevich

Acknowledgments

First and foremost, I would like to express my deep and sincere gratitude to my Erasmus Mundus program coordinator Dr. Marta Arzarello, and all the associated partner institutions for selecting me to the highly interdisciplinary IMQP program which was a life-changing period in my academic life as well as personal life.

Special mention goes to my first hosting institution IPT and my program coordinator Prof. Luiz Oosterbeek for his endless academic support and guidance through all the stages of the Master's program in Portugal.

As an Erasmus Mundus student, I would like to express my sincerest acknowledgments to the European Commission for granting me a full scholarship that ensured my smooth stay in Europe without any needs for the duration of my study period.

I could not have completed this Master's thesis without the support of my supervisors Dr. Drucker Dorothée and Prof. Fontana Federica. I am extremely grateful to them for assisting me with the practical, technical, and theoretical aspects of my research. Their guidance and encouragement were immeasurable for my professional development as an early-stage researcher.

My gratefulness also goes to the Biogeology group at the University of Tübingen, particularly Prof. Hervé Bocherens and Dr. Drucker Dorothée for granting permission to do my thesis lab work in their laboratory and mentoring in my isotope analysis. Furthermore, I am thankful for the in-lab technical supports by Valentina Gracia-Huidobro, Dr. Magdalena Krajcarz, Dr. Maciej Krajcarz, Dr. Chris Baumann, Emily Milton, Freya Riedel, and Peter Tung.

I would like to say thanks to my professors from my hosting institution – Instituto Politécnico de Tomar (IPT), as well as my mobility institution – Università degli studi di Ferrara (UNIFE) for their dedication in teaching us, guidance, and support during the semesters.

Thanks should also go to my professors from my undergraduate degree, colleagues, and friends, especially to my best friend Elena Ovliyakuli and Jemal Shirguliyeva for their continuous support, insightful advice, and their belief in me.

In the end, I believe my biggest thanks belongs to my loved family: my dear mum Hesel Amanova and my brothers Mekan, Serdar, and Mergen, for their support, encouragement, and endless love throughout my life, in personal as well as academic life. I would like to dedicate this piece of achievement to my late father Myrat Amanov Babayevich who died in a car accident in 2018, for whom I could not have a moment to say goodbye and 'I love you, Dad'.

INDEX

INDEX OF FIGURES

INDEX OF TABLES

Chapter 1 – INTRODUCTION

The aim of this introductory chapter is to put the necessary foundations for this thesis as a whole. It introduces the key concept of stable isotopes in palaeoecological reconstruction, which is the main focus of this research, and underscores its significance in the field of archaeology. It also provides a general overview of the climatic background during the Late Pleistocene and of the palaeoecological context of North-Eastern Italy. Lastly, it outlines the structure of the thesis, providing a brief overview of each of the chapters that will follow.

1.1 Aims and Objectives of the Research

Analysis of stable isotopes from tooth enamel bioapatite ($\delta^{13}C$ and $\delta^{18}O$) is a powerful tool for reconstructing paleoenvironments, especially when combined with other available environmental proxies. This type of analysis allows us to detect the diet and/or habitat conditions experienced by modern and extinct animals through their early lifetimes. The carbon isotopic composition of herbivore tooth enamel can be used to determine the fractions of C_3 and C_4 biomass in diets of both modern and fossil mammals and to identify the closed-canopy effects in their diets (Bocherens et al., 1996; Cerling & Harris, 1999; Cerling et al., 1997; Kohn & Cerling, 2002). In open environments, the $\delta^{13}C$ values are relatively higher than in areas with dense forest cover, like dense canopy forest, where reduction of solar radiation and CO_2 mixing with the general atmosphere at the forest floor are observed (Tieszen, 1991; van der Merwe & Medina, 1991). The $\delta^{13}C$ values of herbivore teeth is influenced by the isotopic composition of the plants they fed on and can thus be related to their diet and habitat. The oxygen isotopic composition of terrestrial mammal's teeth is driven by the isotopic composition of the plant water they consumed and ingested drinking water, which is supplied by meteoric water (Koch, 2007). The $\delta^{18}O$ value in meteoric water also varies geographically and temporally, meaning with higher values in warm regions or seasons, and lower values in colder regions or seasons (Koch, 2007; Kohn et al., 1998). The $\delta^{18}O$ isotopic values from the terrestrial animal teeth can be used as a proxy for short-term palaeoclimatic conditions, such as winter and summer seasonal variations experienced during the early lives of animals (Kohn et al., 1998). In general,

tooth enamel isotope signatures are a faithful recorder of diet and/or habitat and winter-summer seasonality.

In this palaeoecological context, the present study seeks to explore the paleoclimate and paleoenvironment in the region of the south-east Alps during the late Upper Pleistocene. These paleo-conditions are inferred from the analysis of stable isotopes of the red deer (*Cervus elaphus*) teeth collected from the archaeological deposits of Riparo Tagliente, NE Italy. The primary objectives are to reconstruct herbivore's early life diet and/or habitat, as well as the first-life seasonal climatic variations, and then provide insights into the ecology and local climate that the Late Epigravettian hunter-gatherers inhabiting this region faced during the great climatic fluctuations of the Late Glacial period between GS-2.1a and GI-1. Red deer, the primary large prey for local hunter-gatherers, is an opportunistic mixed feeder and lives in variable habitats from open steppe to close temperate forest (Heptner et al., 1989) allowing us to explore the range of ecosystems exploited by local foragers.

Animal tooth enamel stable isotope ($\delta^{13}C$ and $\delta^{18}O$) analyses have been widely applied in Europe and outside to explore paleoecological scenarios (e.g. Balasse, 2002; Bocherens et al., 1996; Drucker et al., 2024; Wiedemann et al., 1999), as well as the current ecology and climate changes (e.g. Makarewicz & Pederzani, 2017; Stevens et al., 2011). However, these biogeochemical analyses have been so far applied sparsely in the Eastern sector of the Italian Alps to investigate environmental and climatic variations except for paleodietary reconstructions of human individuals (Gazzoni et al., 2013; Oxilia et al., 2021) and paleoecology of ungulates (Manzella et al., 2024). In this regard, this isotopic study of Riparo Tagliente rock-shelter is the first extensive one for the late Upper Pleistocene period in the south-east Alps and will contribute to the reconstruction of the local environment and climatic conditions experienced by the Late Epigravettian groups.

1.2 General climatic background

Generally accepted chronostratigraphical and geochronological timescale, the Quaternary period, the beginning of which is dated at 2.58 Ma, is placed under the Cenozoic Era and the Phanerozoic Eon (see Cohen et al., 2013). The Quaternary system includes the Pleistocene and Holocene epochs, each of which with subseries divisions, i.e. the lower/early (L/E), middle, upper/late (U/L) Pleistocene, and likewise the lower/early (L/E), middle, upper/late (U/L) Holocene. The Pleistocene and Holocene series are also subdivided into stages (see more in Cohen & Gibbard, 2019). These Quaternary subdivisions are based on the

identification of the repeated major global climatic oscillations throughout its stratigraphic record, to practically group these climatic variations in the younger and older cycles (e.g. Cohen & Gibbard, 2019). In general, the onset of the Quaternary/Pleistocene is associated with the first evidence of the paleoenvironmental changes on land and the glacial-interglacial climatic cycles.

The occurrence of these climatic oscillations during the Quaternary has been correlated with the global-distributed oceanic drilling and continental proxy-records to summarize the common signal in the global datasets and establish calibrated age models (e.g. Cohen & Gibbard, 2019). Isotopic studies of the major deep-ocean proxy, i.e. a fossil foraminifera (stable oxygen isotope composition, $\delta^{18}O$), have revealed around 52 cold and interspersed warm climate periods during Quaternary which referred to as glacials and interglacials (e.g. Suggate, 1965). These deep-sea-based records are climatically defined as marine oxygen isotope stages or (MIS) (Lisiecki & Raymo, 2005). In total, 102 marine isotope stages were recorded during the last 2.58 Ma, and even numbers represent glacials while odd numbers are interglacials. The Penultimate Glacial Maximum (PGM) and the Last Glacial Maximum (LGM) are the cold maxima within MIS 6 and MIS 2 respectively. In terrestrial records, Last Glacial Maximum ice advances differ in timing from region to region (Hughes & Gibbard, 2015), and do not necessarily coincide with the LGM as labeled along deep marine benthic foraminiferal $\delta^{18}O$ records (***Fig. 1)***. An additional option to define the global LGM event – dated back 27.5-23.3 ka and coeval to the GS-3 – is related to its correspondence to the global sea level minima records as proposed by Hughes and Gibbard (2015).

A major continental record, the annual layer counts on multi-proxy Greenland North-GRIP ice-cores data (measured stable $\delta^{18}O$ isotope of the ice) delivered the high-resolution Greenland Isotope Division schemes extending from the lower half of the Late Pleistocene (late part of the Last Interglacial, Eemian) up to the end of Last Glacial (11.7 ka 'before 2000 CE') (Rasmussen et al., 2006). In the Greenland records based on synchronization of the NGRIP, GRIP, and GISP2 ice-core proxies, the high climate instability is represented by a sequence of stadials (full glacial phase) and interstadials (relatively mild). This has led to identification of 25 Greenland Stadials (GS) and 24 Greenland Interstadials (GI) for the Last Glacial period (beginning at ca. 116 ka) (Rasmussen et al., 2014). In addition, another correlation proxy data from the sea surface temperature of North Atlantic sediments, the so-called the Heinrich events, record about six (H1–H6) brief intervals of increased discharge of icebergs and reduced foraminiferal fluxes during times of colder stadials for the past 80 ka (Bond et al., 1993; Heinrich, 1988).

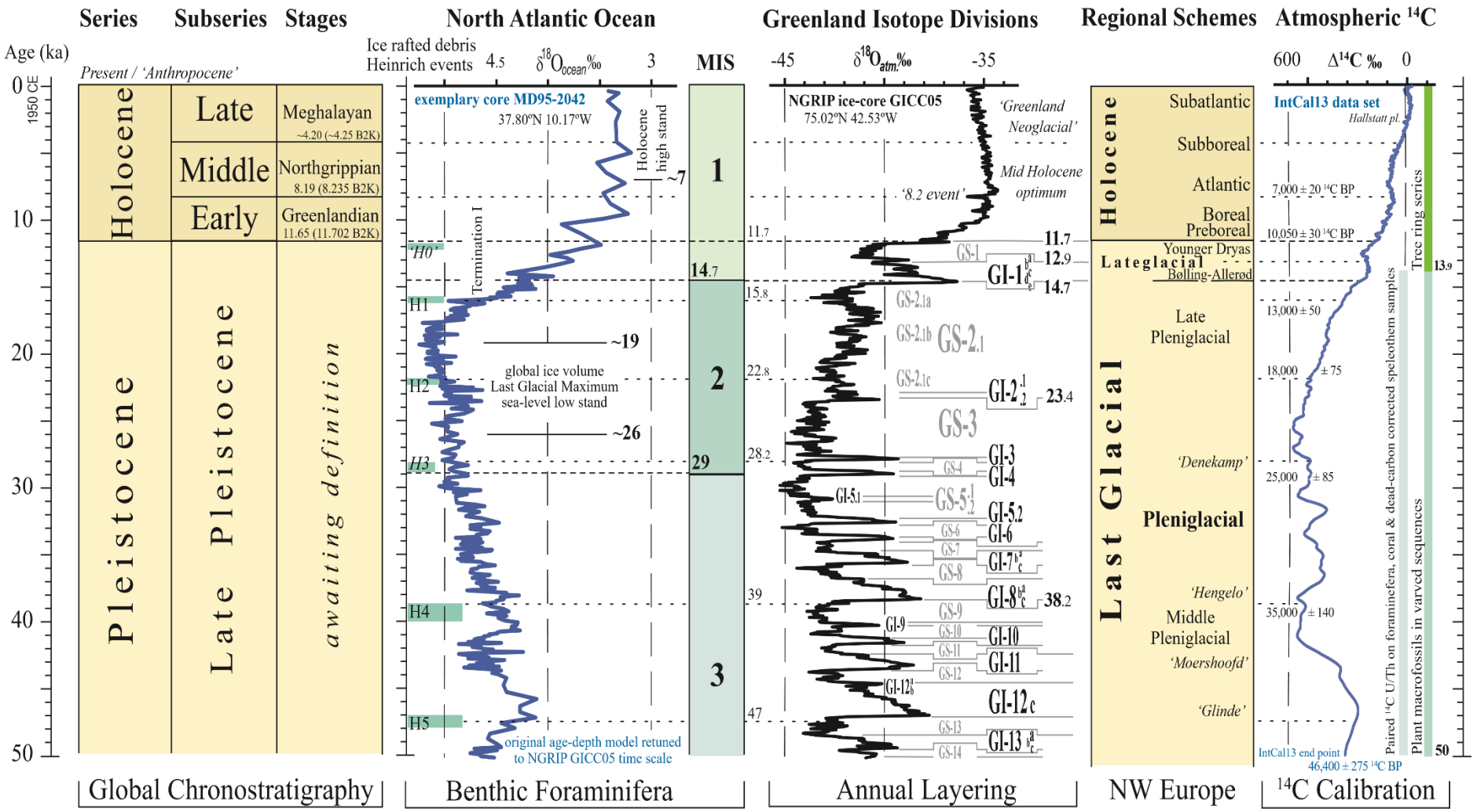

Fig. 1. Global chronostratigraphical correlation table for the last 50 ka (see Cohen & Gibbard, 2019)

The late Upper Pleistocene is of great importance in the history of the environment and prehistoric colonization of high latitude regions as well as mountain territories. It corresponds to the last part of the Upper Pleistocene, the beginning of which almost coincides with the onset of the Last Interglacial Eemian regional Stage in NW Europe referred to ca.129 ka (MIS 5e) (e.g. Kukla et al., 2002). The last part of the late Upper Pleistocene is characterized by several climatic oscillations, which correspond to MIS 2 and the first part of MIS 1 (e.g. Bond et al., 1997; Heinrich, 1988; Lisiecki & Raymo, 2005; Rasmussen et al., 2014). After the LGM, when the south continent of Europe became a refuge for northern terrestrial organisms, a series of climatic fluctuations can be observed in the Greenland ice-core records. Particularly, GS-2 is marked by the progressive increase in temperature and separated into three climatic events (GS-2.1c, -2.1b, -2.1a); it is, then, followed by a short period of relative warming (GI-1), when a rapid increase of temperatures and development of wooded environment is recorded. Lastly, an abrupt climatic event of cooling (GS-1), characterizes the very end of the Upper Pleistocene. The latter part of GS-2 is also accompanied by the H1 (Heinrich event 1), which is a relatively arid phase, resulting in a series of dramatic glacial collapses across the Alpine district (Ravazzi et al., 2007; Ravazzi et al., 2014). The Late Glacial period, ca. 17.5-11.7 ka cal. BP, was an episode of changing environmental conditions in Europe, in which the climate system shifted from glacial to interglacial conditions (e.g. Björck et al., 1998; Magny et al., 2006). The Late Glacial is a regional stage, to which paleoclimatic and paleoenvironmental studies attribute a sequence of climatic periods: the Oldest Dryas, Bølling-Allerød, and Younger Dryas. The Oldest Dryas corresponds to GS-2 where the gradual increase in temperature is marked. The beginning of the Bølling-Allerød Interstadial is consistent with the onset of the GI-1, a relatively warm period with several minor oscillations, i.e. Bølling (GI-1e), Older Dryas (GI-1d), Allerød (GI-1a-c3), which particularly have been observed in the northern Alpine region. The Younger Dryas is a cold phase, broadly equivalent to GS-1. These chronozone subdivisions are based on pollen records and were first proposed for the Scandinavian region (Mangerud et al., 1974). The series of climatic oscillation events that occurred during the Late Glacial led up to gradual changes of the landscape and resulted in the formation of a complex system of environments for hunter-gatherers.

1.3 Paleoenvironment and paleoclimate in the South-eastern Italian Alps during the Late Glacial

Most of the extensive research conducted in the eastern region of the Italian Alps have been focusing on the human occupation during and after the end of the Alpine LGM (Peresani et al., 2021). However, a few numbers of studies on climatic evolution in the region mainly come from paleolimnological (Filippi et al., 2007; Heiri et al., 2007), palynological (Pini et al., 2010; Ravazzi et al., 2007) and stalagmite studies (Frisia et al., 2005).

In Northeast Italy, the available palaeoclimate and palaeovegetation reconstructions record similar climatic events as recorded from Northern and Central Europe, i.e. Late Glacial gradual deglaciation after the LGM and Late Glacial Interstadial warming, followed by the Younger Dryas cooling phase before climatic conditions reach comparatively stable and warmer Holocene (e.g. Leroy et al., 1996; Rasmussen et al., 2014). During the MIS 2 (GS-3 and GS-2), the environments in central and northern Europe were with much reduced forest cover and mostly treeless areas (Magyari et al., 2014; Willis et al., 2000). While these regions were with apparently limited resources for hunter-gatherers, in Southern Europe several regions, including the south-eastern Alps provided more favorable conditions, where the development of open boreal forests and highly productive wetlands are supported during the LGM and early Late Glacial (Monegato et al., 2015; Willis et al., 2000).

Pollen studies from lacustrine sites are the main proxies to explore the climatic and environmental changes between the end of GS-2 and GI-1 in the Southern Alps (Pini et al., 2010; Ravazzi et al., 2007; Ravazzi et al., 2014). During the first part of the Late Glacial, GS-2b and GS-2a, no forest increase and retreating glaciers are detected, while some pre-alpine lakes, especially in the inner valleys, are still subject to intense periglacial conditions (Ravazzi et al., 2007). Furthermore, dry, cold, and continental events were recorded in the Garda Lake during the late part of GS-2, prior to the Bølling-Allerød Interstadial when a quick increase in forest density is already evident in the Southern part of the Alps (Ravazzi et al., 2007; Ravazzi et al., 2014). These climate and environmental changes from the southern Alpine and Prealpine pollen records are also attested by macro- and micro-mammals assemblages from the Late Epigravettian layers of Riparo Tagliente (see more chapters 2 and 5).

In addition, similar climatic and environmental interpretations are revealed by the isotopic data of stalagmite SV1 from the south-east of the Alps for the past 17 ka BP, indicating temperature increase and ice-sheet melting since 16.5 ka BP, and reflecting warm and wet climatic settings for GI-1 Interstadial while the climate during GS-1 was colder and dry (Frisia

et al., 2005). Since the first phases of deglaciation (the onset of the Late Glacial), the retreatment of major glaciers from the south-eastern pre-Alpine foothills with less vegetation cover is evident from the 'Lago di Lavarone' lake sediment records, as well as its fossil chironomid assemblages (Trentino, NE Italy) (Filippi et al., 2007; Heiri et al., 2007). Based on this paleolimnological data from the lake at the altitude of 1100 m a.s.l, the reforestation, and warmer ecosystems are enhanced during the phase of Bølling-Allerød (GI-1).

In summary, the deglaciation process and transformation of the grasslands into tree forest cover between GS-2 and GI-1, along with the relative warming during GI-1 in the south-eastern fringe of the European Alps have been extensively observed.

1.4 Thesis outline

This thesis is organized into six chapters:

Chapter One begins with the aims and objectives of the research work, explaining the importance of the research topic, its key concepts, and the objectives of this project. A brief review of the paleoclimate giving a precedency on the late Upper Pleistocene climate fluctuations, followed by the available paleoenvironmental and paleoclimate data from north-east Italy.

In Chapter Two, the research study area is introduced. The archaeological history of the site, i.e. Riparo (rock-shelter) Tagliente as well as the Late Epigravettian culture and its occupational sequence in the site are reported. In addition, all paleoecological studies applied in these Late Epigravettian deposits are also given.

Chapter Three presents the research methodology employed to attain the objective of the current study. How the samples were selected and sampled to collect the enamel powder for further isotope analysis, as well as the carbonate pre-treatment procedure of tooth enamel powders are demonstrated in this chapter. Furthermore, the sample preparation for the isotope ratio mass spectrometry (IRMS) measurement is presented and then followed by the method for calculation of the mean monthly (MMT) and mean annual (MAT) temperatures for Riparo Tagliente.

Chapter Four provides all results obtained from the stable isotope ratio measurements in the following order. First, the reliability of the carbonate content within the teeth is monitored in order to compile the set with reliable data for further isotope interpretations. Afterward, the carbon and oxygen stable isotope ratios are reported in separate sub-chapters. Lastly, the

calculated mean monthly and mean annual temperatures relative to the meteorological station Feletto Umberto and European continent are respectively indicated.

In Chapter Five, the earlier reported results are discussed, giving explanations, interpretations, as well as the limitations of the study. In particular, two topics: palaeoenvironmental and palaeoclimatic implications for the Southern Alps during the Late Glacial stage are open for discussion.

Final Chapter Six, concludes this research work by summarizing the key findings, main contributions of the research, as well as the weaknesses of the study, ending up with the future perspectives for research.

In summary of the introductory stage, the importance and relevance of the research topic were explained, meaning that stable isotope tracking is one of the powerful proxies for reconstructing paleoecology and paleoclimate seasonality. The general climatic background of the Late Glacial period is reported, which is of great importance to this research, followed by the summary of the reconstructed environmental and climatic shifts in the south-east of Italian Alps after the end of the LGM. In the following chapter, the archaeological context of the study area with a focus on the Late Epigravettian deposits will be presented.

Chapter 2 – THE STUDY AREA

Earlier in the introduction chapter, the topic was about the aims and objectives of the thesis, the general climatic background of Europe, focusing on the LGM, Late Glacial, as well as the paleoenvironmental and paleoclimatic proxies in the regional context of North-east Italy. This part was followed by the overall structure of the entire research work.

This chapter begins by giving priority to the Late Epigravettian techno-complex with respect to the Late Upper Paleolithic (LUP) of Europe. Additionally, it will deal with the re-occupation of the southern Alps by the Late Epigravettian groups during the Late Glacial and the state of the art on their subsistence strategies. The next sub-chapter presents a general overview of the archaeological site of Riparo Tagliente, including a brief history, location, structure of the site, and excavation areas. The following subsection comes with some data on the Late Epigravettian occupation of the Tagliente rock-shelter, focusing on the structural organization of the stratigraphic sequence, main findings, and chronological aspects. Several paleoenvironmental data revealed from the intense archaeological research and studies on the Late Epigravettian series are described in the final subpart of the chapter.

2.1 The Late Epigravettian in the South-Eastern Alps

The late Upper Paleolithic is characterized by the geographical separation of the European cultural techno-complexes at the end of the Gravettian period. With the end of the LGM, the Solutrean is followed by the Late Glacial Magdalenian complex, both of which are recorded in archaeological sites in the Iberian Peninsula, western France and central Europe; contemporaneously the Epigravettian industries are documented in southern and eastern Europe (Italy, Greece, the Balkans) during Late Glacial period. The Epigravettian was one of the last archaeological industries and cultures of the European Upper Paleolithic and it is divided into the Early and Late which are respectively dated to the Last Glacial Maximum (LGM) and the Late Glacial (LG) (Peresani, 2006). The Early Epigravettian is mostly characterized by shouldered projectile points and the distribution in peninsular Italy spanning chronologically between ca. 24,000 and 19,000 cal BP (ca. 20,000 – 16,000 uncal BP) particularly along the Adriatic side of the peninsula (e.g. Cancellieri, 2018).

The difference between the Early and the Late Epigravettian is mostly based on the typology and technology of lithic assemblages. The main technological difference between Early and Late Epigravettian is the presence of a wide variety of rectilinear laminar blanks (large blades, bladelets, microbladelets), associated to a wide array of armatures, i.e. backed and curved backed points, backed bladelets, and backed and truncated bladelets (e.g. Béres et al., 2021; Fontana et al., 2009). The sites with Late Epigravettian layers reported in the Southern Alps are more than fifty. Only some present a context allowing a multidisciplinary investigation; in others, the archaeological documentation is limited to the lithic industry. Some of the major Late Epigravettian sites of northeastern Italy include Riparo Tagliente, Riparo Soman, Le Regole, Riparo La Cogola, Riparo Villabruna, Grotta Clusantin, Val Lastari, Riparo Dalmeri, and Riparo Biarzo (Bertola et al., 2007). According to the known archaeological record, the Late Epigravettian hunter-gatherers began to re-occupy the Alpine highlands (e.g. cave Clusantin at 520m a.s.l., Riparo Dalmeri at 1240m a.s.l., Val Lastari at 1060m a.s.l., Riparo La Cogola at 1070m a.s.l., Le Regole at 1240m a.s.l) starting at the beginning of the temperate (Bølling-Allerød) Interstadial (Bertola et al., 2007). Thus, the Epigravettian sites at the highest elevations are post-dating the occupation of Riparo Tagliente which has yielded the most complete Late Glacial stratigraphic series testifying the earliest evidence of re-occupation of the Southern Alpine fringe after the end of the LGM (Fontana et al., 2018; Ravazzi et al., 2007). Comparisons with other Late Epigravettian sites distributed in different areas of the Italian peninsula is currently limited, due to the low number of sites for this early phase (17,000-15,000 cal. B.P). However, some sites are roughly contemporaneous to the most recent Late Epigravettian occupation of this site (i.e. Riparo Villabruna, Grotta Clusantin).

Thanks to the intensive zooarchaeological studies in the south-eastern Alps, the primary role played by hunting in the subsistence strategies of the Late Epigravettian groups has been attested. Ibex (*Capra ibex*), red deer (*Cervus elaphus*), and chamois (*Rupicapra rupicapra*) were the most hunted species while elk (*Alces alces*), bison/auroch (*Bos/Bison*), roe deer (*Capreolus capreolus*), and wild boar (*Sus scrofa*) occupy a secondary role. Among carnivores, fox (*Vulpes vulpes*), wolf (*Canis lupus*), *mustelidae*, and brown bear (*Ursus arctos*) were hunted frequently (Bertola et al., 2007). Exploitation of birds is also documented at some sites such as Riparo Dalmeri (Trento) where bird bones are characterized by butchering marks (Fiore et al., 2022). In addition to hunting practices of Epigravettian groups, gathering and fishing activities are also recorded by archaeological data. Fishing is evidenced at a few sites including Riparo Dalmeri (Trento), Villabruna (Belluno), and Riparo Soman (Verona) with the presence of fish

remains. Important traces of fish consumption come also from Riparo Tagliente, where the identification of species is still in progress (Fontana et al., 2009; Gazzoni et al., 2013).

2.2 Riparo Tagliente

2.2.1 General context of the site

The site of Riparo Tagliente is a rock-shelter located in the village of Stallavena di Grezzana, Verona, Italy. It is considered a key site of the Upper Pleistocene in the south-east Alps. Tagliente rock-shelter is located under a rock wall formed by oolitic limestone, on the west slope of Valpantena, one of the main valleys of the pre-Alpine massif of Lessini (Monti Lessini), at an altitude of 226 m above sea level (***Fig. 2***). It occupies a strategic position at the crossroads of different topographic situations: the plain, the valley-bottom, the rocky slopes, and the top of the massif (Bartolomei et al., 1982; Fontana et al., 2009). The shelter was intensively exploited by Middle and Upper Paleolithic groups thanks to the presence of lithic and mineral resources such as a wide variety of cherts (e.g. Fontana et al., 2009; 2018).

The rock-shelter was first discovered in 1958 by Mr. Francesco Tagliente (Zorzi & Mezzana, 1962), and the initial excavations were carried out between 1962-1964 by the Museo Civico di Storia Naturale di Verona. From 1967, excavations were resumed by the University of Ferrara, and since then systematic excavations have been conducted. The research was initially (until the mid-1970s) focused on the excavation of the long trench running transversally to the rock-shelter in order to investigate the whole sequence of the site. This trench separates the site into two sectors of excavation: the southern sector and northern sector (e.g. Bartolomei et al., 1982; Fontana et al., 2009). Both sectors include an inner area protected by the rock-wall and an outer area. Excavations on the transversal trench have reached up to 4.60 m deep in the outer area and uncovered the stratigraphy formed by two main deposits separated by a river erosion. The lower deposit is characterized by Mousterian and Aurignacian cultural evidence (the latter detected only in a small portion of the internal area and the trench). Although the radiometric dating is not available for the Mousterian deposits (Middle Paleolithic), it has been attributed to MIS 4-3 based on the analyses of the lithic and faunal assemblages, along with sedimentological studies (Arnaud et al., 2016; Bartolomei et al., 1982). The upper unit provided a rich Late Epigravettian evidence attesting occupation during the Late Glacial (GS-2.1a and the first part of GI-1) (Bartolomei et al., 1982; Fontana et al., 2009; Fontana et al., 2018; Fontana et al., 2015).

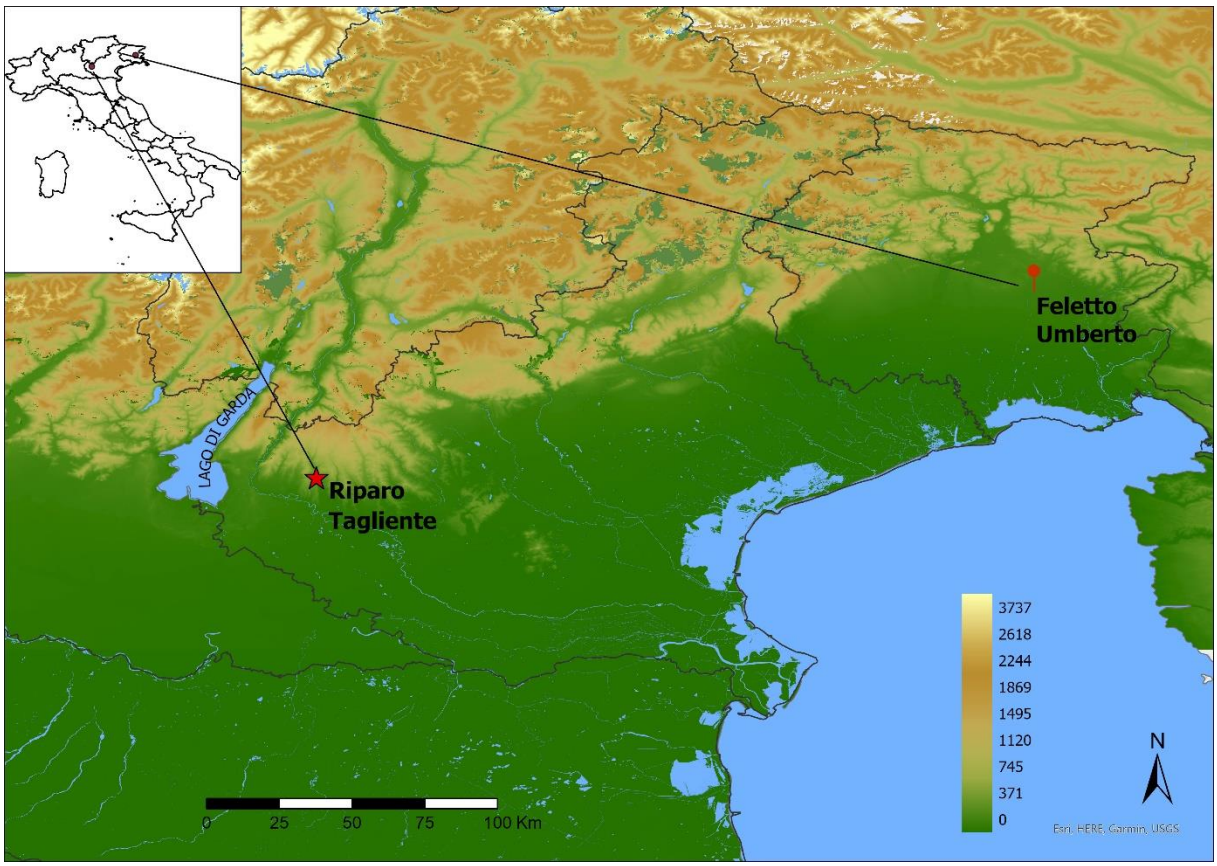

Fig. 2. Geographic location of Riparo Tagliente rock-shelter (226m a.s.l.) in Veneto, and Feletto Umberto meteorological station (135m a.s.l) in Friuli, NE Italy (ArcGIS Pro 3.2.0 elaboration by M. Amanova).

The late Upper Paleolithic deposits (Late Epigravettian) appeared in the inner and outer zones of the site, corresponding to layers 4 – 18 of the transversal trench. Extensive excavations have been carried out in these layers starting from the late 1970s particularly over the northern sector of the site, reaching an area of about 80 m^2 (Fontana et al., 2009; Fontana et al., 2018).

2.3 The Late Epigravettian occupation

2.3.1 General context of the sequence

As we mentioned above, the upper unit of the trench area stratigraphy dates back to the Late Glacial and is culturally associated with the Late Epigravettian. The Late Epigravettian sediments deposited not evenly, being thinner in the internal part of the shelter (about 50 cm) and relatively thicker in the external one (over 2 m). This complex situation was explained as

due to two main factors: (1) the river erosion escarpment at the base of the Late Epigravettian occupation leaning steeply outside the shelter; (2) the different use of the two areas by the Epigravettian groups, namely the cleaning of inner zones and the consequent accumulation of waste products in the outer ones. In addition, medieval excavation works were also carried out in the shelter, which destroyed large portions of the inner stratigraphic sequence, allowing their preservation only some areas and especially the lowermost Late Epigravettian deposits (Bartolomei et al., 1982; Fontana et al., 2009; Fontana et al., 2018; Fontana et al., 2015).

From a sedimentological viewpoint, the Epigravettian deposit is divided into two sub-units in the external area: the lower Epigravettian sequence (cuts 18 – 15) and the upper one (cuts 14 – 5) (***Fig. 3***). Both sub-units are set in a loess matrix with the lower deposits a much denser coarse breccia than the upper ones. Based on the different proxies such as sediments, pollens, malacofauna, small mammals and large mammal remains, the lower levels 18 – 12 indicate a steppe environment with cold and arid climate conditions, whereas the upper units 11 – 5 testify a temperate climate with a grassland and woodland with conifers and deciduous trees. The Late Epigravettian sequence is characterized by intense human occupation, testified not only by lithic industries and faunal remains, but also by dwelling structures, mobile art objects, ornaments (from shells, animal teeth), coloring materials (iron oxides), and *in situ* burial (Bartolomei et al., 1982; Fontana et al., 2009).

The malacological collection of ornamental beads is composed of 728 items one third of which is characterized by at least one intentional perforation. Almost all identified species (29 *taxa*) are still widely diffused in the Mediterranean Sea. Only one fossil specimen belonging to warm-related habitats *Aspa marginata* disappeared from the Mediterranean at the end of the Pliocene. In the area of Monti Lessini, only one Pliocene age deposit is known, near Salò, in the Garda Lake area. In general, the genus *Cyclope* dominates the assemblage, seemingly as a consequence of human selection (Cilli et al., 2006; Fontana et al., 2009).

All Epigravettian layers are rich in lithic industry and characterized by considerable masses of products and debris, documenting intense knapping activities and the transformation of blanks. Techno-economical studies in the latest years testify several *chaînes opératoires* for producing a wide variety of rectilinear laminar blanks (large blades, bladelets, and microbladelets) and laminar flakes. Exploited lithic raw materials come from the Lessini area, corresponding to those in the surrounding territory within a range of about 15 km from the site, although the bottom layers have yielded some artifacts (cores, blanks and tools) made on exogenous cherts from the central Adriatic area (Bertola et al., 2018).

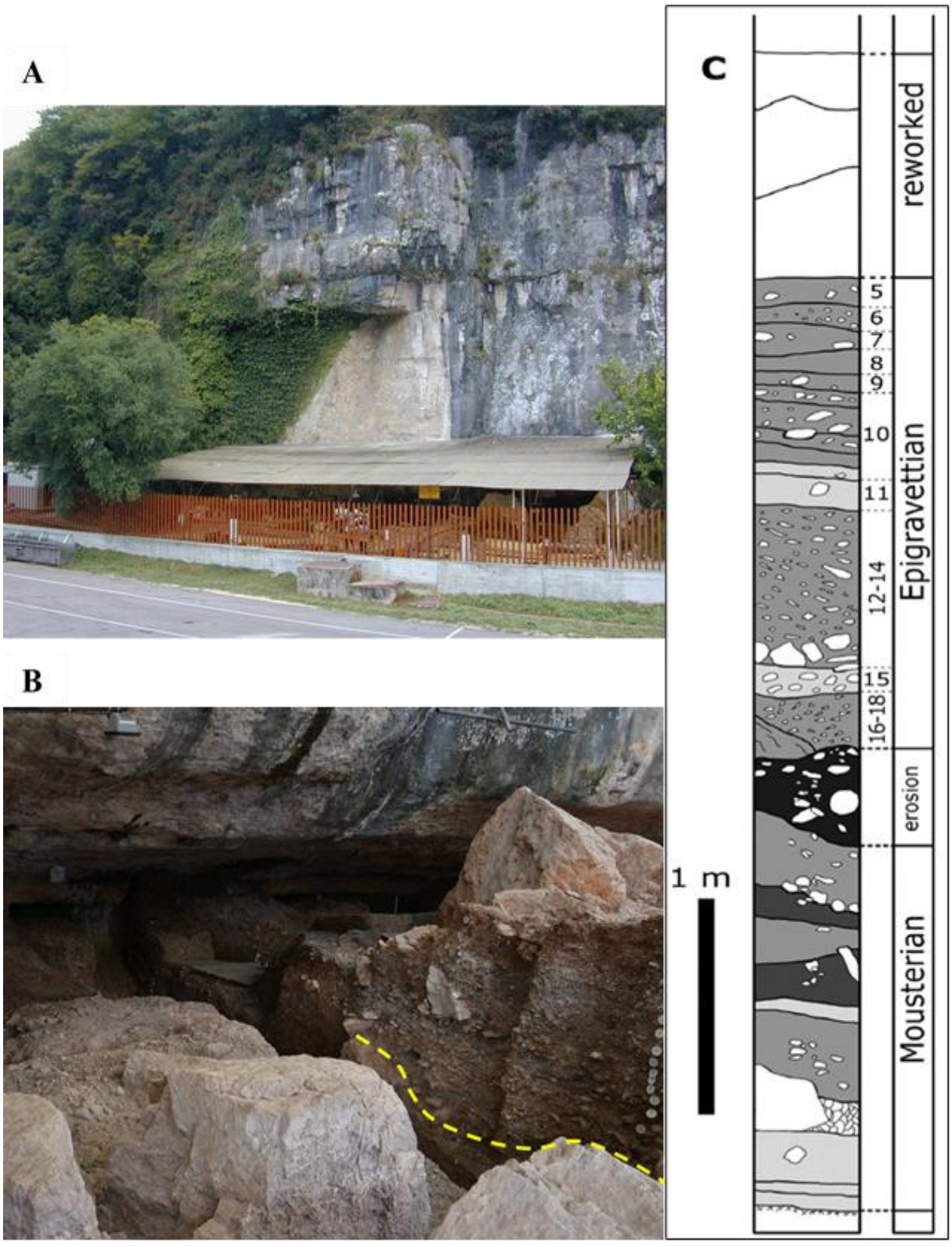

Fig. 3. A) Riparo Tagliente archaeological site (photo by A. Guerreschi). B) The stratigraphic sequence of the external trench zone. The dashed line indicates the erosion surface separating the Late Epigravettian sequence from the Mousterian and Aurignacian one. Modified from (Fontana et al., 2018). C) The stratigraphic section of the external trench. In this area, the Aurignacian levels are not detected. Modified from (Bartolomei et al., 1982).

Two different phases have been recognized from the analysis of the Epigravettian lithic assemblages: phase I (layers 17 – 12) is characterized by four different reduction sequences, each one aimed at obtaining a specific type of blank; phase II (layers 11 – 6) is marked by a simplification of the reduction sequences (Bartolomei et al., 1982; Bertola et al., 2007; Fontana et al., 2009; Fontana et al., 2015). As a result of the last 40 years of excavation works, a high quantity of yellow and red ochre nodules (approximately 8 kg) was also recovered in the northern sector of the Tagliente rock-shelter (Cavallo et al., 2017). Moreover, great importance is the faunal assemblage recovered in the southern sector, comprising small and large mammal remains, which were in a high level of fragmentation: 91% was smaller than 2 cm (Fontana et al., 2009)

Concerning the spatial organization of remains, within the outer area of the northern sector the presence of a recurrent pattern of distribution of living floors has been observed during the excavation activities of the last two decades. The inner protected area of the shelter can be considered a dwelling area due to the presence of several hearths, whereas different categories of waste were found in the outer zone (Fontana et al., 2009; Peretto et al., 2004). Other important finds of the sequence are mobile art objects engraved with geometric and figurative shapes, and a burial discovered in the 1970s of the last century in the southern sector of the sheltered area (coeval to level 13) dated to the 16,634 – 15,286 cal. BP (Gazzoni et al., 2013).

According to radiocarbon dates which range from 17,219-16,687 cal. BP (layer 13 alpha) to 14,572–13,430 cal BP (levels 10–8), the Epigravettian series is one of the most complete in northern Italy, formed between the first part of the Oldest Dryas (GS-2.1a) and the first half of the Bølling–Allerød Interstadial (GI-1c1) (Fontana et al., 2009; Fontana et al., 2018). Taking into account the external area of the long trench from where all of the analyzed red deer teeth for this study were collected, the radiocarbon dates range from 16,932-15,495 cal BP (levels 15–16) to 14,572-13,430 cal. BP (levels 8–10) (Gazzoni et al., 2013) (***Table 4***).

In this regard, the site represents the most ancient deposit known on the southern slope of the Alps to be re-occupied by human groups after the Last Glacial Maximum (Alpine LGM, 26 – 17 ka ago (see Monegato et al., 2017)). Last but not least, the results from the recent radiocarbon dates of the lower deposit of the internal sequence (levels 13a alpha, 13a, and 300), which corresponds roughly to layers 13 to 15/18 in the outer zone, appear older than the dates from the lower levels of the outer part (15 – 16) (Berto et al., 2018). This suggests, the radiometric dates from the 1980s that were applied on charcoal samples from levels 15 – 16, should be considered carefully.

2.3.2 Paleoenvironmental background

The large mammal remains recovered from the southern sector and the trench area of the Tagliente rock-shelter testify to a change of the exploited species by Late Epigravettian hunter-gatherers throughout time. The study of the large mammals allowed divided the faunal assemblage of the Late Epigravettian sequence into two phases: the lower levels 18 – 13, and upper levels 12 – 5 (Bartolomei et al., 1982). The distribution of ungulates and other mammals in the lower layers is characterized by species adapted to an open environment and dominated by Alpine ibexes (*Capra ibex*) (NISP=832). The upper layers (12 – 5) document the development of milder climatic conditions with the increase of temperate species such as *Cervus elaphus*, *Capreolus capreolus*, and *Sus scrofa*. Only in level 13, which is coeval to the burial, the two associations are equivalent (Fontana et al., 2009; Rocci Ris, 2006). Red deer (*Cervus elaphus*) is the most represented species within the whole stratigraphic sequence (NISP=4522) with 52.5% identified specimens. It is documented from layer 15 and increases from levels 12-10 to the top, becoming the most abundant in the upper layers (71.5% of identified specimens in layer 8). The second most represented ungulate is roe deer, already present in layer 14. Water-related species such as *Alces alces* have a relatively high percentage in layers 11 – 15. Most remains are represented by adult individuals. The analysis of butchering marks confirms that herbivores represented one of the main food resources of the Late Epigravettian groups (Fontana et al., 2009).

The distribution of small mammals (e.g. marmot, hare, beaver), which are present in all the layers, confirms the environmental settings attested by the large mammal records. The marmot (*Marmota marmot)* remains (NISP=463) are mostly recovered from the lower layers 17 – 14. The second abundant small mammal is the hare (*Lepus europaeus* and *Lepus timidus*) with NISP=163 (Fontana et al., 2009). The beginning of the GI-1 in the Southern Alps is characterized by a quick increase in forest density, even at altitudes up to 1350 m a.s.l. (Ravazzi et al., 2007). However, the small mammal collection in the upper levels (5 – 10) does not reflect such an increase in forest.

The micro-mammal assemblage is dominated by *Microtus arvalis* and *Microtus (Terricola)* gr. *multiplex-subterraneus* along the whole stratigraphic series 14 – 5 (Bartolomei et al., 1982; Berto et al., 2018). These species are dominating in levels 12 and 13 – 14, testifying that the landscape surrounding the site was a periglacial one, mainly open, and with scarce forest patches. *Microtus arvalis* start to decrease from level 11 reflecting an increase in

woodland and water components, as suggested by the presence of water-related species, *Arvicola amphibius*. Level 10 is the last recording of the occurrence of cold climate-related species *Cricetus cricetus.* It also testifies to a strong decrease in *Microtus (T.)* gr. *multiplex-subterraneus*. The first slight increase in mean annual temperature (MAT) (from 8.0 °C to 8.5 °C) and mean temperature of the coldest month (MTC) (from 0.4 °C to 1.7 °C) is also recorded in this unit. A strong decrease of cold-related species and an increase of temperate climate-related species (e.g. *Chionomys nivalis*) can be related to a transitional moment when the landscape was changing from a dense grassland to a degraded environment as an effect of the strong deglaciation process occurred in the Southern Alps during Late Glacial. The disappearance of species *Cricetus cricetus* from the upper levels (5 – 9) indicates general, mild climate warming corresponding to the temperate (Bølling–Allerød) Interstadial (GI-1) (Berto, 2013; Berto et al., 2018).

Another climate proxy – pollen analyses – which was carried out along the Epigravettian series of Riparo Tagliente, indicates similar variations of environmental parameters. In the pollen diagrams, the lower layers 16 – 15 testify that during the first part of the Late Glacial (GS-2.1a), the landscape was dominated by herbaceous plants (*Gramineae, Artemisia*) with some conifers and colonizing plants (*Pinus sylvestris-mugo, Juniperus, Salix*). In the Late Glacial Interstadial, the area surrounding the shelter was characterized by a woodland expansion with conifers (*Pinus sylvestris-mugo*) and deciduous trees (*Quercus* sp., *Tilia* sp., *Ulmus* sp., *Ostrya carpinifolia, Fraxinus, Corylus*). The latter are associated with layers 14 – 5 (Bartolomei et al., 1982).

The analysis of malacological assemblages recovered from the trench area also testify to a progressive climate improvement along the Epigravettian sequences. In layers 12 – 10, the xero-thermophilous species dominate the malacofauna collection, indicating the onset of warm climatic conditions, while cold-associated species are registered in the bottom layers (18 – 15) of the Late Epigravettian series (Bartolomei et al., 1982).

To conclude, in the North-Mediterranean area, the term Epigravettian describes the archaeological techno-complexes that emerged during and after the LGM by dividing this period respectively into an Early and Late phase. So far, after the cold phase LGM, the earliest occupation of Late Epigravettian hunter-gatherers in the Southern Alps, is documented in the archaeological deposits of Riparo Tagliente. The most complete sequence of the Late Epigravettian was discovered at Tagliente rock-shelter and has been extensively investigated

since the late 1970s. After intensive archaeological interdisciplinary studies, it was observed that Epigravettian groups exploited the internal and external areas of the shelter differently. According to studies carried out on different proxies (macrofaunal remains, microfauna, pollen, malacofauna, sediments), the Epigravettian deposits are divided into two "phases", where different environments were detected, although the transition between the two is not coeval. Based on macro-faunal assemblages, the lower layers (17 – 14) are characterized by the cold-associated species with open steppe grassland, whereas the upper layers (12 – 5) are dominated by the warm-related species in the temperate climate. Layer 13 represents a transitional phase, where the two faunal associations are equivalent. This two phases of occupation confirm that occupation at the site of Riparo Tagliente occurred between the end of the Greenland Stadial-2 (GS-2) and the beginning of the warmer Bølling–Allerød Interstadial (GI-1).

Chapter 3 – MATERIALS AND METHODS

In the previous chapter, the general archaeological context of the study area was reported, by focusing on the Late Epigravettian culture in terms of the Late Upper Paleolithic of Europe, and its role in the re-occupation of the Southern Alps after the Last Glacial Maximum (LGM). In addition, several paleoecological data acquired from the deposits of the Epigravettian series at Riparo Tagliente were also discussed.

This focal chapter aims to present the methodological approach applied in this research. We first discuss the sample materials that can be analyzed, focusing on special concerns when dealing with fossils, and then describe the analytical basics.

This chapter was organized according to the four following steps. The first is a selection of materials, where we are describing in detail the main principles of collecting materials. Such as how and what archaeofaunal fragments were chosen (in our case, red deer teeth), the purpose of selection, sample quantities, as well as their distribution sequence along the stratigraphy at Riparo Tagliente. The second is a sampling of materials, which explains how to process the teeth specimens and extract a required amount of fine powders from the dental tissue (enamel). The third one is the carbonate pre-treatment phase, where the analytical steps of sampling purification are outlined. The last stage is the measurement of the pretreated samples in the isotope ratio mass spectrometry (IRMS) and consequently, the processing of the resulting isotope ratio values.

3.1 Selection of materials

Initially, a total of 48 prehistoric teeth of red deer (*Cervus elaphus*) from 38 different individuals have been selected from the faunal assemblage of Riparo Tagliente. Dental material chronologically records the diet of an individual during a particular period of time in their life as well as the corresponding climatic signals. The key sample selection was focused on collecting the latest-forming permanent third molars (M3), and whenever possible the second molars (M2), to reconstruct the adult diet and habitat, and avoid the isotopic effect of breast milk intake (Chinique de Armas et al., 2022; Fuller et al., 2006; Tsutaya & Yoneda, 2015). Moreover, third molars mineralize during early life stages (i.e., infant to young-adult period) (Koch, 2007) by preserving in enamel the information from early life diets of red deer as well as their habitat and local seasonal variation (e.g. Kohn & Cerling, 2002; Kohn et al., 1998).

Recorded seasonal cycles from third molars correspond to the duration of the crown formation (mineralization) of these teeth (e.g. Balasse et al., 2003). The mineralization period of teeth in typical herbivore, continues during a tooth eruption and completely finishes before the tooth eruption ends (Kohn & Cerling, 2002; Kohn et al., 1998). Red deer second molars erupt between 12 and 16 months and third molars erupt between 21 and 32 months after birth (Azorit et al., 2002; Brown & Chapman, 1991a; Godawa, 1989). Based on the radiographic observations on modern red deer jawbone dentition by (Brown & Chapman, 1991b) it was identified that the mineralization of the second molar in red deer takes place between 3 and 9 months and that the third molar mineralizes between 9 and 26 months. It thus means second molars likely provide a record of one summer and/or winter of the first year and third molars the whole one-year seasons of the second year of red deer life.

In this regard, for each individual, it was carefully chosen the right or left third molars and associated second molars for some individuals. All permanent teeth were from the lower jawbone (mandible). For the case of selected second molars, they were still enclosed in the jawbone, otherwise, they are not identifiable as an isolated tooth like the third molars do. We tried to select the intact teeth by avoiding breaks, and large fractures, since they might contain potential diagenetic carbonates that can contaminate our samples for isotope analysis.

The collected teeth come from the upper stratigraphic unit of the external trench area, which dates back to the Late Glacial and contains the Late Epigravettian assemblages (Aspes, 2002; Bartolomei et al., 1982). Namely, they belong to the following layers (or *tagli* as they were originally named): 1, 4, 4a, 4b, 5, 6, 7, 7b, 8, 9, 10a, 10b, 10c, 10d and 13. The specimens selected for stable isotopic analysis were confined to the stratigraphic sequence between layers 5 and 13, due to different factors. First, we excluded the specimens from layers 1, 4, 4a, and 4b, which were reworked and could not be attributed to a specific phase of occupation. Then, we need to take into account that the lowermost levels lack temperate species like red deer because these species started to increase in the rock-shelter from layers 14 and 13 to the upper layers. In our case, we don`t have any adequate samples from layer 14. After excluding the teeth from the uppermost levels (1, 4, 4a, 4b), a total of 42 red deer teeth were left, i.e. 33 lower third molars and 9 lower second molars, have been chosen as an ultimate set of samples for the carbonate (CO_3) isotopic analysis. These 42 lower molars have been analyzed for stable oxygen ($^{18}O/^{16}O$) and carbon ($^{13}C/^{12}C$) isotope ratios. The detailed distribution of teeth specimens along the stratigraphic series can be found in ***Table 1.***.

Although several radiocarbon dates have been obtained at the Tagliente shelter, there is not yet precise radiocarbon dates for all of our selected levels (SU 13-5). We know from other

sources that the Epigravettian series spanned between the Oldest Dryas (GS-2) and the first part of the Bølling–Allerød temperate Interstadial (GI-1) (Fontana et al., 2009; Gazzoni et al., 2013). According to other studies, the radiocarbon dates of the Epigravettian sequence range from 16,932–15,495 cal BP (layers 16 – 15) to 14,572–13,430 cal BP (layers 10 – 8) (Alessio et al., 1970; Aspes, 2002; Stuiver & Reimer, 1993) (***Table 4***).

A crown and a root are the two main elements that form the general structure of the teeth. Three major calcified tissues of teeth are *dentine* – a firm and resilient tissue that forms the fundamental structure of a tooth, *enamel* – a hard and shiny layer covering the dentine in the crown part only, and *cement (cementum)* – a bone-like tissue with which coated the dentine root and in some animal species the enamel surface too (Hillson, 2005, pp. 146-147). Dental enamel, the highly mineralized material with useful seasonal isotope changes (Cerling & Sharp, 1996; Dettman et al., 2001; Koch et al., 1989), was analyzed for the stable O and C isotope ratios in this study. As a PO_4 component (from enamel, dentine, and bone), enamel, even in samples as old as the Miocene, is physically and chemically most resistant to alteration (Ayliffe et al., 1994; Bocherens et al., 1996; Wang & Cerling, 1994).

3.2 Sampling of materials

As we mentioned above, the sample set includes only the lower M3 left (M3L) or right (M3R) and lower M2 right (M2R) side only. 33 individuals (total 42 teeth) were sampled, including two individuals from layer 5, three from layer 6, five from layer 7 and one from layer 7b, four from each layer 8 and layer 9, six from layer 10a, two from each layer 10b and 10d, one from 10c and three individuals for layer 13 (***Table 1***). Enamel sampling was always performed on the buccal (labial) side of the teeth, except for one tooth where a wide crack covered the buccal (lab code: RPT-36) (***Fig. 4*** and ***Fig. 7***). The M3 was sampled on the mesial (anterior) or middle lophs (***Fig. 7*** – ***Fig. 9***). Whenever possible, sampling was performed on the distal (posterior) loph of the M2 that is adjacent to the mesial loph of M3, which might help record a more continuous seasonal sequence. Again, above all, one needs to avoid fractures enclosing contaminated sediment (diagenetic calcite) and work accordingly. Moreover, it is important to be cautious while collecting enamel powder without touching the underlying dentine, as this may alter the isotopic values of the enamel bioapatite. It should be noted that the sampling fulfillment of specimens was carried out by two people and in two different places.

Fig. 4. Photo after sampling (Lower M3R). Sampled lingual side.

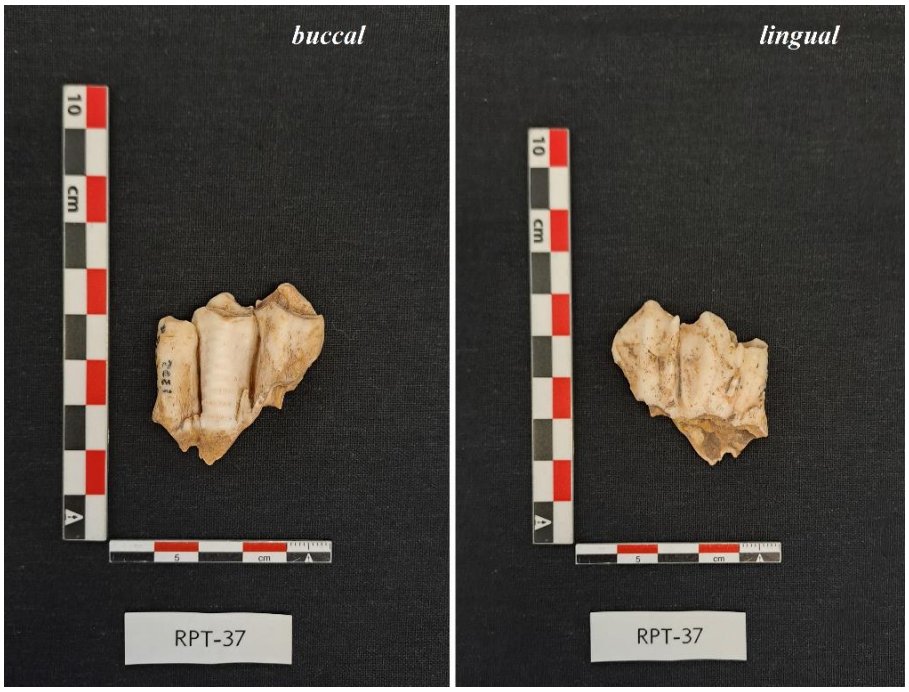

Fig. 5. Photo after sampling (Lower M3R). Sampled buccal side.

Most of the teeth sampling was performed by my thesis supervisor, Prof. Dorothée G. Drucker, partly at the Department of Humanities of the University of Ferrara, and partly in the field during the archaeological excavations at Riparo Tagliente, Verona, Italy. Being responsible for the sampling of three red deer teeth, I have experienced the entire process, beginning from the tooth sampling until carbonate pretreatment procedures, in the Biogeology laboratory at the

Geoscience Department of Tübingen University (February and March 2024). These three teeth were lower M3R (RPT-36, RPT-37, RPT-38) from three different individuals (***Fig. 4*** – ***Fig. 9***).

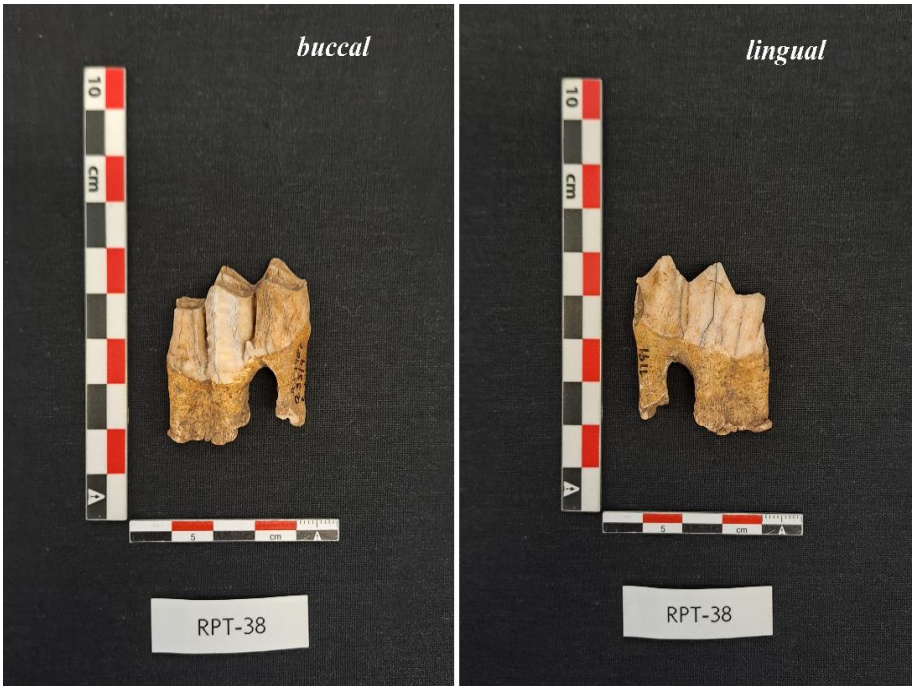

Fig. 6. Photo after sampling (Lower M3R). Sampled buccal side.

Primarily, teeth surfaces were cleaned with a diamond drill bit. After, the series of horizontal bands of enamel was extracted along the crown using the diamond-coated drill bit. These successive bands were sampled from the top to the bottom, an enamel-root junction (ERJ) boundary, of the crown (***Fig. 7*** – ***Fig. 9***). ERJ point was used as a reference point for measurement and the origin (starting point) in the plotted graphs with the results. In some teeth, for example, an isolated tooth with a broken root or a tooth still held in the jawbone that covers the ERJ line of the tooth, it was difficult to see the ERJ point, so we marked a point 0 in the bottom of the crown.

Up to 11 bands or a minimum of 5 bands per tooth were obtained from the molars M3 whose crowns' heights range from 27.6 mm and 13.0 mm, while for the molars M2 it was taken maximum of 9 bands and at least 5 bands where the crown height ranges between 19.0 mm and 12.7 mm. The more bands the higher possibility to record the complete seasonal cycle (summer and winter). As long as this sampling strategy is applied consistently to all the specimens, this approach succeeds in preserving the chronological order of seasonal changes. For each sampled band, about 10 – 15 milligrams (mg) of enamel fine powders were collected. Here the root dentine, in the amount of 18 – 20 mg, was also collected only from each M3 in order to control

the quality of the isotope analysis of our samples. Powders sampled from every band were put into separate plastic vials with a flip lid (volume: 1.5 ml). Afterwards, these vials were arranged into a set of 24 pcs (22 vials of our samples and 2 vials with the in-lab standards), which is consistent with the centrifuge (Thermo Scientific Heraeus Biofuge) slots. In total 303 tubes with enamel powder and 31 with root dentine powder were prepared for the pre-treatment phase (***Table 1***). After finishing the dental sampling, drawings of every sampled tooth with all details (cracks, strip heights, etc.) were produced (e.g. ***Fig. 7*** – ***Fig. 9***).

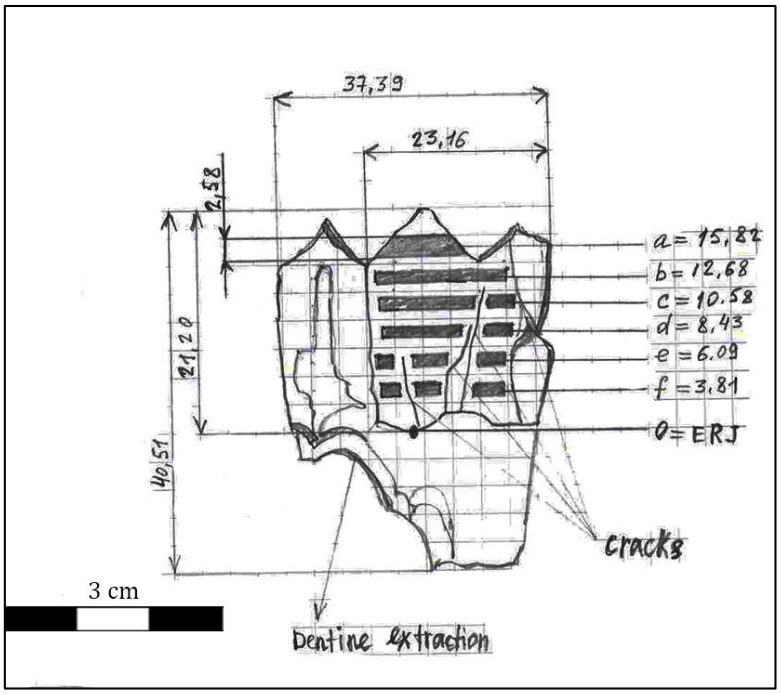

Fig. 7. RPT-36. Sampled on the lingual side along the middle and distal lophs (Lower M3R).

3.3 Carbonate pre-treatment

Like other living dental tissues, the archaeofaunal dental enamel is composed of inorganic (formed entirely of minerals) and organic compounds (Hillson, 2005, pp. 146-147). Its mineral composition makes up almost 99% calcium phosphate from which ~3% is carbonate, while the organic part takes about 1% only (Bocherens & Drucker, 2007). This inorganic component is also called a bioapatite (biological apatite), which is mainly based on calcium phosphate ($CaPO_4$) minerals. Most of the bioapatite in teeth is hydroxylapatite $Ca_{10}(PO_4)_6(OH)_2$ (Hillson, 2005, p. 146) where some phosphates are substituted by CO_3 (carbonate) components.

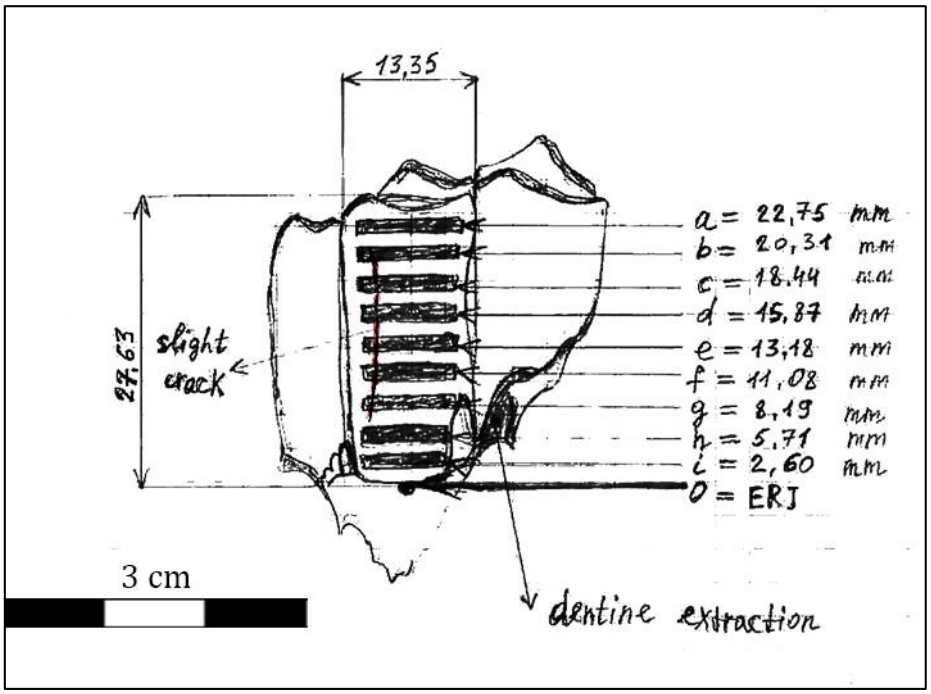

Fig. 8. Sampled bands of RPT-37 (Lower M3R).

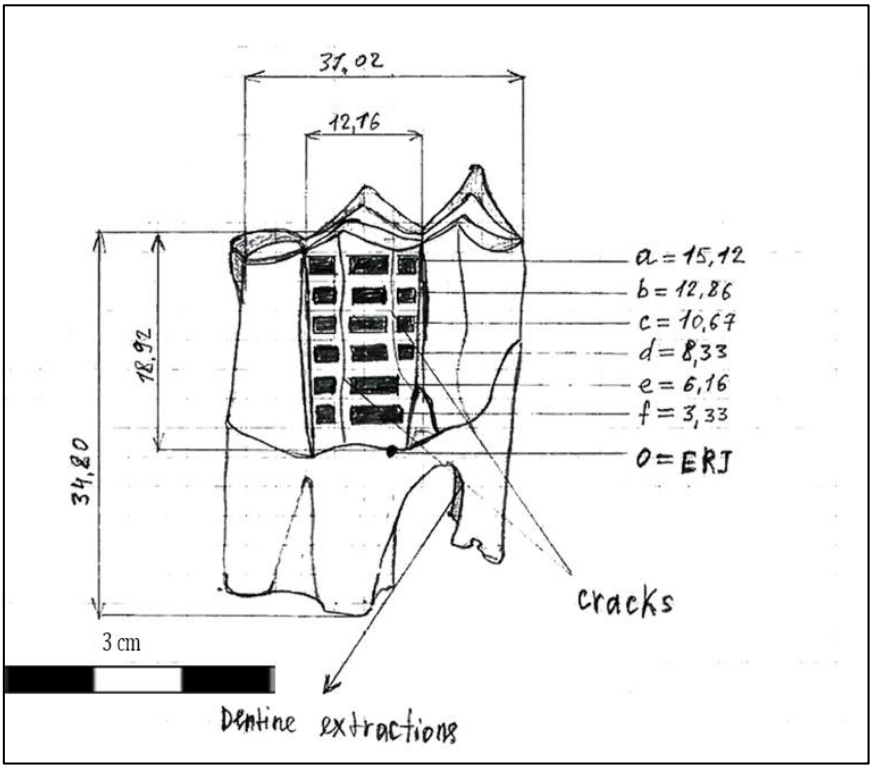

Fig. 9. Sampled bands of RPT-38 (Lower M3R).

Only the CO_3 component that substitutes for PO_4 and OH, diagenetically highly resistant (Kohn & Cerling, 2002), was analyzed for O and C isotopes, and other labile carbonates were removed during the pre-treatment (e.g. Rey et al., 1991).

The pre-treatment procedure of the samples was carried out following the protocol used at the laboratory of the working group Biogeology from the Department of Geosciences of the University of Tübingen (see description below). It is again worth noting that I performed myself the pre-treatment procedure of the four sets of samples (24 tubes/set) at the Biogeology laboratory in Tübingen.

Generally, the enamel powder samples take three consecutive days to be pretreated while dentine powder can take longer when containing organic matter that needs to be removed. The pre-treatment phase of samples includes the following laboratory steps:

(1) Each sampled powder was treated by adding 1.35 ml of sodium hypochlorite (NaOCl) at a concentration of 2.5% to remove the organic composition. Every tube was first shaken on the mini-shaker to mix the solution and then placed in the shaking plate (Heidolph Vibramax 100) and left for 24 hours. This step was repeated twice for the dentine powder.

(2) After 24 hours, samples were centrifuged for 5 min at 5000 rpm (revolutions per minute) to separate liquids from solids. Then NaOCl (2.5% Cl) solution was removed and samples were rinsed three times with Millipore water (Milli-Q H_2O) to wash NaOCl off. Every rinsing also was accompanied by shaking on the mini-shaker followed by centrifugation. Afterward, to remove all the diagenetic carbonates, the samples were reacted with 1 M acetic acid buffered solution (CH_3COOH) for 24 hours by adding 1.35 ml to each tube (e.g. Koch et al., 1997; Wright & Schwarcz, 1998; 1999). Before terminating this step, the tubes were shaken on the mini shaker to mix sample solids and solution well, and placed on the shaking plate at 450 rpm.

(3) The next day, after 24 hours samples were centrifuged for 5 min and the buffered solution was removed. And rinsed three times with Milli-Q water as explained before. In the end, samples had to be dried in the oven set at 35 °C for 72 hours. The treatment procedure can cause a sample weight loss in a considerable proportion (e.g. Balasse et al., 2002; Balasse et al., 2003). In this pre-treatment, it varies between 30 – 50%.

3.4 IRMS measurement

Once we had pretreated enamel hydroxylapatite, the isotope compositions were measured using the isotope ratio mass spectrometry (IRMS) in the Senckenberg Centre for

Human Evolution and Palaeoenvironment at the University of Tübingen. For IRMS, we took 2.5-3.0 mg of treated enamel, and dentine samples as well as in-lab standards (enamel of elephant and hippo from the archaeological site Chad) which underwent the same pretreatment as our other samples. In addition to this sample set, we included the international standards (IAEA-603, NBS-18, and LM) weighing 0.10 to 0.15 mg.

Vials with carbonates (treated samples) were then placed in the heated sample tray in the MultiFlow-Geo preparation system, where they were reacted with highly concentrated (~99%) phosphoric acid (H_3PO_4) at 70 °C for 4 hours. From this equilibration, the carbonate was obtained as CO_2 gas and sent through MultiFlow-Geo system to the Elementar IsoPrime100 IRMS where CO_2 was measured for four times within 15 minutes to get isotope values. Measured isotopic ratios are reported in mean values that were calibrated with two international standards (IAEA-603 with $\delta^{13}C$ = +2.46‰ and $\delta^{18}O$ = –2.37‰ and NBS-18 with $\delta^{13}C$ = –5.01‰ and $\delta^{18}O$ = –23.20‰) as well as two in-lab standards (elephant with $\delta^{13}C$ = –10.55‰ and $\delta^{18}O$ = +1.80‰ and hippo with $\delta^{13}C$ = –3.80‰ and $\delta^{18}O$ = –2.10‰) using the "LyticOS" software (see description in Drucker et al., 2024).

Theoretically, oxygen and carbon isotope ratios are measured as:

$$\delta(‰) = [(R_{sample}/R_{standard}) - 1] \qquad \textbf{3.1}$$

where R=$^{13}C/^{12}C$ or R=$^{18}O/^{16}O$ ratios of the sample and the standards, which is PDB for carbon and SMOW for oxygen (Gifford-Gonzalez, 2018; Koch et al., 1997); and will be written as ‰ (parts per mil.).

Final carbonate $\delta^{13}C_{carbonate}$ and $\delta^{18}O_{carbonate}$ mean values obtained from the IRMS measurements are presented versus Vienna Pee Dee Belemnite limestone (‰ vs. VPDB) standard. For further orthographic brevity, we simplify $\delta^{18}O_{carbonate}$ to $\delta^{18}O_{carb}$.and the $\delta^{13}C_{carbonate}$ to $\delta^{13}C_{carb}$. In addition, $\delta^{18}O_{carb}$ values in VPDB were also recalculated to the Vienna Standard Mean Ocean Water scale (‰ vs. VSMOW) and will be indicated in tables and graphs of the following chapters. The next equation by (Coplen, 1988) was applied from VPDB to VSMOW conversion:

$$\delta^{18}O_{VSMOW} = 1.03091 \times \delta^{18}O_{VPDB} + 30.91 \qquad \textbf{3.2}$$

The measurement uncertainty was monitored using three in-house standards (pure carbonate Laaser Marmor with $\delta^{13}C$ = +1.50‰ and $\delta^{18}O$ = –5.20‰, pretreated enamel of elephant with

$\delta^{13}C$ = –10.55‰ and $\delta^{18}O$ = +1.80‰, pretreated enamel of hippo with $\delta^{13}C$ = –3.80‰ and $\delta^{18}O$ = –2.10‰). Overall analytical precision is higher than 0.1‰ for carbon ($\delta^{13}C$) and better than 0.2‰ for oxygen ($\delta^{18}O$) isotopic values.

3.5 Calculation methods for air temperature (T_{air})

The mean annual air temperature (MAT) and mean monthly air temperature (MMT) values for our red deer samples were calculated (e.g. Gasparik et al., 2023). To calculate these temperatures, we use two equations relating the precipitation $\delta^{18}O$ to the temperature and call them as MAT and MMT equations. It is worth pointing out that with the short crown red deer teeth, it is possible to reconstruct the temperature of no more than one or two seasons using one or another equation.

For MAT and MMT calculations, we first converted the measured oxygen isotope values of enamel carbonate ($\delta^{18}O_{carb}$ against VSMOW) to local meteoric water $\delta^{18}O_{meteoric\ water}$ values (hereinafter $\delta^{18}O_w$). Red deer obtain their water through drinking and from the plants ingested. The main source of drinking water for terrestrial animals is meteoric water, which is important for assessing seasonal isotope effects showing higher $\delta^{18}O$ values in warm regions or seasons, and lower $\delta^{18}O$ values in colder regions or seasons (Gat, 1996; Koch, 2007). Meteoric water (environmental water) is supplied by the precipitations and therefore we should have drinking water isotope values to describe the relationship of our red deer $\delta^{18}O_{carb}$ isotopic results with the present air temperature. The $\delta^{18}O_{carb}$ composition of the biogenic apatite of mammal teeth is in direct relationship with that of the environmental water ($\delta^{18}O_w$), from which the MAT and MMT temperatures can be estimated.

In our calculations of $\delta^{18}O_w$ for the red deer sample, it was used the following equation by Iacumin *et al.* (1996) where modern deer (*Cervus elaphus*) samples and local meteoric water were calibrated and obtained a direct positive relationship between $\delta^{18}O_{carb}$ and $\delta^{18}O_w$ values:

$$\delta^{18}O_c = 0.998 \times \delta^{18}O_w + 33.63 \qquad \textbf{3.3}$$

Here, the $\delta^{18}O_w$ values are also introduced in (‰ vs. VSMOW).

In the next step, we tried to describe the current relationship between meteoric water $\delta^{18}O_w$ and recent air temperature (T_{air}) for two locations from where the MAT and MMT equations derived.

Table 1. Final list of the selected specimens

SU=Stratigraphic Unit; *ERJ*=Enamel Root Junction; *Dent. Ext.* = dentine extracted teeth; *M3L* = third molar left side; *M3R* = third molar right side; *M2R* = second molar right side. The ***total -303*** is the number of samples (enamel only) prepared for isotope analysis.

Lab ID	***Site***	***Excavation ID***	***Culture***	***Species***	***SU***	***Tooth***	***Bands N***	***ERJ point***	***Crown height (mm)***	***Dent. Ext.***
RPT-R6	Riparo Tagliente	RT81 Q3519 #9138	Late Epigravettian	*Cervus elaphus*	5	Lower M3L	7	Yes	23.5	Yes
RPT-R7	Riparo Tagliente	RT q20/4 #6574	Late Epigravettian	*Cervus elaphus*	5	Lower M3L	5	No	17.6	Yes
RPT-R8	Riparo Tagliente	RT q631 #6757	Late Epigravettian	*Cervus elaphus*	6	Lower M3R	8	Yes	21.1	Yes
RPT-R9	Riparo Tagliente	RT81 q5015 #9488	Late Epigravettian	*Cervus elaphus*	6	Lower M3L	7	No	18.0	Yes
RPT-R10	Riparo Tagliente	RT81 q5016 #9475	Late Epigravettian	*Cervus elaphus*	6	Lower M3L	6	Yes	16.6	Yes
RPT-R11	Riparo Tagliente	RT q23 #7001	Late Epigravettian	*Cervus elaphus*	7b	Lower M3R	9	Yes	23.2	Yes
RPT-R12	Riparo Tagliente	RT q9 #6920	Late Epigravettian	*Cervus elaphus*	7	Lower M3R	10	Yes	24.0	Yes
RPT-R13	Riparo Tagliente	RT81 q21/8	Late Epigravettian	*Cervus elaphus*	7	**Lower M2R**	8	Yes	15.5	No
RPT-R13	Riparo Tagliente	RT81 q21/8	Late Epigravettian	*Cervus elaphus*	7	Lower M3R	8	Yes	19.1	Yes
RPT-R14	Riparo Tagliente	RT q6 #6839	Late Epigravettian	*Cervus elaphus*	7	Lower M3R	7	Yes	18.6	Yes
RPT-R15	Riparo Tagliente	RT81 q35/7 #7002	Late Epigravettian	*Cervus elaphus*	7	Lower M3R	8	Yes	19.3	Yes
RPT-R16	Riparo Tagliente	RT q6 #6850	Late Epigravettian	*Cervus elaphus*	7	**Lower M2R**	5	No	12.7	No
RPT-R16	Riparo Tagliente	RT q6 #6850	Late Epigravettian	*Cervus elaphus*	7	Lower M3R	6	No	13.0	Yes
RPT-17	Riparo Tagliente	RT62 Q20/7 #7636	Late Epigravettian	*Cervus elaphus*	8	Lower M3R	8	Yes	20.7	Yes
RPT-18	Riparo Tagliente	RT8 q6 #7628	Late Epigravettian	*Cervus elaphus*	8	**Lower M2R**	9	No	17.3	No

Lab ID	*Site*	*Excavation ID*	*Culture*	*Species*	*SU*	*Tooth*	*Bands N*	*ERJ point*	*Crown height (mm)*	*Dent. Ext.*
RPT-18	Riparo Tagliente	RT8 q6 #7628	Late Epigravettian	*Cervus elaphus*	8	Lower M3R	8	Yes	21.1	Yes
RPT-19	Riparo Tagliente	RT Q3613 #7643	Late Epigravettian	*Cervus elaphus*	8	**Lower M2R**	6	Yes	16.6	No
RPT-19	Riparo Tagliente	RT Q3613 #7643	Late Epigravettian	*Cervus elaphus*	8	Lower M3R	6	Yes	18.6	Yes
RPT-20	Riparo Tagliente	RT Q6 #7556	Late Epigravettian	*Cervus elaphus*	8	**Lower M2R**	5	Yes	14.0	No
RPT-20	Riparo Tagliente	RT Q6 #7556	Late Epigravettian	*Cervus elaphus*	8	Lower M3R	7	Yes	15.8	Yes
RPT-21	Riparo Tagliente	RT Q80/9 #9727	Late Epigravettian	*Cervus elaphus*	9	**Lower M2R**	5	Yes	14.1	No
RPT-21	Riparo Tagliente	RT Q80/9 #9727	Late Epigravettian	*Cervus elaphus*	9	Lower M3R	6	Yes	13.0	Yes
RPT-22	Riparo Tagliente	RT Q23 #8512	Late Epigravettian	*Cervus elaphus*	9	**Lower M2R**	5	Yes	13.7	No
RPT-22	Riparo Tagliente	RT Q23 #8512	Late Epigravettian	*Cervus elaphus*	9	Lower M3R	6	Yes	14.7	No
RPT-23	Riparo Tagliente	RT Q64/5-8 #8536	Late Epigravettian	*Cervus elaphus*	9	Lower M3R	9	Yes	21.5	Yes
RPT-24	Riparo Tagliente	RT Q6 #9536	Late Epigravettian	*Cervus elaphus*	9	**Lower M2R**	9	Yes	19.0	No
RPT-24	Riparo Tagliente	RT Q6 #9536	Late Epigravettian	*Cervus elaphus*	9	Lower M3R	8	Yes	18.9	Yes
RPT-25	Riparo Tagliente	RT Q19/4 #1181	Late Epigravettian	*Cervus elaphus*	10a	Lower M3L	7	Yes	16.7	Yes
RPT-26	Riparo Tagliente	RT Q35/6 #1176	Late Epigravettian	*Cervus elaphus*	10a	Lower M3R	6	Yes	17.5	Yes
RPT-27	Riparo Tagliente	RT Q22	Late Epigravettian	*Cervus elaphus*	10a	**Lower M2R**	6	Yes	15.5	No
RPT-27	Riparo Tagliente	RT Q22	Late Epigravettian	*Cervus elaphus*	10a	Lower M3R	7	Yes	17.9	Yes
RPT-28	Riparo Tagliente	RT Q38/6 #1198	Late Epigravettian	*Cervus elaphus*	10b	Lower M3R	7	Yes	17.5	Yes
RPT-29	Riparo Tagliente	RT Q80/7 #1237	Late Epigravettian	*Cervus elaphus*	10b	Lower M3R	11	Yes	22.3	No

Lab ID	*Site*	*Excavation ID*	*Culture*	*Species*	*SU*	*Tooth*	*Bands N*	*ERJ point*	*Crown height (mm)*	*Dent. Ext.*
RPT-30	Riparo Tagliente	RT Q37/6 #1166bis	Late Epigravettian	*Cervus elaphus*	10c	Lower M3R	8	Yes	23.2	Yes
RPT-31	Riparo Tagliente	RT Q50 #1229	Late Epigravettian	*Cervus elaphus*	10d	Lower M3R	8	Yes	22.8	Yes
RPT-32	Riparo Tagliente	RT Q79/9 #1239	Late Epigravettian	*Cervus elaphus*	10d	Lower M3R	8	Yes	19.1	Yes
RPT-33	Riparo Tagliente	RT Q15 #4727	Late Epigravettian	*Cervus elaphus*	13	Lower M3L	8	Yes	23.7	Yes
RPT-34	Riparo Tagliente	RT Q511-7 #4118	Late Epigravettian	*Cervus elaphus*	13	Lower M3L	7	Yes	21.1	Yes
RPT-35	Riparo Tagliente	RT Q15 #4695	Late Epigravettian	*Cervus elaphus*	13	Lower M3L	8	Yes	18.2	Yes
RPT-36	Riparo Tagliente	RT Q22 #3055	Late Epigravettian	*Cervus elaphus*	10a	Lower M3R	6	Yes	21.2	Yes
RPT-37	Riparo Tagliente	RT Q54 #1302	Late Epigravettian	*Cervus elaphus*	10a	Lower M3R	9	Yes	27.6	Yes
RPT-38	Riparo Tagliente	RT Q9519 #1191	Late Epigravettian	*Cervus elaphus*	10a	Lower M3R	6	Yes	18.9	Yes
Total							***303***			

(1) The MAT temperature values for our teeth samples were estimated related to the entire continent of Europe using an already published relationship by Skrzypek *et al.* (2011), where the $\delta^{18}O_w$ calculation was based on fossil mammal teeth:

$$T_{air} = 1.41 \times \delta^{18}O_w + 21.63 \qquad \textbf{3.4}$$

(2) To assess whether the seasonal changes in red deer intra-tooth $\delta^{18}O_{carb}$ isotope signatures reflect seasonal climate variations, we need to compare the teeth isotope results with the temperature in the region of Riparo Tagliente site. We then used data from the Global Network of Isotopes in Precipitation (GNIP) (IAEA/WMO, 2024) for the MMT estimations (e.g. Gasparik et al., 2023; Skrzypek et al., 2011; Tütken et al., 2007). This GNIP database did not provide any meteorological stations in Verona that can provide data with the $\delta^{18}O$ composition of precipitation. However, we could find the closest GNIP station to the study area, that is Feletto Umberto in the Friulia region, Italy. The Feletto Umberto station (46.1° N, 13.22° E) is located in the south-east of the pre-Alps at the elevation of 135 m a.s.l. and approximately 250 km (retrieved from Google Maps) northeast of the Riparo Tagliente. From the data provided by this GNIP station, we derived an equation having a good linear relation between two variables. Finally, we estimated the mean monthly air temperature (MMT) for Riparo Tagliente using this derived equation and the $\delta^{18}O_w$ that was calculated based on tooth $\delta^{18}O_{carb}$.

To summarize the chapter, the red deer teeth from the study site were chosen based on the followings (1) latest-forming lower permanent molars M3R or M3L and M2 to record the diet, habitat, and seasonal variability during the first and second year of deer early life; (2) less fractured permanent molars. To perform the carbonate isotope analysis, in total 42 teeth (33 third molars and 9 second molars) were selected out of the stratigraphic levels 13-5 from the trench area. After we cleaned the buccal surface of the crown from where we extracted horizontal strips of fine enamel powders, without touching the underlying dentine. Tubes holding 10-15 mg of sampled enamel bioapatite were pretreated following the laboratory protocol: (1) treated with sodium hypochlorite-NaOCl (2.5% Cl) to remove organic matter, (2) then reacted with 1 M acetic acid buffered solution (CH_3COOH) to remove diagenetic carbonates. These purified bioapatite carbonates (or hydroxylapatite carbonates) were then measured in the IRMS. The obtained oxygen ($\delta^{18}O_{carb}$. in ‰ vs. VSMOW) and carbon ($\delta^{13}C_{carb}$ in VPDB) isotope ratio values will be brought out in detail in the following chapter.

Chapter 4 – RESULTS

In the last chapter, the materials and methods for carrying out this research were explicitly discussed. Briefly, we selected archaeological red deer teeth, third and second molars. Then we analyzed the isotopic signals in the red deer teeth enamel by measuring the carbonate $\delta^{18}O_{carb}$ and $\delta^{13}C_{carb}$ values to obtain a deeper insight into the red deer diet, and habitat at first-life seasonal stages. In the previous chapter, all analytical procedures were also presented stepwise: starting from tooth enamel sampling and pretreatment until the preparation of samples to Mass Spectroscopy measurement. Afterward, we discussed how we deal with measured results by focusing on the conversion of isotopic values from one standard unit (V-PDB) to another (V-SMOW), as well as comparing the $\delta^{18}O_{cacb}$ values with the local meteoric water to estimate the mean monthly (MMT) and mean annual (MAT) air temperatures (T_{air}) for archaeological site Riparo Tagliente.

Now it is that chapter where we report, all obtained results from the carbonate isotope analysis of red deer teeth enamel. In this crucial stage of the research, we are going to determine bands that gave a reliable result for further isotopic interpretation, and why some were excluded from the final data set, by applying quality control criteria.

In general, this chapter will be covered in four sub-chapters. First, we begin with the results of bio-apatite carbonate preservation in our samples. Here we will investigate whether the $CaCO_3$ content of each sample matches the expected carbonate content, expressed in weight percent, or deviates from it likely due to contamination and/or incomplete chemical reaction during the pretreatment. In the following two sub-chapters, first $\delta^{13}C_{carb}$ and then $\delta^{18}O_{carb}$ values results will be described separately for each tooth. In these steps, intra-tooth and inter-tooth ranges, minimum and maximum values as well as mean values for both an individual and whole population will be calculated to detect dietary signals ($\delta^{13}C_{carb}$) and seasonal changes ($\delta^{18}O_{carb}$). In the last sub-chapter, the MMT and the MAT temperature for the Riparo Tagliente site will be provided, which were calculated based on data from the GNIP meteorological stations, including two locations: the entire Europe and Feletto Umberto.

4.1 Enamel Carbonate preservation

Carbonate content ($CaCO_3$) was determined by measurement of the amount of CO_2 generated from tooth enamel under acid reaction during IRMS measurement. The weight

percent carbonate for enamel hydroxylapatite is estimated by [(weight CO_3/weight sample) ×100] (Koch et al., 1997). We expected the weight percent of carbonate content ($CaCO_3$) for our samples in the ranges of 2.3 – 5.8 % for enamel (Koch et al., 1997; Rink & Schwarcz, 1995; Zazzo et al., 2005) as well as 4.4 – 8.9 % for dentine (Zazzo et al., 2006) which preserves a higher carbonate content than an enamel (e.g. Drucker et al., 2024). These percentages are based on the reported analyses of the modern enamel (e.g. bovid, elephant, hippo, horse). If there is a diagenetic alteration or impurity of the enamel, the values are expected to be much more varied from the above-defined percent ranges, respectively (e.g. Drucker et al., 2024). The reliability test on the obtained data from the $CaCO_3$ content was further done by comparing the values yielded by enamel and dentine, and then the intra-tooth $CaCO_3$ results were also used as a diagnostic tool for identifying contaminating signs within the tooth carbonate (e.g. Drucker et al., 2024; Martin et al., 2008) (***Fig. 10*** and ***Fig. 11***).

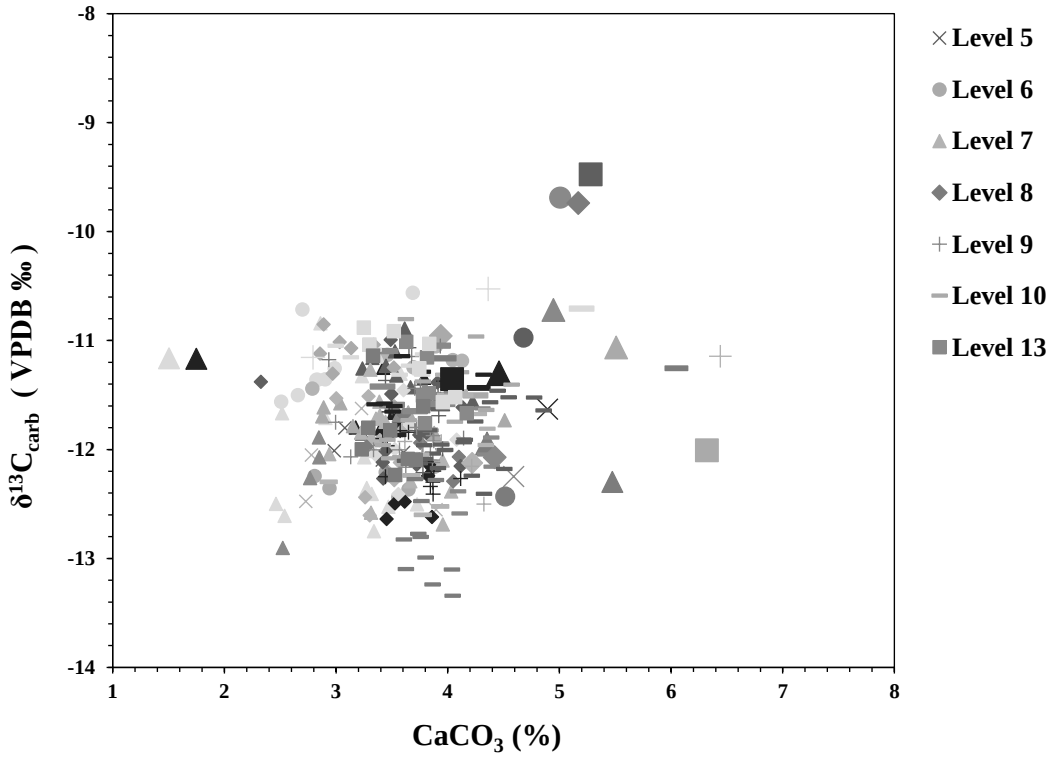

Fig. 10. The quality control of obtained isotopic results from carbonate ($CaCO_3$) content for all teeth samples. A comparison of enamel and dentine $\delta^{13}C_{carb}$ values.
Each symbol indicates one stratigraphic unit. The large signs represent dentine values and the small ones are enamel results.

Results for 303 enamel hydroxylapatite samples yielded reliable data on carbonate content, albeit not in all samples. The overall percent carbonate for treated enamel samples

ranges from 2.3 % to 4.9 %, and for dentine, which was collected to monitor the quality of our enamel carbonate, it ranges between 1.5 % and 6.4 % (***Table A. 1***). The intra-tooth variation of weight percent carbonate (the differences between maximum and minimum values of $CaCO_3$ (%) within one given tooth) ranges between 0.1% – 1.8%. We will further take a look at the results of intra-tooth carbonate content by the stratigraphic layers.

Specimens (two M3L) from layer 5 provided a carbonate content ranging between 2.7% – 3.9% in weight for enamel and the reference dentine gave the range of 4.6% – 4.9%.in weight percent $CaCO_3$ (***Table A. 1***). One tooth (RPT-R9) from the SU 6 provided two bands with a lower carbonate content than the rest samples in the tooth (2.8 – 2.9% against 3.4 – 3.9%) as well as an unexpected scattering of oxygen values. These records were excluded from the set of reliable data.

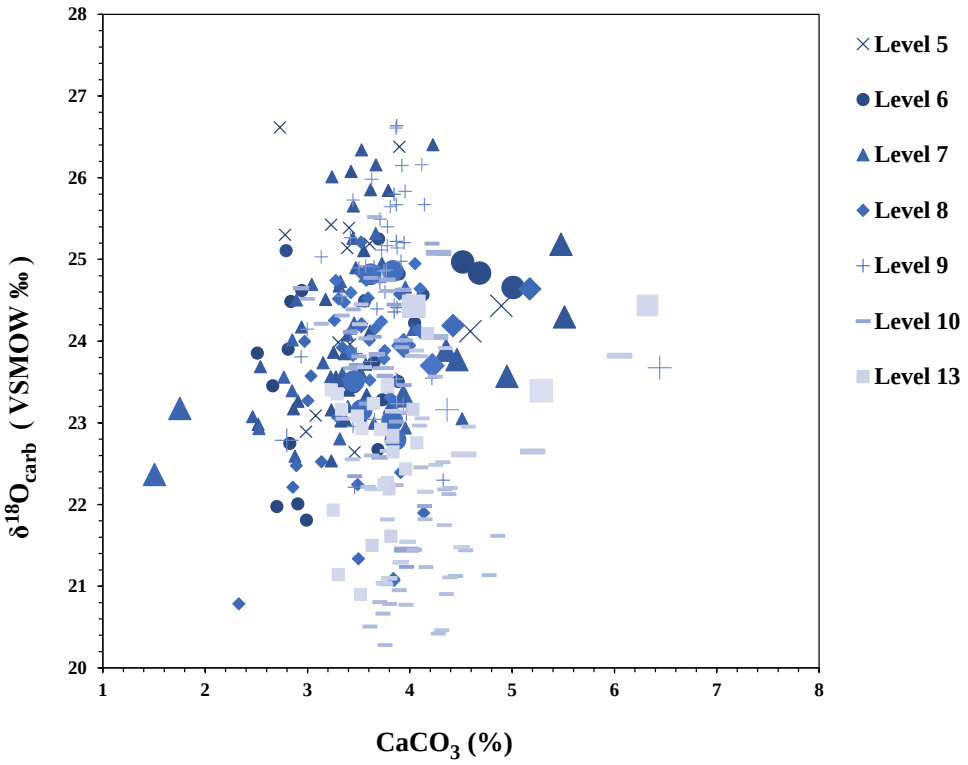

Fig. 11. The quality control of obtained isotopic results from carbonate ($CaCO_3$) content for all teeth samples. A comparison of enamel and dentine $\delta^{18}O_{carb}$ values.
Each symbol indicates one stratigraphic unit. The large signs represent dentine values and the small ones are enamel results.

These deflections of RPT-R9 were perhaps caused by possible contamination with dentine or bone during sampling since the tooth has a cracked crown surface and still was enclosed in the jawbone. Another suspicious molar RPT-R10 had a relatively high intra-tooth range for

carbonate weight percent (1.3 %) and some scattered $\delta^{18}O_{carb}$ values that traced the imprecise seasonal turning points. Conversely, the tooth RPT-R9 did record a sloping line pattern, so no incremental change could be observed (***Fig. A.1 - 2***). Within the specimen RPT-R10, one enamel band with the lowest carbonate content (2.8%) that provided the lowest $\delta^{13}C_{carb}$ value was excluded, after which we got a more reliable distribution pattern of isotopic signals (notably in $\delta^{18}O_{carb}$) (***Fig. 12***). The teeth from this level yielded the weight percent carbonate that varies between 4.5% – 5.0% for dentine and 2.5% – 4.1% for enamel, and after the state of exclusion the intra-tooth range became 0.7% – 1.2% (***Table A. 1***).

In the SU 7, only four teeth (RPT-R13-M2/M3, RPT-R14, RPT-R16-M3) out of eight showed satisfactory isotopic data. Enamel samples from this layer provided the percent carbonate ranging between 2.5% – 4.5% and dentine gave the ranges of 1.5% – 4.5% (***Table A. 1***). The intra-tooth carbonate content varied from 0.5% to 1.6%. One band in the tooth RPT-R11 gave lower isotopic values than the rest rows and therefore it was eliminated so that we could make RPT-R11 more reliable for further isotopic interpretation. The three bands in RPT-R15 that made the tooth with the highest intra-tooth variability (1.6%) among the specimens in layer 7, were excluded. After the exclusion of these bands (one gave the highest 4.5% in weight $CaCO_3$ and two gave the lowest 2.9%), we got a more reliable tendency, at least in oxygen isotopic values (***Fig. 12***). Even if the dentine of RPT-R16 yielded the lowest rate (1.5%) in weight $CaCO_3$ it well recorded one-year seasonal contrast (summer and winter), whereas RPT-R16-M2 with its dentine carbonate content of 1.8%, displayed the inconclusive pattern of $\delta^{18}O_{carb}$ values. One band of RPT-R16-M2 was not considered as reliable due to its lowest carbonate weight through the crown (3.3% against 3.7% – 4.0%). It is perhaps due to likely dentine contamination as these second and third molars were sampled on the adjacent lophs holding in the jawbone. Last the RPT-R12, the collected three bands from its crown were not trustworthy due to relatively low carbonate contents (2.5 – 2.9% against 3.2 – 3.6%), and the $\delta^{18}O_{carb}$ values recorded more plain sinusoidal pattern (**Fig. A.1 - 3**).

Red deer molars from level 8 provided a carbonate content that varies from 2.3% to 4.1% for enamel and 3.9% – 5.2% for dentine material. Intra-tooth enamel carbonate content ranges between 0.4% – 1.8% (***Table A. 1***). We had doubting results from four specimens (RPT-18-M2 and RPT-18-M3, RPT-19-M3, RPT-20-M3) whereas the other three showed satisfying values of carbonate content. No incremental changes were observed in the $\delta^{18}O_{carb}$ values of RPT-19-M3 molar (a quite flat graph with high $\delta^{18}O_{carb}$ values) and one sampled band was excluded because of the higher $CaCO_3$ content than other intra-tooth samples (4.1% versus 3.4% – 3.7%). After the exclusion of a band in doubt, the flat curve in $\delta^{18}O_{carb}$ values is still

kept. It might be considered as an ecological signal, reflecting that the individual spent the cold winter in a milder environment away from the shelter. With the highest 1.8% intra-tooth variation, the specimen RPT-18-M2 had enamel bands lack of reliability; one band gave very low carbonate content (2.3% against 3.5% – 4.1%), and the other two had no comparable isotopic values $\delta^{13}C_{carb}$ and $\delta^{18}O_{carb}$. These bands thus were eliminated from the sample set of the tooth. Therefore, the intra-tooth range dropped to 0.6% and we obtained a more readable seasonal graph (unfinished U-shape curve) for oxygen values (***Fig. 12***). A similar amendment was applied to RPT-18-M3 and RPT-20-M3 each of which one band that deviating in intra-tooth carbonate values was excluded. These samples were probably contaminated by possible alterations from their surface fractures. As a result of this exclusion, the carbonate content within the tooth finally declined to 0.3% (RPT-18-M3) and 0.4% (RPT-20-M3) (***Fig. 12***). Specimens from the US 9 provided the percent carbonate content 2.9% – 4.3% in enamel and 2.8% – 6.4% in dentine and intra-tooth carbonate content ranges from 0.1% to 1.2%. In the tooth RPT-21-M3, the $\delta^{18}O_{carb}$ values distributed without giving any clear trend profile, and a band close to the root gave relatively high carbonate content, which was excluded from the further isotopic explanations (***Table A. 1*** and ***Fig. A.1 - 5***). Two specimens RPT-22-M2 and RPT-22-M3 yielded one (3.6% versus 3.9% – 4.3%) and two strips (4.1% and 2.9%) with no reliable carbonate content, respectively. Doubtful bands were taken away and oxygen values then managed to record only half of the reversed U-shape curve corresponding to half of one season, which was still not efficient for further consideration. The last tooth RPT-24-M2 supplied the imperfect data due to its three bands with lower carbonate content (3.0% – 3.3% against 3.6% – 3.9%). When we did not count these three bands, almost one-year incremental changes could be observed in oxygen values (***Fig. 12***).

There are twelve specimens in the SU 10, from which only six gave more demonstrative isotopic results for further interpretation. The dentine results of RPT-26 one of these six teeth, were excluded from the reliable data set because it provided unacceptable values (23.5% in $CaCO_3$ and the very lowest $\delta^{13}C_{carb}$ value) (***Table A. 1***). In this case, the dentine material definitely underwent the diagenesis process. In addition, RPT-25 was also included in this set after a small correction in the intra-tooth rows. A couple of strips that gave slightly higher $CaCO_3$ content, 4.0% and 3.8%, than the rest of the crown (3.4% – 3.6%) were discarded. We then got the $\delta^{18}O_{carb}$ values exhibiting an almost summer season pattern along the tooth crown (***Fig. 12***). The tooth RPT-31 was analyzed twice. As a result of two measurements, it provided two bands, relatively lowest (3.6%) and highest (4.6%) than the rest (3.8 – 4.3%), which ultimately were discarded.

Fig. 12. Summary of red deer teeth with the revised results of carbonate ($CaCO_3$) content
Unreliable bands were excluded during the reliability test of weight percent carbonate content for these specimens. These are thus considered for further isotopic interpretations (e.g. in definition of $\delta^{18}O_{carb}$).

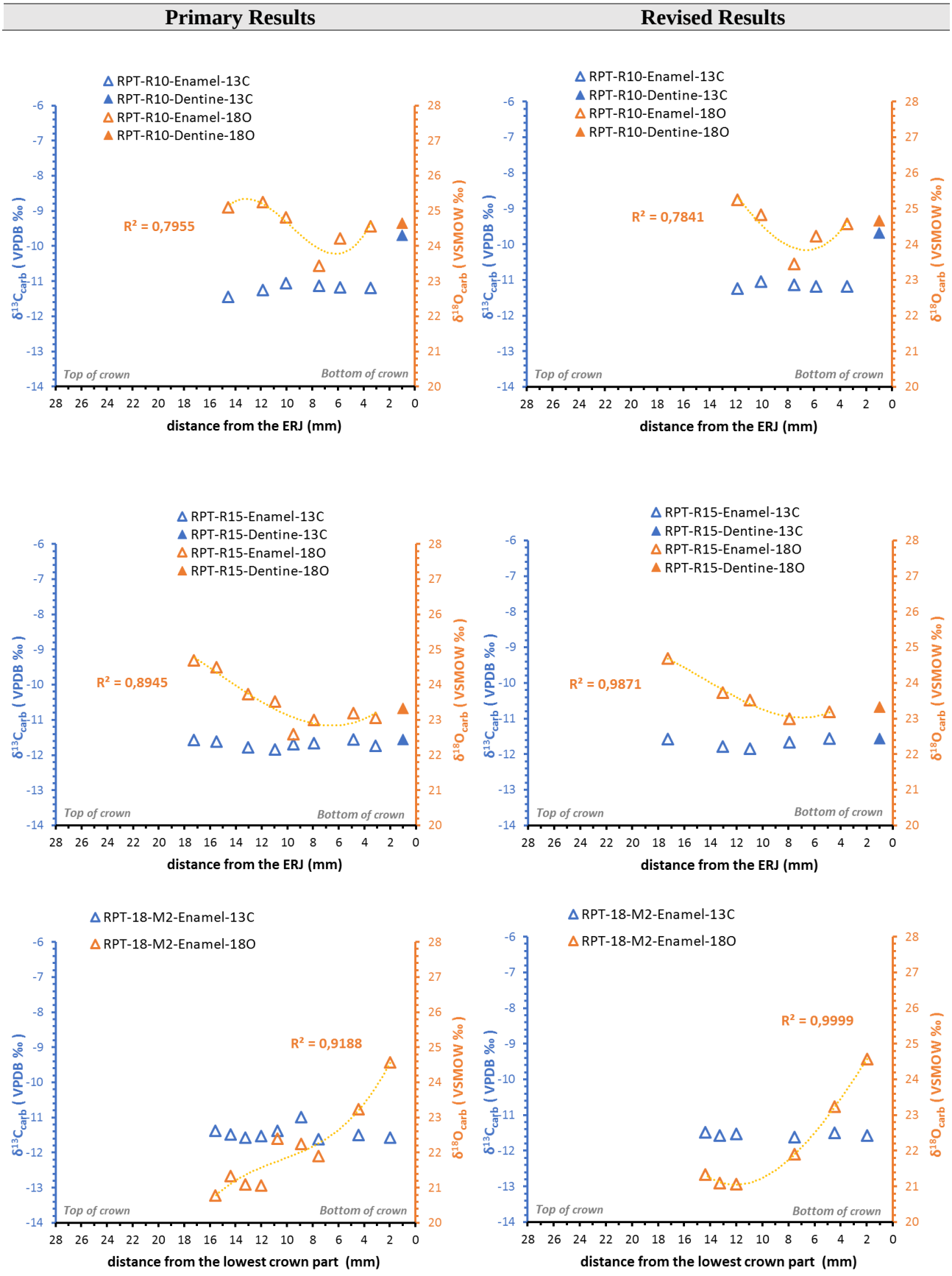

Primary Results	Revised Results

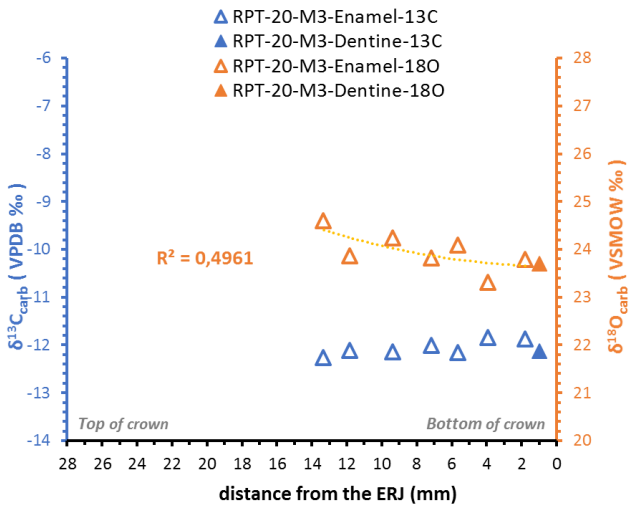

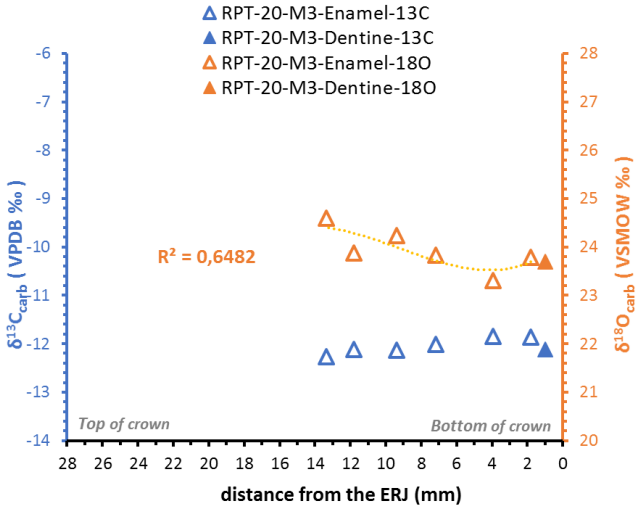

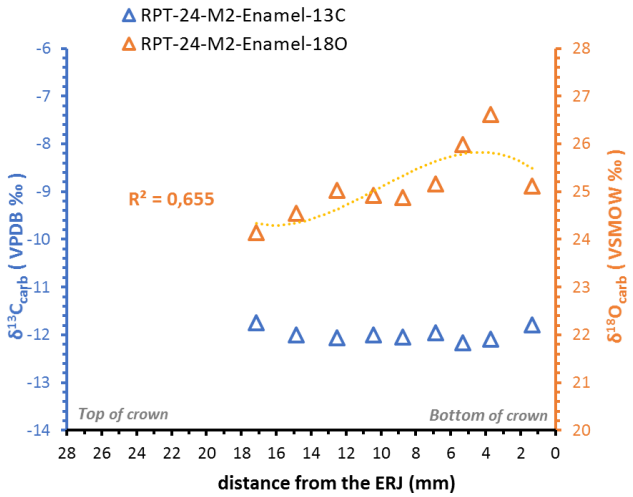

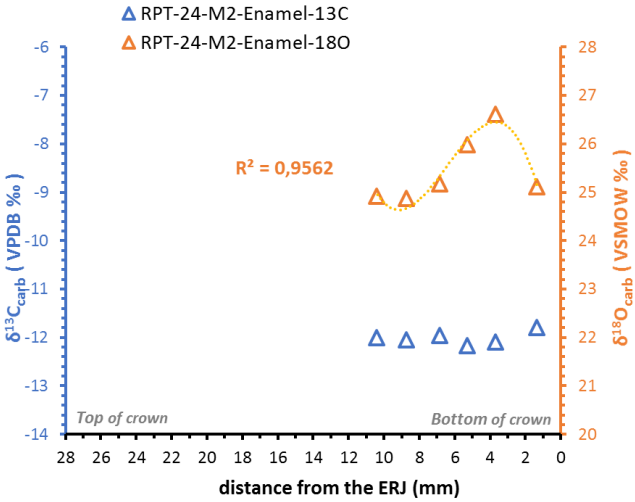

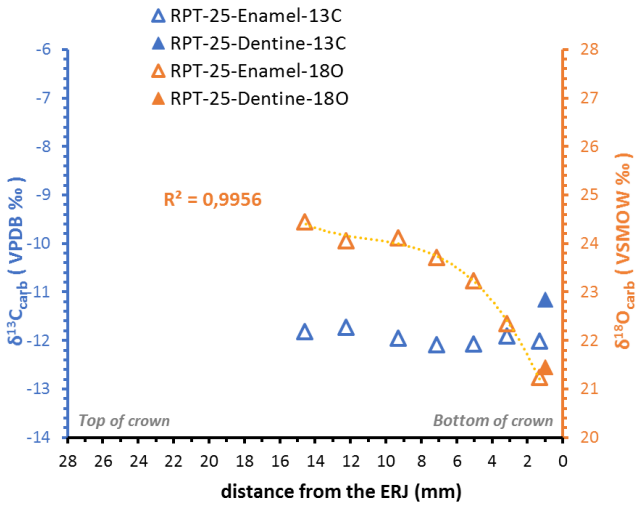

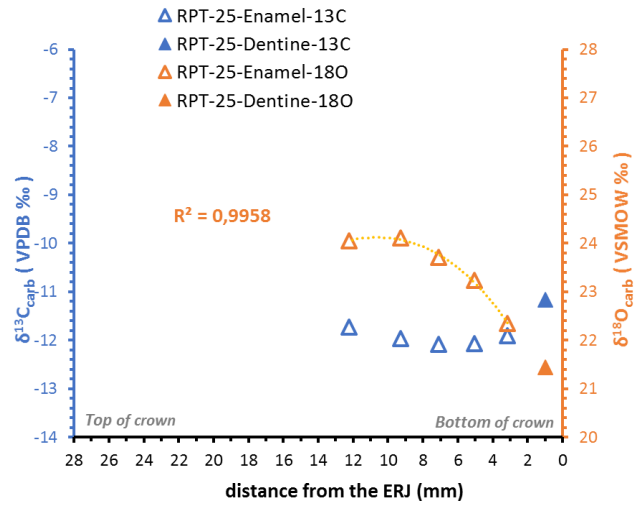

Its dentine yielded a carbonate content of 6.1% in weight and the intra-tooth enamel carbonate range is 0.9%. Moreover, isotopic values were spread randomly by giving an unclear trend model. It was thus considered contaminated with dentine material. The specimen RPT-27-M2 with intra-tooth carbonate content range 1.0% gave one strip with the lower weight (2.9% in contrast with 3.7% – 3.9%), which was excluded too. No any doubtful signals were detected in the carbonate content of the RPT-27-M3, which generated a stable flat curve with high $\delta^{18}O_{carb}$ values similar case with RPT-19 (level 8) and RPT-35 (level 13) (***Fig. A.1 - 6*** and ***Table A. 1***). From the last layer 13, only one tooth (RPT-34) out of three, yielded adequate data for further consideration. The specimens from this level yielded carbonate content ranging from 3.2 % to 4.2 % in enamel and 4.0 % to 6.3 % in dentine as well as the intra-tooth variability in weight percent carbonate is between 0.5% – 0.8% (***Table A. 1***). Even though RPT-33 gave a low-level intra-tooth range (0.5%) in weight $CaCO_3$ and stable isotopic results comparable to the corresponding dentine, oxygen values were simply scattered in the unwished sloping course. Likewise, the specimen RPT-35 with its intra-tooth results of 0.6% produced a higher $\delta^{13}C_{carb}$ value in dentine that is not comparable to the enamel isotopic data. The $\delta^{18}O_{carb}$ values occurred in the horizontal flow along the tooth crown, although no dubious signals in carbonate content and oxygen isotope values were observed. The flat curve with high $\delta^{18}O_{carb}$ values in the specimen RPT-35 can be considered as an ecological signal, suggesting red deer spent the winter in a milder conditioned environment, perhaps away from the site (***Fig. A.1 - 7***).

4.2 Carbonate $\delta^{13}C$ isotopic results

The $\delta^{13}C_{carb}$ values for all analyzed teeth are similar and range from –13.3 ‰ to –10.6 ‰ in the entire stratigraphic sequence of Late Epigravettian at Riparo Tagliente (Table 2). The mean $\delta^{13}C_{carb}$ values per tooth varied from –12.8 ‰ to –11.2 ‰ with a standard deviation between 0.05 ‰ and 0.5 ‰. The sole one red deer RPT-29 from level 10b has a lower mean $\delta^{13}C_{carb}$ value (also in $\delta^{18}O_{carb}$ values) whereas the rest of the specimens range between – 12.5 ‰ and – 11.2 ‰ on average (***Fig. 13***).

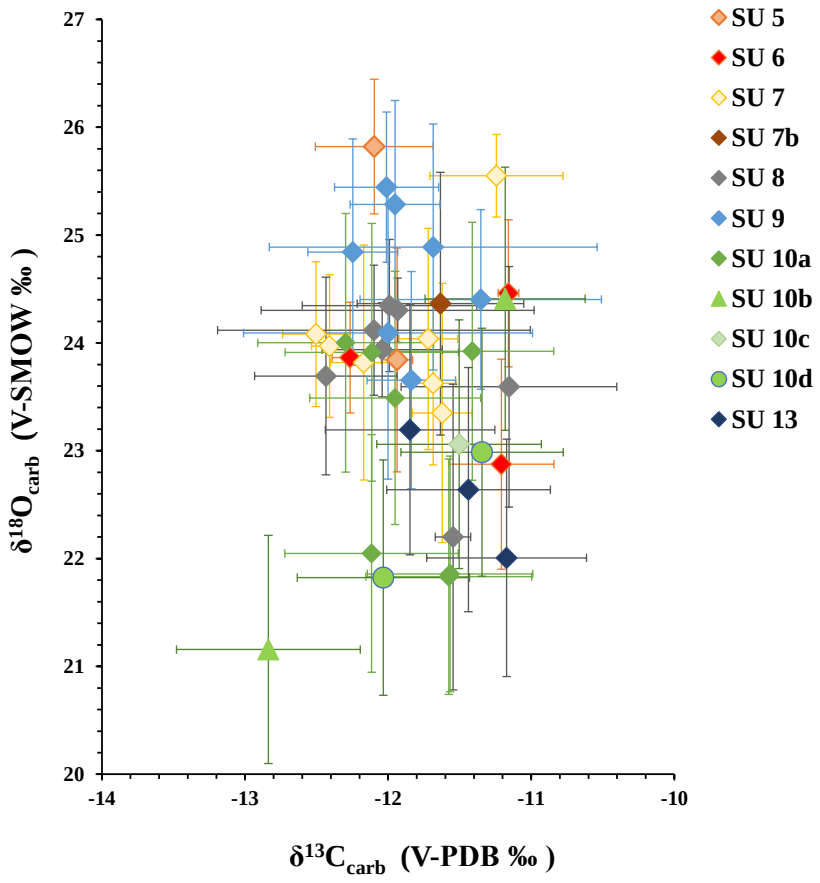

Fig. 13. The mean values and standard deviations of $\delta^{13}C_{carb}$ and $\delta^{18}O_{carb}$ for each sampled red deer teeth (third molars – 33 pcs, second molars – 9 pcs)

Furthermore, the variations in the $\delta^{13}C_{carb}$ values of carbonate hydroxylapatite in herbivores reflect differences between plants, which are primarily controlled by different photosynthetic (i.e. C_3, C_4, CAM types) pathways (DeNiro & Epstein, 1978; Lee-Thorp et al., 1989; Lüttge, 2004). The data of $\delta^{13}C_{carb}$ measurements for the analyzed red deer confirm a diet based on terrestrial C_3 plants with the carbon values mentioned above. Moreover, using diet-bioapatite ^{13}C-trophic discrimination factor of +13.6 ‰ (see more Drucker et al., 2024) for the mean $\delta^{13}C_{carb}$ values (between –12.8 ‰ and –11.2 ‰), the $\delta^{13}C_{diet}$ of the diet can be estimated to around – 26.4 ‰ to – 24.8 ‰ , which are expected values for terrestrial C_3 plants.

The intra-tooth $\Delta\delta^{13}C_{carb}$ variability in teeth (that is a difference between the highest and lowest values per tooth) ranges from 0.1 ‰ to 1.5 ‰, which is not as high as in $\Delta\delta^{18}O_{carb}$ variation (0.5‰ – 3.5‰) (***Table 2***). It reflects that there is not a significant seasonal variance in the red deer diet. In addition, the relatively flat incremental changes of $\delta^{13}C_{carb}$ values can be also observed in the graphical materials (***Figure A. 1***). However, some incremental plots of $\delta^{13}C_{carb}$ values display a considerable contrast between winter and summer (e.g. increasing

values in RPT-R8, RPT-17, and the declines in RPT-20-M2, RPT-26, RPT-27-M2) (***Figure A. 1***). It refers to the lower $\delta^{13}C$ values in summer and higher $\delta^{13}C$ values in winter, by confirming that trees and shrubs were dominating in red deer diet during summer, while in winter, to some extent, red deer adapted to grazing behavior to feed on the open grassland. Out of 33 third molars, only one specimen RPT-R12 gave an inversed U-shape pattern (layer 7) and four specimens RPT-R7, RPT-R16, RPT-30, and RPT-35 generated a sinusoidal pattern in $\delta^{13}C_{carb}$ through the stratigraphic units 5, 7, 10c, 13, respectively (***Figure A. 1***). Twenty specimens displayed quite horizontal profiles or unclear tendency with the range values less than 1‰ (0.3 – 0.9 ‰) and the rest have slightly sloping profiles that tending toward either winter (RPT-R8, RPT-29, RPT-34, RPT-38) or summer (RPT-18, RPT-19, RPT-22, RPT-23) seasons. From the set of second molars, three of which (RPT-19, RPT-20, RPT-27) gave a slight reflection of the summer season effect, although have not completed the incremental curves (***Figure A. 1***). One specimen (RPT-22) produce unclear profile in $\delta^{13}C_{carb}$ values with the range value of 1.0‰. Finally, the rest of the second molars generate more plane models without seasonal fluctuations with intra-tooth ranging from 0.1 to 0.7 ‰ (***Figure A. 1***).

The $\delta^{13}C_{carb}$ values in all third molars varied from –13.3 ‰ to –10.6 ‰ and in all second molars, it is between –12.7 ‰ and –10.9 ‰. The $\delta^{13}C_{carb}$ values of these second molars (from –12.7‰ to –10.9‰) are a little higher than the corresponding third molars which recorded the $\delta^{13}C_{carb}$ values within –12.9 ‰ and –11.0 ‰ (***Table 2***). It supports a slight change in the summer-winter diet, and/or environment within the specimen. As previously mentioned that we have collected both third and second molars for the nine specimens from levels 10a, 9, 8, and 7. Red deer (RPT-27) from level 10a have $\delta^{13}C_{carb}$ values ranging from – 11.6 to –11.0 ‰ in the third molar, which were higher than –12.6 and –12.0 ‰ in the second molar. It should confirm a significant difference between summer (second molar) and winter (third molar), although the $\delta^{18}O_{carb}$ values provided a flat profile where no seasonal tendency could be seen. Red deer from other stratigraphic layers, for which both second and third molars were sampled, did not provide as high inter-tooth (M3 and M2) variation in $\delta^{13}C_{carb}$ values as in level 10a (***Table 2***).

Taking all samples (42 teeth) into account, red deer do not produce a significant differences in $\delta^{13}C_{carb}$ values when grouped according to the stratigraphic units; with mean $\delta^{13}C_{carb}$ values of –12.0 ± 0.1 ‰ (n = 2) for level 5, –11.6 ± 0.6 ‰ (n = 3) for level 6, –11.9 ± 0.4 ‰ (n = 8) for level 7, –11.9 ± 0.4 ‰ (n = 7) for level 8, –11.9 ± 0.3 ‰ (n = 7) for layer 9, –11.9 ± 0.3 ‰ (n = 7) for layer 10a, –12.0 ± 1.2 ‰ (n = 2) for layer 10b, –11.5 ± 0.2 ‰ (n = 1) for layer 10c, –11.7 ± 0.5 ‰ (n = 2) for layer 10d, and –11.5 ± 0.3 ‰ (n = 3) for the last layer

13 (***Table 2***). However, the graph plotted based on mean values of $\delta^{13}C_{carb}$ and $\delta^{18}O_{carb}$, still shows that there are some red deer teeth with relatively high $\delta^{13}C_{carb}$ values in the layers SU 13, 10b as well as in the upper layers 8, 7, and 6. Moreover, the lowest mean $\delta^{13}C_{carb}$ values were observed in the specimens from layer 10b together with layers 7 and 8 (***Fig. 13***).

4.3 Carbonate $\delta^{18}O$ isotopic results

The range of $\delta^{18}O_{carb}$ isotopic values covers from +20.3 ‰ to +26.6 ‰ including all red deer teeth analyzed at the archaeological site (***Table 2***). The intra-tooth variation of $\Delta\delta^{18}O_{carb}$ values spans from 0.5 ‰ to 3.5 ‰ and is much more pronounced than in carbon values (from 0.1 ‰ to 1.5 ‰). The higher amplitude within the teeth should allow us to observe the expected one-year or single winter/summer seasonal fluctuations. The seasonal contrast could be discovered in most incrementally sampled teeth except for thirteen specimens, which recorded an unclear trend (RPT-R12-M3, RPT-21-M3, RPT-22-M3, RPT-31-M3), S-shaped curve (RPT-R16-M2), horizontal (RPT-19-M3, RPT-20-M3, RPT-27-M3, RPT-35-M3) or inclined (RPT-R9-M3, RPT-22-M2, RPT-38-M3, RPT-33-M3) profiles with no incremental changes (***Figure A. 1***). The incomplete state of S-shaped teeth (RPT-R16-M2) is likely due to its lowest crown of 12.7 mm (was collected only 5 bands and with no ERJ). Only six specimens exhibited the expected sinusoidal profile in $\delta^{18}O_{carb}$ values including one summer followed by one winter (RPT-R7-M3, RPT-R10-M3, RPT-R14-M3, RPT-R16-M3, RPT-30-M3) and one winter preceding one summer (RPT-21-M2) with the intra-tooth range between 1.3‰ and 2.6‰. The sequential $\delta^{18}O_{carb}$ patterns were an inconclusive U-shaped curve for nine specimens (RPT-R8-M3, RPT-R11-M3, RPT-R13-M3, RPT-19-M2, RPT-28-M3, RPT-29-M3, RPT-32-M3, RPT-36-M3, RPT-37-M3) and either a reversed unfinished J-shape for three teeth (RPT-R6-M3, RPT-R15-M3, RPT-17-M3) or a J-curve (RPT-18-M2), but they still showed a trend to reflect mainly the winter season. Finally, the last ten specimens generated the profiles corresponding mainly to the summer season, including an unfinished inversed U-curve (RPT-R13-M2, RPT-18-M3, RPT-20-M2, RPT-24-M2, RPT-23-M3, RPT-26-M3) and half an inverted U-shape (RPT-24-M3, RPT-25-M3, RPT-27-M2, RPT-34-M3) (***Figure A. 1***). Indeed the third molars could provide a record of one-year seasonal pattern; however, the limited seasonal records of this study are probably due to the presence of fractures on the crown surface of the teeth. It also could be due to the complex nature of enamel maturation that is sometimes not able to obtain an uninterrupted time period of the isotopic variation experienced by the animal (e.g. Balasse, 2002; Zazzo et al., 2005).

Table 2. Summary statistics results of carbonate $\delta^{13}C$ and $\delta^{18}O$ isotope values for each red deer tooth

SU – stratigraphic unit. L – left side, R – right side, and all teeth are lower permanent molars (M3 and M2). N – number of analyzed samples (bands) per tooth. Minimum (Min), maximum (Max), mean and standard deviation (SD) of $\delta^{13}C_{carb}$ and $\delta^{18}O_{carb}$ values per tooth. Numbers in bold indicate the seasonal contrast, winter (Min) and summer (Max), detected in the profiles of the $\delta^{18}O_{carb}$ values.

					$\delta^{13}C_{carb}$ (‰ VPDB)					$\delta^{18}O_{carb}$ (‰ VSMOW)				
Lab ID	**Excavation ID**	**SU**	**Tooth**	**N**	**Min**	**Max**	**Range**	**Mean**	**SD**	**Min**	**Max**	**Range**	**Mean**	**SD**
RPT-R6	RT81 Q3519 #9138	5	M3 L	7	-12.1	-11.8	0.3	-11.9	0.1	**22.6**	25.2	2.6	23.8	1.0
RPT-R7	RT q20/4 #6574	5	M3 L	5	-12.6	-11.6	0.9	-12.1	0.4	25.3	26.6	1.3	25.8	0.6
RPT-R8	RT q631 #6757	6	M3 R	8	-11.6	-10.6	1.0	-11.2	0.4	**21.8**	24.5	2.7	22.9	1.0
RPT-R9	RT81 q5015 #9488	6	M3 L	7	-12.4	-12.1	0.4	-12.3	0.1	23.3	24.6	1.3	23.9	0.5
RPT-R10	RT81 q5016 #9475	6	M3 L	5	-11.2	-11.1	0.2	-11.2	0.1	**23.4**	25.3	1.8	24.5	0.7
RPT-R11	RT q23 #7001	7b	M3 R	8	-11.8	-11.3	0.6	-11.6	0.2	**23.1**	26.1	3.0	24.4	1.2
RPT-R12	RT q9 #6920	7	M3 R	10	-12.4	-10.8	1.5	-11.6	0.5	23.0	24.1	1.1	23.4	0.4
RPT-R13	RT81 q21/8	7	**M2 R**	8	-11.6	-10.9	0.7	-11.2	0.2	23.5	**26.4**	2.9	25.6	1.0
RPT-R13	RT81 q21/8	7	M3 R	8	-12.0	-11.3	0.8	-11.7	0.2	**23.2**	25.3	2.1	24.0	0.7
RPT-R14	RT q6 #6839	7	M3 R	7	-12.7	-12.2	0.5	-12.5	0.2	**23.1**	25.0	1.9	24.1	0.8
RPT-R15	RT81 q35/7 #7002	7	M3 R	5	-11.8	-11.6	0.3	-11.7	0.1	**23.0**	24.7	1.7	23.6	0.7
RPT-R16	RT q6 #6850	7	**M2 R**	5	-12.7	-12.1	0.6	-12.4	0.2	22.8	25.3	2.5	24.0	1.1
RPT-R16	RT q6 #6850	7	M3 R	6	-12.9	-11.7	1.2	-12.2	0.4	**22.9**	**24.8**	**1.9**	23.8	0.7

					$\delta^{13}C_{carb}$ (‰ VPDB)					$\delta^{18}O_{carb}$ (‰ VSMOW)				
Lab ID	**Excavation ID**	**SU**	**Tooth**	**N**	**Min**	**Max**	**Range**	**Mean**	**SD**	**Min**	**Max**	**Range**	**Mean**	**SD**
RPT-17	RT62 Q20/7 #7636	8	M3 R	8	-11.6	-10.9	0.8	-11.2	0.2	**22.2**	25.2	3.0	23.6	1.1
RPT-18	RT8 q6 #7628	8	**M2 R**	6	-11.6	-11.5	0.1	-11.5	0.05	**21.1**	24.6	3.5	22.2	1.4
RPT-18	RT8 q6 #7628	8	M3 R	7	-12.6	-11.5	1.1	-12.1	0.4	23.1	**24.7**	1.7	24.1	0.6
RPT-19	RT Q3613 #7643	8	**M2 R**	6	-12.6	-12.1	0.5	-12.4	0.2	**22.8**	24.9	2.1	23.7	0.9
RPT-19	RT Q3613 #7643	8	M3 R	6	-12.4	-11.5	1.0	-11.9	0.3	24.0	24.8	0.8	24.3	0.3
RPT-20	RT Q6 #7556	8	**M2 R**	5	-12.3	-11.7	0.6	-12.0	0.2	23.5	**24.9**	1.4	24.3	0.6
RPT-20	RT Q6 #7556	8	M3 R	6	-12.3	-11.8	0.4	-12.0	0.2	**23.3**	24.6	1.3	23.9	0.4
RPT-21	RT Q80/9 #9727	9	**M2 R**	5	-12.1	-11.8	0.3	-12.0	0.1	**24.4**	**26.6**	**2.3**	25.3	1.0
RPT-21	RT Q80/9 #9727	9	M3 R	6	-12.0	-11.7	0.3	-11.8	0.1	22.2	24.9	2.7	23.7	1.0
RPT-22	RT Q23 #8512	9	**M2 R**	5	-12.5	-11.5	1.0	-12.0	0.4	22.3	25.7	3.4	24.1	1.4
RPT-22	RT Q23 #8512	9	M3 R	6	-11.9	-11.1	0.8	-11.4	0.3	23.2	25.7	2.4	24.4	0.8
RPT-23	RT Q64/5-8 #8536	9	M3 R	9	-12.2	-11.1	1.1	-11.7	0.4	23.0	**26.1**	3.2	24.9	1.1
RPT-24	RT Q6 #9536	9	**M2 R**	6	-12.2	-11.8	0.4	-12.0	0.1	**24.9**	**26.6**	**1.7**	25.4	0.7
RPT-24	RT Q6 #9536	9	M3 R	8	-12.4	-12.1	0.3	-12.2	0.1	23.2	**26.2**	2.9	24.8	1.0
RPT-25	RT Q19/4 #1181	10a	M3 L	5	-12.1	-11.7	0.4	-12.0	0.1	22.3	**24.1**	1.8	23.5	0.7
RPT-26	RT Q35/6 #1176	10a	M3 R	6	-12.4	-11.9	0.5	-12.1	0.2	22.0	**25.2**	3.2	23.9	1.3
RPT-27	RT Q22	10a	**M2 R**	6	-12.6	-12.0	0.6	-12.3	0.2	22.6	24.8	2.2	24.0	0.9
RPT-27	RT Q22	10a	M3 R	7	-11.6	-11.0	0.6	-11.4	0.2	23.7	24.4	0.7	23.9	0.2

					$\delta^{13}C_{carb}$ (‰ VPDB)					$\delta^{18}O_{carb}$ (‰ VSMOW)				
Lab ID	**Excavation ID**	**SU**	**Tooth**	**N**	**Min**	**Max**	**Range**	**Mean**	**SD**	**Min**	**Max**	**Range**	**Mean**	**SD**
RPT-28	RT Q38/6 #1198	10b	M3 R	7	-11.3	-11.0	0.3	-11.2	0.1	23.7	25.5	1.8	24.4	0.6
RPT-29	RT Q80/7 #1237	10b	M3 R	11	-13.3	-12.3	1.1	-12.8	0.4	**20.3**	22.6	2.3	21.2	0.7
RPT-30	RT Q37/6 #1166bis	10c	M3 R	8	-11.9	-11.1	0.7	-11.5	0.2	**21.8**	**24.4**	**2.6**	23.1	1.0
RPT-31	RT Q50 #1229	10d	M3 R	8	-11.7	-10.8	0.9	-11.3	0.3	22.2	23.9	1.7	23.0	0.6
RPT-32	RT Q79/9 #1239	10d	M3 R	8	-12.2	-11.8	0.4	-12.0	0.1	**21.0**	23.1	2.1	21.8	0.8
RPT-36	RT Q22 #3055	10a	M3 R	6	-11.7	-11.5	0.3	-11.6	0.1	**21.1**	23.6	2.4	21.8	0.9
RPT-37	RT Q54 #1302	10a	M3 R	9	-12.0	-11.3	0.6	-11.6	0.2	**20.4**	23.8	3.4	21.9	1.1
RPT-38	RT Q9519 #1191	10a	M3 R	6	-12.6	-11.6	1.0	-12.1	0.3	20.5	23.8	3.4	22.0	1.2
RPT-33	RT Q15 #4727	13	M3 L	8	-11.8	-11.0	0.7	-11.4	0.2	21.5	24.1	2.6	22.6	0.9
RPT-34	RT Q511-7 #4118	13	M3 L	7	-11.6	-10.9	0.7	-11.2	0.3	**20.9**	22.8	1.9	22.0	0.7
RPT-35	RT Q15 #4695	13	M3 L	8	-12.2	-11.1	1.1	-11.8	0.3	22.9	23.5	0.5	23.2	0.2

As a result, the maximum and minimum values of $\delta^{18}O_{carb}$, only those that recorded summer and winter tendencies, can be observed in the plotted graph (***Fig. 14***).

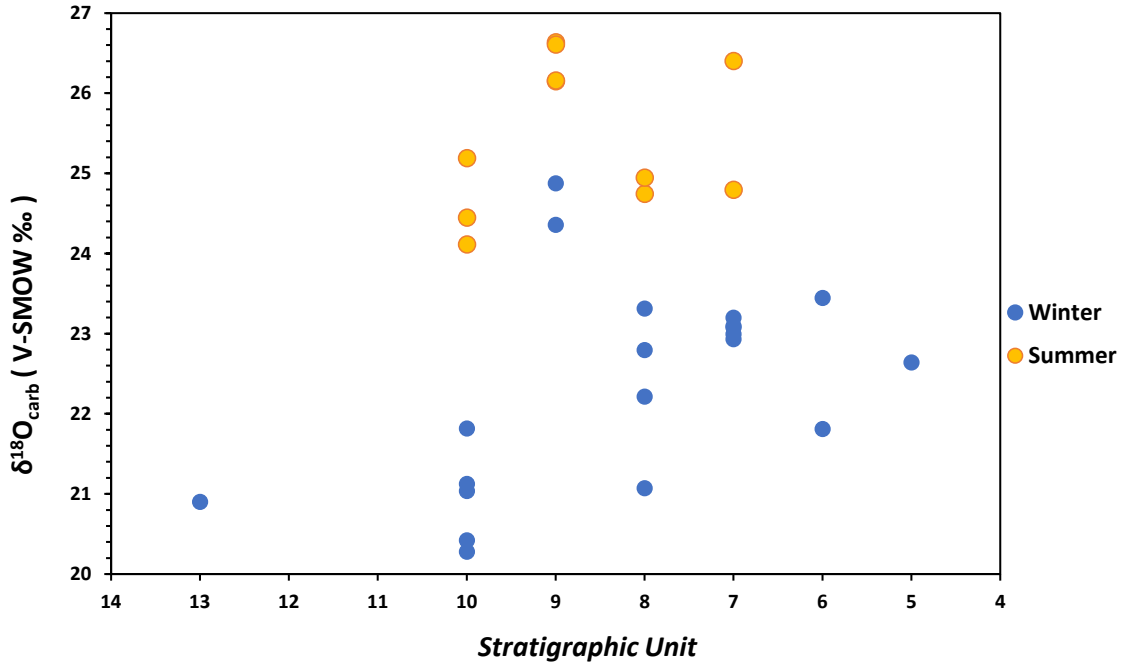

Fig. 14. The maximum and minimum values of oxygen isotope ratios ($\delta^{18}O_{carb}$) for those sampled red deer teeth that recorded the seasonal contrasts through the crown length.

In addition, their corresponding $\delta^{13}C_{carb}$ values were also grouped and demonstrated to check whether they support these seasonal phases in $\delta^{18}O_{carb}$ data (***Fig. 15***). In figure 15, the high $\delta^{13}C_{carb}$ values in layers 13, 8, 6, and 5 were clearly exhibited as expected, whereas levels 9 and 7 also somehow showed the high points of $\delta^{13}C_{carb}$, representing summer phases.

Briefly, thirteen third molars well provided the sole winter seasonal signal and just five specimens reflected the summer trend, while only summer was detected effectively in four second-molars, and the winter period was exhibited in two second-molars (***Figure A. 1***). This evidence supports the principle that the second molars of red deer mainly record summer, the first season in red deer life, and third molars mostly reveal the winter of the year after (e.g. Drucker et al., 2024; Stevens et al., 2011). A couple of third molars (RPT-R12 and RPT-35) where an unclear trend was detected in $\delta^{18}O_{carb}$ values, however, they showed a seasonal signal in $\delta^{13}C_{carb}$ values (–12.4 to –10.8 ‰ and –12.2 to –11.1 ‰, respectively) reflecting the winter season. In five specimens, it could be clearly seen the summer season in $\delta^{18}O_{carb}$ pattern with the decreasing model of $\delta^{13}C_{carb}$ values at a similar pace (M3=RPT-18, RPT-23, RPT-26; M2= RPT-20, RPT-27).

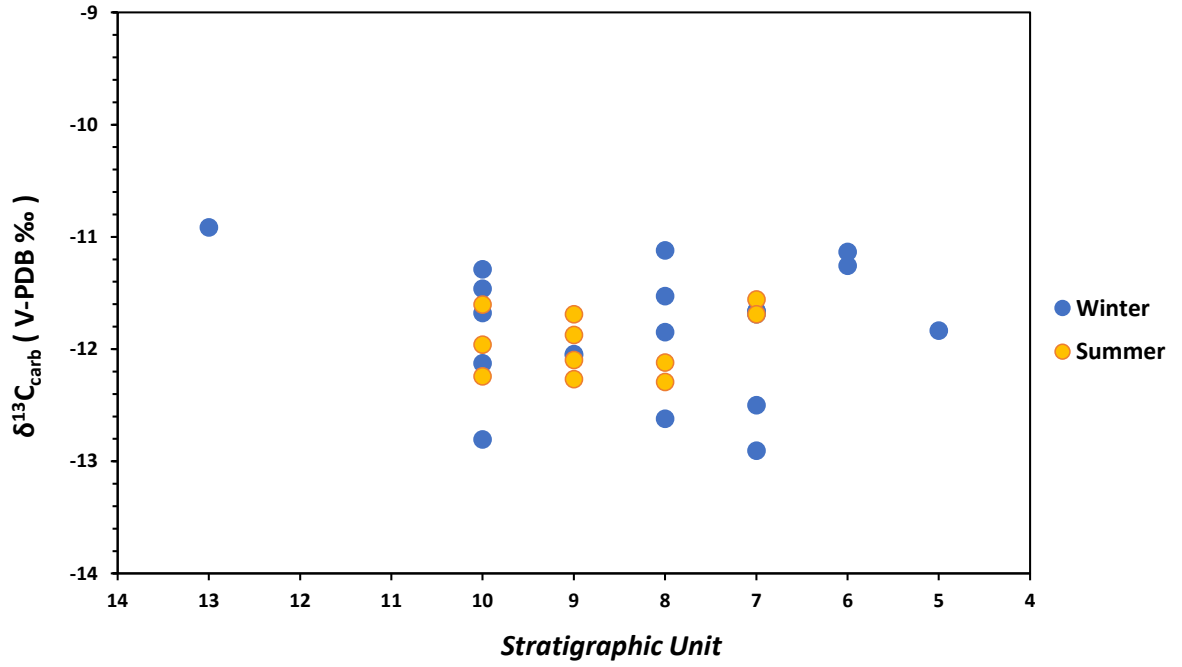

Fig. 15. The values of carbon isotope ratios ($\delta^{13}C_{carb}$) corresponding to the maximum and minimum values of oxygen isotope ratios for those sampled red deer teeth that recorded the seasonal contrasts through the crown length.

In most specimens that generate the sole winter phase in the $\delta^{18}O_{carb}$ values (including both second and third molars), there is no prominent variation in the level of the $\delta^{13}C_{carb}$ values ranging less than 1.0‰, except for five teeth (RPT-17, RPT-19-M2, RPT-34, RPT-36, RPT-37) where we can see the reversal increase in carbon isotope values even if it is a significantly small (***Figure A. 1***).

For the whole specimens, the highest intra-tooth variation in $\delta^{18}O_{carb}$ values (5.2 ‰) was observed in level 10, including all sub-layers (10a, b, c, d), while the smallest was detected in layer 13 with a range of 3.2‰ (from max: +24.1‰ to min: +20.9‰). Even if considering the archaeological layer 10a alone, it still yields the highest intra-tooth range of 4.8 ‰ (from max: +25.2‰ to min: +20.4‰) among the entire stratigraphic series. In addition, the highest winter-summer contrasts were also observed in the teeth from layer 10 (a, b, c, d) with the seasonal range 4.9 ‰ (amplitude between minimum point of winter and maximum point of summer). Similar to the intra-tooth ranges, the intra-individual variation was also compared with individuals for which both second and third molars were collected (nine red deer). Within an individual, the largest range in $\delta^{18}O_{carb}$ values is 4.4 ‰ (RPT-21, SU 9) and the lowest is 1.6 ‰ (RPT-20, SU 8).

In the cumulative plotting of $\delta^{18}O_{carb}$ values from the samples of nine red deer, substantial intra-individual (between M2 and M3) $\delta^{18}O_{carb}$ variation and some variation between individuals can be detected (see ***Fig. 16***). In general, $\delta^{18}O_{carb}$ values are higher or lower in the second molars in comparison with the corresponding third molars, from which can still be observed the broadly sinusoidal pattern across the second and third molars.

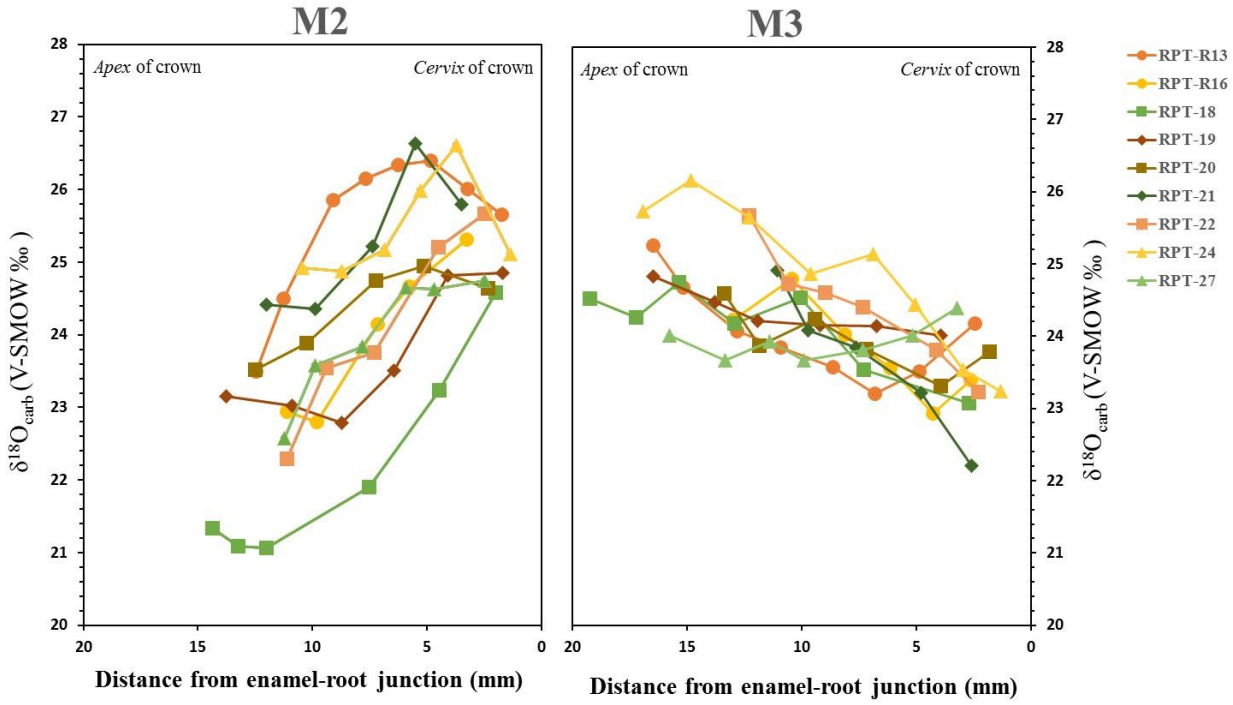

Fig. 16. Incremental plots of intra-tooth oxygen isotope ratios ($\delta^{18}O_{carb}$) for second (M2) and third molars (M3) for 9 sampled red deer

Moreover, the $\delta^{18}O_{carb}$ patterns in the third molars seem to directly continue the pattern measured in a second molar despite small temporal overlaps or gaps trended in $\delta^{18}O_{carb}$ isotopic values. It should be noted that the mineralization of permanent third molars of red deer starts (between 9 to 26 months) just after the end of the preceding mineralization phase of the second molars (from 3 to 9 months) (Brown & Chapman, 1991b).

The case with the following specimens was intriguing; three molars with the winter model (RPT-R8, RPT-14, RPT-29) showed a tendency alarming the following spring or early summer with the coeval increase of both $\delta^{18}O_{carb}$ and $\delta^{13}C_{carb}$ values. In addition, we can observe how the $\delta^{13}C_{carb}$ isotope level is slightly increasing with the beginning of the summer trend in second molars RPT-19 and RPT-22. On the contrary, RPT-R11 showed how coevally decreased the $\delta^{13}C_{carb}$ value with the end of the preceding summer trend. Similar seasonal contrast can be

also observed in RPT-R16-M3, which generated a strong sine wave trend in $\delta^{18}O_{carb}$ and where the $\delta^{13}C_{carb}$ value dropped in the winter stage and increased with the summer. These cases were detected from the stratigraphic levels 6, 7, 8, 9, and 10b. Samples RPT-R10-M3 (SU 6) and RPT-21-M2 (US 9) with sinusoidal trend detected no seasonal fluctuations in $\delta^{13}C_{carb}$ values ranging from 0.2‰ to 0.3‰, respectively. In contrast, third molars RPT-R7 (SU 5) and RPT-30 (SU 10c) showed a sine wave even in the $\delta^{13}C_{carb}$ value with the range 0.9 ‰ and 0.7 ‰, suggesting little seasonal changes in diet and habitat during the formation of the teeth (***Figure A. 1***).

4.4 Reconstruction of the seasonal and annual temperatures

Global Network for Isotopes in Precipitation (GNIP) database (IAEA/WMO, 2024) was used to acquire data for the local climatic variations. At the selected Feletto Umberto GNIP station, the locally registered data (air temperature, precipitation amount, and precipitation $\delta^{18}O$) were for three consecutive years 1985, 1986, and 1987 with the missed data in both $\delta^{18}O_{precipitation}$ and precipitation for just one month (see ***Table 3***). To obtain the seasonal range in temperature for this GNIP location, we need to generate the positive relationship between precipitation water $\delta^{18}O_w$ and temperature T_{air}. Therefore, we correlated acquired data in the mean annual model as well as a mean monthly model of air temperature. In the model of mean annual air temperature (MAT), the plotted set of data is more scattered which can be considered unreliable. The coefficient of determination is R^2=0.7 for this model. On the other side, a good positive relationship exists between $\delta^{18}O_w$ and mean monthly air temperature (MMT) (r^2 = 0.82) (***Fig. 17***). In the end, the equation derived from the model of mean monthly T_{air} is more reasonable for our study. The following is that a derived MMT equation for the Feletto Umberto location based on the relationship of the local precipitation water $\delta^{18}O_w$ and air temperature T_{air}:

$$T_{air} = 3.8175 * \delta^{18}O_w + 42.186 \qquad \textbf{4.1}$$

To be able to compare the tooth $\delta^{18}O_{carb}$ isotopic values with the modeled precipitation $\delta^{18}O_w$ and air temperature, we calculated the isotopic composition of drinking water consumed by the red deer. First, following the equation (**3.2**) by (Coplen, 1988) that was stated in the methods chapter, the red deer $\delta^{18}O_{carb}$ values in the VPDB (‰) scale were converted to the VSMOW (‰) scale, and all results were indicated in (***Table A. 1***).

Table 3. Summary of meteorological data obtained from GNIP/IAEA, WISER database for Feletto Umberto station

GNIP Project Region: Friulia, NE, Italy. Location – 46.1° N, 13.22° E. Altitude – 135 m. (a.s.l).

Month	Precipitation $\delta^{18}O_w$ (‰ vs. VSMOW-SLAP)	Precipitation (mm)	Air temperature (°C)
1985-01	-11,08	90	-0,5
1985-02	-10,9	79	2,4
1985-03	-7,69	102	7,3
1985-04	-6,5	156	10,5
1985-05	-7,85	151	16,5
1985-06	-7,47	172	18,7
1985-07	-4,83	39	23,1
1985-08	-4,97	162	22,2
1985-09	-5,35	24	20,4
1985-10	-5,85	46	14,6
1985-11	-7,66	98	6,7
1985-12	-7,9	74	5,9
1986-01	-9,9	89	2,3
1986-02	-11,22	96	2
1986-03	-7,41	99	7
1986-04	-6,84	107	11,8
1986-05	-7,62	61	19,4
1986-06	-7,02	76	20
1986-07	-	-	22,3
1986-08	-4,52	160	23
1986-09	-6,89	102	18,5
1986-10	-7,19	69	14,3
1986-11	-10,2	88	8,4
1986-12	-12,05	66	2,7
1987-01	-9,98	80	0,3
1987-02	-10,76	99	4,1
1987-03	-8,12	103	3,7
1987-04	-6,89	128	11,3
1987-05	-7,22	94	14,8
1987-06	-6,64	60	19
1987-07	-6,7	48	23,1
1987-08	-5,99	94	21
1987-09	-6,32	132	21,1
1987-10	-8,18	94	13,7
1987-11	-9,69	76	8,2
1987-12	-10,12	104	4,3

From: IAEA/WMO (2024). Global Network of Isotopes in Precipitation. The GNIP Database. Accessible at: https://nucleus.iaea.org/wiser.

Then using the equation (**3.3**) that is the relationship between modern red deer bone carbonate and local meteoric water, established by (Iacumin et al., 1996), the drinking water $\delta^{18}O_w$ of the red deer was calculated. The meteoric water $\delta^{18}O_w$ values were calculated only for those specimens that gave sufficient seasonal patterns since other teeth with unclear trends are not comparable with a seasonal temperature (see ***Table 4***).

Based on the MMT equation (**4.1**) derived for the Feletto Umberto GNIP station, the MMT was estimated for all specimens with the seasonal tendency (see ***Table 4***). According to the estimated MMT, the coldest winter at Riparo Tagliente the period of tooth enamel mineralization for this red deer population was recorded in the archaeological level 10 and level 13, whereas warmer summers and milder winters are indicated in levels 9 and 7 (***Fig. 18***). In detail, –8.4 °C for layer 10a and –8.9 °C for layer 10b where we even detected the lowest $\delta^{13}C_{carb}$ and $\delta^{18}O_{carb}$ values, and for level 13 for which the calculated temperature is dropped down to –6.5 °C.

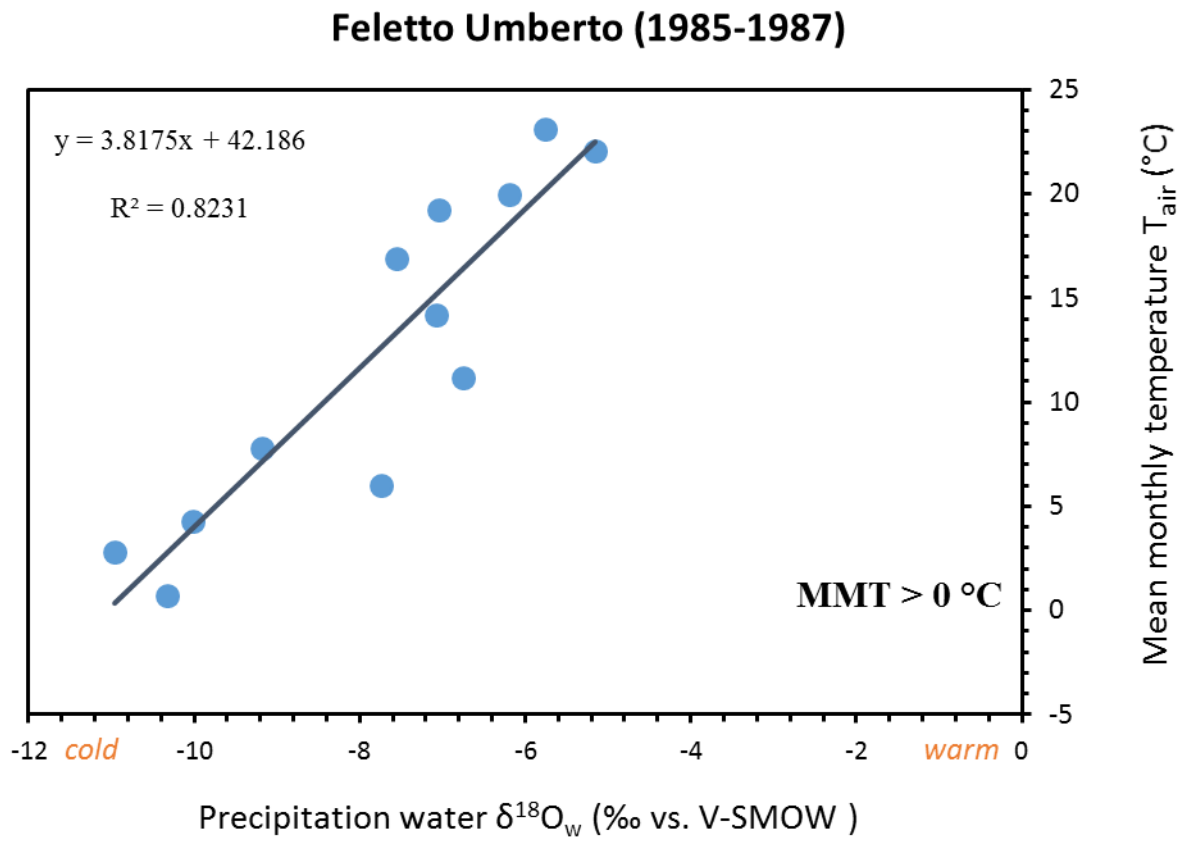

Fig. 17. Present-day linear relationship between the mean monthly air temperature T_{air} and the mean monthly $\delta^{18}O_w$ value of environmental water, extracted from the GNIP/WISER database for Feletto Umberto meteorology station
Its MMT is higher than 0 °C.

According to the pollen chronozone and isotopic chronological subdivision, the archaeological level 13 is associated with Oldest Dryas (GS-2.1a) and level 10a is within Oldest Dryas (GS-2.1a) and Bølling–Allerød (GI-1), however, 10b has not yet been determined chronologically (***Table 4***). Moreover, we can observe an abrupt increase in temperature in the stratigraphic level 9 with the mean MMT of 14.5 °C in summer and 7.7 °C in winter. In total four summer stages were detected through the whole stratigraphic series: a summer in level 10 with the mean MMT of 7.6 °C, in level 9 with a mean of 14.5 °C, in level 8 with a mean of 8.6 °C, and in level 7 with a mean of 11.5 °C.

In general, the estimated mean monthly T_{air} for the study area ranges between the lowest –8.9 °C and the highest 15.4 °C including all winter and summer seasons. If we compare the amplitude of winter-summer seasonal changes in temperature by grouping red deer according to stratigraphic units, we can then observe significant differences. The mean monthly minimum temperature (in winter) recorded on the level 10 (including all sub-layers) is –8.9 °C and the mean monthly maximum temperature (in summer) is 9.9 °C. For stratigraphic unit 9, the minimum in winter is 6.7 °C, and the maximum in summer is 15.4 °C. In layer 8, the recorded mean monthly minimum temperature is –5.9 °C and the mean monthly maximum temperature is 9.0 °C, whereas the layer 7 recorded the winter minimum of 1.2 °C and the summer maximum of 14.5 °C. The levels 13, 6, and 5 for which only winter phases were detected, recorded the mean monthly minimum temperature of – 6.5 °C, –3.1 °C and 0.1 °C, respectively (***Fig. 18*** and ***Table 4***).

As a supplement to the MMT results, the mean annual air temperature (MAT) for the study area was also estimated based on the already published general MAT equation (**3.4**) for continental Europe as we mentioned in the methods chapter. This equation was generated by (Skrzypek et al., 2011) using more than 13,000 station records from the GNIP/WISER database. The continental estimates of the MAT temperature are slightly less variable by showing only positive degrees of temperature in all years through the entire stratigraphic sequence (see ***Table 4***). It shows the lowest mean annual temperature (MAT) of 3.6 °C for level 13 as well as 3.0 °C for level 10a and 2.8 °C for layer 10b (***Table 4***). In general, this estimated mean annual T_{air} of the continental scale ranges between a minimum of 2.8 °C and a maximum of 11.7 °C including all stratigraphic layers. The mean annual minimum temperature recorded on level 10 (including all sub-layers) is 2.8 °C and the mean annual maximum temperature is 9.7 °C. For stratigraphic unit 9, the MAT minimum is 8.5 °C, and the MAT maximum is 11.7 °C. In layer 8, the recorded MAT minimum temperature is 3.9 °C and the MAT maximum temperature is 9.4 °C, whereas the layer 7 recorded the MAT minimum of 6.5 °C and the MAT maximum of 11.4 °C (***Fig. 21***

and ***Table 4***). From these calculations, a big difference between the results of the MMT and the MAT is clearly observed.

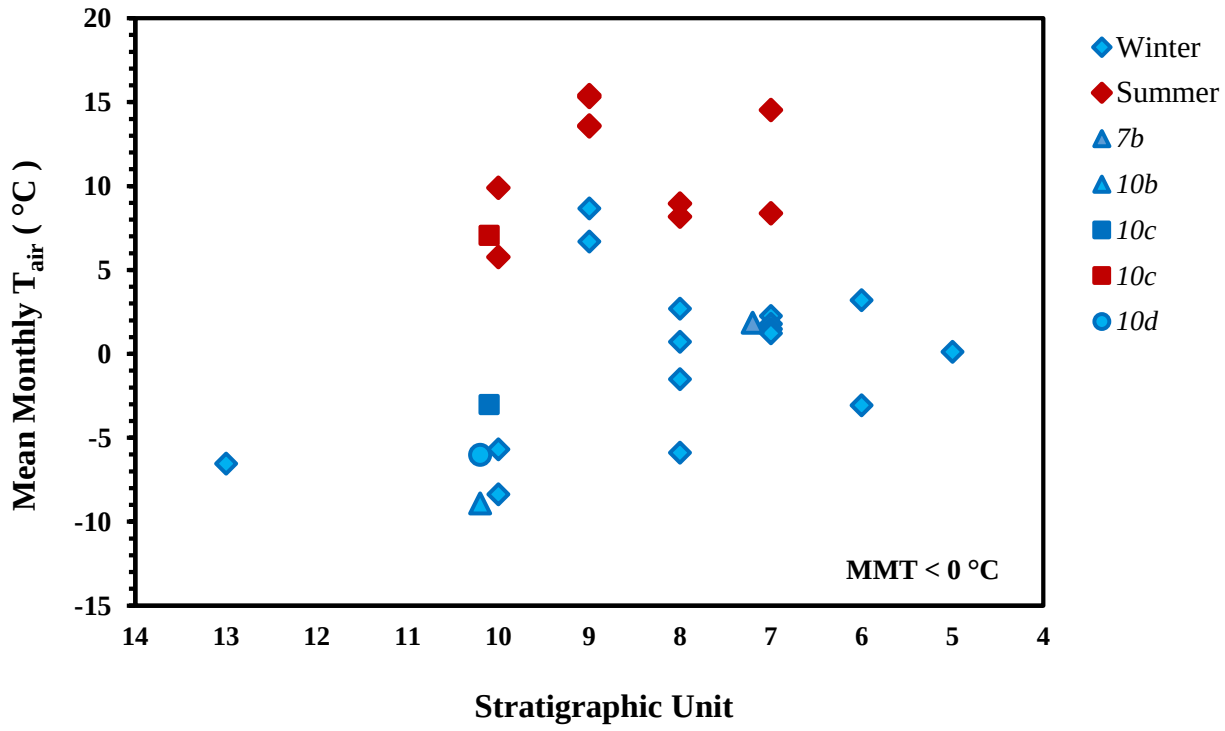

Fig. 18. Calculated Mean Monthly Air Temperature (°C) for the archaeological sequence at Riparo Tagliente, based on the linear equation (5) derived from the meteorological data of GNIP station, Feletto Umberto.
In this plot, levels 10 and 7 were separated into sub-levels for clarity. Level 10 is 10a as a main stratigraphic unit.

In a summary of the reported results obtained from the carbonate isotope analysis of red deer teeth enamel, we have observed that not the whole set of sampled teeth gave a reliable result. First, we controlled the expected range of weight percent of carbonate content (ranges of 2.3 – 5.8 % for enamel, 4.4 – 8.9 % for dentine) in the analyzed samples and its potential effects on their corresponding $\delta^{13}C_{carb}$ and $\delta^{18}O_{carb}$ isotopic values. As a consequence of this reliability test, one or two horizontally sampled bands from more than ten specimens were excluded from the reliable data set. The values of carbon isotope ratios revealed not high ranges neither in the intra-tooth nor between individuals of the whole red deer population. Despite the one specimen, which gave the lowest carbonate isotope values, the mean values of $\delta^{13}C_{carb}$ per tooth range between –12.8 ‰ and –11.2 ‰, which reflects the C_3 based plant diet with open grassland and no prominent seasonal dietary changes. Conversely, oxygen isotope ratios gave

high intra-tooth ranges that is associated with winter and summer seasonal stages. The $\delta^{18}O_{carb}$ isotopic values of 29 red deer teeth out of 42, recorded a good seasonal contrast for those later the present-day air temperature was inferred. To obtain the temperature, the winter minimum and summer maximum values of $\delta^{18}O_{carb}$ were first converted into drinking water (equation 3 by (Iacumin et al., 1996)), and then into mean monthly air temperature correlated with the data from Feletto Umberto GNIP station. In the result, it was recorded only winter phases in levels 13, 6, and 5 while both winter and summer seasons were well detected in levels 10, 9, 8, and 7. The minimum and maximum mean monthly air temperature (MMT) for the entire archaeological sequence of Riparo Tagliente ranges from – 8.9 °C (level 10) to 15.4 °C (level 9). Further, in the discussion chapter, we will consider the possible interpretations, implications, and limitations of these described results.

Table 4. Calculated the mean annual air temperature (MAT), the mean monthly air temperature (MMT) and calculated meteoric water ($\delta^{18}O_W$) for the sampled red deer teeth from Riparo Tagliente

L – left side, R – right side. SU – stratigraphic unit. (-) – non determined yet.

Lab ID	Tooth	SU	Age	Stage	$\delta^{13}C_{carb}$	$\delta^{18}O_{carb}$	$\delta^{18}O_W$	MAT	MMT	Season
			Cal BP		(‰, VPDB)	(‰, VSMOW)	(‰, VSMOW)	(°C)	(°C)	
			Gazzoni et al.[1]					Europe	Feletto Umberto	
RPT-R6	M3 L	5	-	Older Dryas (GI-1c2)[2]	-11.8	22.6	-11.0	6.1	0.1	Winter
RPT-R8	M3 R	6	-	Older Dryas (GI-1c2)[2]	-11.3	21.8	-11.8	4.9	-3.1	Winter
RPT-R10	M3 L	6	-	Older Dryas (GI-1c2)[2]	-11.1	23.4	-10.2	7.2	3.2	Winter
RPT-R11	M3 R	7b	-	Older Dryas (GI-1c2)[2]	-11.7	23.1	-10.6	6.7	1.9	Winter
RPT-R13	**M2 R**	7	-	-	-11.6	26.4	-7.2	11.4	14.5	Summer
RPT-R13	M3 R	7	-	-	-11.7	23.2	-10.5	6.9	2.3	Winter
RPT-R14	M3 R	7	-	-	-12.5	23.1	-10.6	6.7	1.8	Winter
RPT-R15	M3 R	7	-	-	-11.7	23.0	-10.7	6.6	1.5	Winter
RPT-R16	M3 R	7	-	-	-11.7	24.8	-8.9	9.1	8.4	Summer
					-12.9	22.9	-10.7	6.5	1.2	Winter
RPT-17	M3 R	8	14,572–13,430	Bølling–Allerød (GI-1)[3]	-11.1	22.2	-11.4	5.5	-1.5	Winter
RPT-18	**M2 R**	8	14,572–13,430	Bølling–Allerød (GI-1)[3]	-11.5	21.1	-12.6	3.9	-5.9	Winter
RPT-18	M3 R	8	14,572–13,430	Bølling–Allerød (GI-1)[3]	-12.1	24.7	-8.9	9.1	8.2	Summer
RPT-19	**M2 R**	8	14,572–13,430	Bølling–Allerød (GI-1)[3]	-12.6	22.8	-10.9	6.3	0.7	Winter
RPT-20	**M2 R**	8	14,572–13,430	Bølling–Allerød (GI-1)[3]	-12.3	24.9	-8.7	9.4	9.0	Summer

Lab ID	Tooth	SU	Age	Stage	$\delta^{13}C_{carb}$	$\delta^{18}O_{carb}$	$\delta^{18}O_{W}$	MAT	MMT	Season
			Cal BP		(‰, VPDB)	(‰, VSMOW)	(‰, VSMOW)	(°C)	(°C)	
			Gazzoni et al.[1]					Europe	Feletto Umberto	
RPT-20	M3 R	8	14,572–13,430	Bølling–Allerød (GI-1)[3]	-11.8	23.3	-10.3	7.1	2.7	Winter
RPT-21	**M2 R**	9	14,572–13,430	Bølling–Allerød (GI-1)[3]	-12.0	24.4	-9.3	8.5	6.7	Winter
					-11.9	26.6	-7.0	11.7	15.4	Summer
RPT-23	M3 R	9	14,572–13,430	Bølling–Allerød (GI-1)[3]	-11.7	26.1	-7.5	11.1	13.6	Summer
RPT-24	**M2 R**	9	14,572–13,430	Bølling–Allerød (GI-1)[3]	-12.1	24.9	-8.8	9.3	8.7	Winter
					-12.1	26.6	-7.0	11.7	15.3	Summer
RPT-24	M3 R	9	14,572–13,430	Bølling–Allerød (GI-1)[3]	-12.3	26.2	-7.5	11.1	13.6	Summer
RPT-25	M3 L	10a	15,632–14,111	Oldest Dryas (GS-2.1a), Bølling–Allerød (GI-1)[3]	-12.0	24.1	-9.5	8.2	5.8	Summer
RPT-26	M3 R	10a	15,632–14,111	Oldest Dryas (GS-2.1a), Bølling–Allerød (GI-1)[3]	-12.2	25.2	-8.5	9.7	9.9	Summer
RPT-36	M3 R	10a	15,632–14,111	Oldest Dryas (GS-2.1a), Bølling–Allerød (GI-1)[3]	-11.5	21.1	-12.5	4.0	-5.7	Winter
RPT-37	M3 R	10a	15,632–14,111	Oldest Dryas (GS-2.1a), Bølling–Allerød (GI-1)[3]	-11.7	20.4	-13.2	3.0	-8.4	Winter
RPT-29	M3 R	10b	-	-	-12.8	20.3	-13.4	2.8	-8.9	Winter
RPT-30	M3 R	10c	16,596–15,117	Oldest Dryas (GS-2.1a)[3]	-11.6	24.4	-9.2	8.7	7.0	Summer
					-11.3	21.8	-11.8	4.9	-3.0	Winter
RPT-32	M3 R	10d	-	-	-12.1	21.0	-12.6	3.8	-6.0	Winter
RPT-34	M3 L	13	16,634–15,286	Oldest Dryas (GS-2.1a)[3]	-10.9	20.9	-12.8	3.6	-6.5	Winter

References: *1. Gazzoni, V., Goude, G., Herrscher, E., Guerreschi, A., Antonioli, F., Fontana, F. (2013). Late upper Palaeolithic human diet: first stable isotope evidence from Riparo Tagliente (Verona, Italy). Bull. Mem. Soc. Anthropol. Paris 25 (3–4), 103–117.* https://doi.org/10.1007/s13219-012-0079-x.

2. Berto, C., Luzi, E., Canini, G. M., Guerreschi, A., & Fontana, F. (2018). Climate and landscape in Italy during Late Epigravettian. The Late Glacial small mammal sequence of Riparo Tagliente (Stallavena di Grezzana, Verona, Italy). *Quaternary Science Reviews*, *184*, 132–142. https://doi.org/10.1016/j.quascirev.2017.07.022.

3. Rasmussen, S. O., Bigler, M., Blockley, S. P., Blunier, T., Buchardt, S. L., Clausen, H. B., Cvijanovic, I., Dahl-Jensen, D., Johnsen, S. J., Fischer, H., Gkinis, V., Guillevic, M., Hoek, W. Z., Lowe, J. J., Pedro, J. B., Popp, T. J., Seierstad, I. K., Steffensen, J. P., Svensson, A., ... Winstrup, M. (2014). A stratigraphic framework for abrupt climatic changes during the Last Glacial period based on three synchronized Greenland ice-core records: refining and extending the INTIMATE event stratigraphy. *Quaternary Science Reviews*, *106*, 14-25. https://doi.org/10.1016/j.quascirev.2014.09.007

Chapter 5 – DISCUSSION

In the preceding chapter, all results derived from the carbonate measurement for red deer enamel were explicitly discussed. As the first significant sub-chapter, the carbonate ($CaCO_3$) content preservation in the enamel samples was reported. In this stage, mostly the reliability of $CaCO_3$ content and quality of the measured isotopic ratios were monitored, and in the end, unsafe data was disqualified from the due isotopic interpretations. Next, we described the whole package of stable carbon isotope ($\delta^{13}C_{carb}$) data acquired from the carbonate measurement in the Mass Spectrometry. Then it was followed by the elucidation of results from the $\delta^{18}O_{carb}$ isotopic values for red deer enamel. In the last sub-chapter, all calculations related to the mean monthly air temperature (MMT) and the mean annual air temperature (MAT) for the Riparo Tagliente site were explained in detail. All the data resulting in the relevant sub-sections were also displayed in the tables and charts in the previous chapter.

This upcoming section goes through the interpretation of findings, comparison of results with related literature, implications as well as the limitations of the obtained results.

First, one encounters the paleoecological discussion focusing on the paleodiet of the red deer population and paleolandscape reconstructed from the deer enamel hydroxylapatite for the period transition Greenland Stadial (GS-2.1a) and Greenland Interstadial (GI-1) in Northeast Italy. Thereafter, one gets insight into paleoclimate and paleoseasonal variations in the south-east pre-Alps during Late Glacial, which were inferred, based on red deer teeth enamel collected from the Late Epigravettian series at Riparo Tagliente.

5.1 Intra-tooth carbon isotope variation in red deer tooth enamel and environmental implications for the Southern Alps during the Late Glacial.

All of the $\delta^{13}C_{carb}$ values for the red deer enamel analyzed in this study, with $\delta^{13}C_{carb}$ values between –13.3 ‰ and –10.6 ‰, confirm a lack of dense forest ecosystem in their habitat, being consistent with the presence of open canopy woodland in the region during the Late Glacial period (e.g. Cerling et al., 1997; Drucker et al., 2011; Drucker et al., 2008; Manzella et al., 2024). Data in the similar range of $\delta^{13}C_{carb}$ were reported in the other studies, and interpreted as reflecting a C_3 diet for both modern and fossil herbivores (Bocherens et al., 1995; Bocherens

& Mariotti, 1992; Quade et al., 1992). For instance, the enamel $\delta^{13}C_{carb}$ values produced from red deer at Riparo Tagliente overlap the ranges reported by Bocherens and Mariotti (1992) for Pleistocene large herbivores (from –12.4‰ to –10.1‰) for Europe and Alaska. C_3 plant communities, likely composed of mostly trees, shrubs and herbs, and moist climate grasses, have lower $\delta^{13}C_{diet}$ values (–26.5 ± 2‰) than in C_4 arid climate grassland (–12.5 ± 1‰) (Bender, 1968; O'Leary, 1988; Smith & Epstein, 1971). Generally, C_3 diet-based browsers have $\delta^{13}C_{carb}$ values lower than –8‰ (Cerling & Harris, 1999; Uno et al., 2018). Dense forest cover is usually reflected by $\delta^{13}C_{carb}$ values lower than –13.0 ‰ (e.g. Drucker et al., 2011; Drucker et al., 2008; Drucker et al., 2024). Based on C_3 plants the $\delta^{13}C$ values can reach up to −36 ‰ under closed canopy (van der Merwe & Medina, 1989).

In addition to the carbonate isotope analysis, the bone collagen isotopic analysis was carried out, which also revealed relatively high $\delta^{13}C_{coll}$ values (between –21.0 ‰ and –19.0 ‰) in the same red deer specimens from Riparo Tagliente (Drucker et al., 2024b). This also suggests an open woodland cover in the stratigraphic series of Riparo Tagliente during the first part of GS-2 and GI-1.

Moreover, the mean $\delta^{13}C_{carb}$ values of all red deer tooth enamel, that is about –11.8 ‰ and in $\delta^{13}C_{diet}$ = –25.4 ‰ (see Drucker et al., 2024), were in the range of diet of animals eating pure C_3 vegetation, suggesting that the surrounding plants include the temperate or cool growing season grasses and most dicots (trees, shrubs, herbaceous plants, etc.) (e.g. Cerling et al., 1997). Relatively high collagen $\delta^{13}C$ isotope values (between −20.5‰ and −18.4‰) in herbivores (red deer, roe deer, ibex, chamois, bovid) have also been detected at Riparo Tagliente and are therefore consistent with the consumption of C_3 plants (Gazzoni et al., 2013). It should be noted that this was the first stable isotope analysis in the site, which was applied for the sole burial layer, i.e. level 13. The C_3 vegetation that was in the form of browse (dicotyledons) and graze (monocotyledons) (Smith & Epstein, 1971) in the region, can also be inferred from the results of mesowear analysis of the same red deer teeth from Riparo Tagliente, which mostly revealed the browse dominated mixed feeding signals in red deer diet (Saravanan, 2024).

Similar results were attested in other different studies on a regional scale. The bone collagen isotopic analysis for ibex and red deer species from Dalmeri, late Epigravettian rock shelter (NE, Italy), yielded results (between –21.59‰ and −19.42‰) consistent with a C_3 herbivore diet and an open landscape and some patchy forest during Allerød (GI-1a-c3) (Manzella et al., 2024).

The results of this study could also be supported by other intra-site proxies' interpretations. Pollen analyses carried out on the Epigravettian series of Riparo Tagliente

indicate that starting from layer 14, the landscape was dominated by woodland expansion with conifers (*Pinus sylvestris-mugo*) and some deciduous trees (*Quercus sp., Tilia sp., Ulmus sp., Ostrya carpinifolia, Fraxinus, Corylus*), suggesting the periods of the milder conditions in the Late Glacial Interstadial (Bartolomei et al., 1982). According to macro-mammal studies, the lower layers (17–14) were characterized by species adapted to an open environment, while the upper ones (12–5) documented the increase of temperate species (Fontana et al., 2009; Rocci Ris, 2006). The micro-mammal assemblage is mostly composed of fossorial species (*Microtus arvalis* and *Microtus (Terricola) gr. multiplex-subterraneus*) in the layers 14-12, indicating the landscape surrounding the site was a periglacial area, mainly open with scarce forest patches. Starting from level 11, the habitat reflected a slow increase in woodland with the decrease of *Microtus arvalis* in the assemblage (Berto, 2013; Berto et al., 2018).

The variability of $\delta^{13}C_{carb}$ values of the red deer teeth in the entire stratigraphic series of Riparo Tagliente can be explained by both the climatic factors and landscape features. After the LGM, the region is characterized by the vegetation composition shift from a steppe-tundra dominated by grasses to a temperate dense deciduous forest, affecting the carbon isotopic composition of plants and consequently the isotopic signature of herbivores including their increasing or decreasing $\delta^{13}C$ values (Ravazzi et al., 2007). The relatively higher $\delta^{13}C_{carb}$ values from level 13 of Riparo Tagliente, dated to the first part of the Late Glacial (GS-2.1a), can be characterized that the site still was dominated by a wooded grassland (Bartolomei et al., 1982; Gazzoni et al., 2013; Heaton, 1999) (***Fig. 19***). Starting from the level 10 that was dated within the first part of the Late Glacial (GS-2.1a) and beginning of the Bølling – Allerød Interstadial (GI-1), we can observe the decrease of $\delta^{13}C_{carb}$ values, probably due to the beginning of the forest vegetation expansion and increase in browsing by red deer. Also, in the upper layers 6 and 5, dated to the brief cold event in the Older Dryas (GI-1c2), were reflected by higher $\delta^{13}C_{carb}$ values in the red deer samples. This variation is also visible in the large mammal assemblages in layers 7b – 5, where an increase of open habitat species such as *Capra ibex*, *Alces alces* was recorded (Berto et al., 2018; Fontana et al., 2009).

Detected inter-individual range of $\delta^{13}C_{carb}$ values in every level of stratigraphy, such as 2.5‰ for level 10, 1.8‰ for level 8, 2.1‰ for level 7, 1.9‰ for level 6, can reflect the seasonal variability in red deer diet and changes in habitat conditions from one year to another (e.g. Drucker et al., 2003) (***Fig. 20***). Relatively low range of $\delta^{13}C_{carb}$ among the specimens in layers 13, 9, and 5 might confirm that the inter-year variations were averaged on a long-term basis.

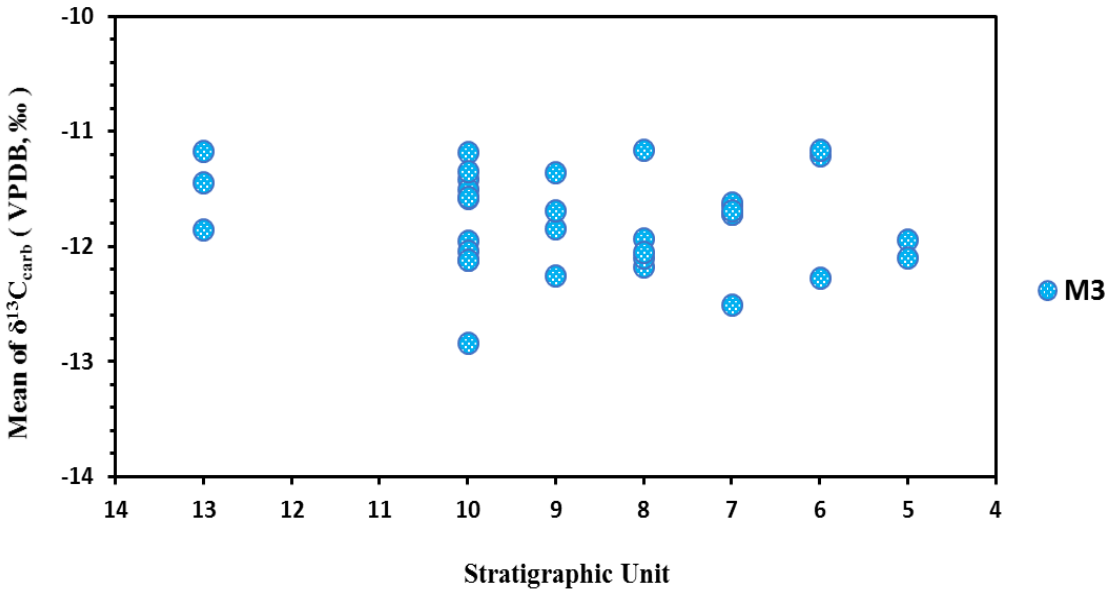

Fig. 19. The mean values of carbon isotopic ratios ($\delta^{13}C_{carb}$) for red deer enamel from Riparo Tagliente, including only third molars

Even if the carbon values in layer 10 indicate the expansion of forest vegetation and humidity, some red deer herbivores still exhibit higher $\delta^{13}C_{carb}$ values that would suggest consumption of different types of grasses, forbs enriched in $\delta^{13}C$ in xeric sites (Cerling & Harris, 1999). Herbivores from level 8 also gave comparatively high $\delta^{13}C_{carb}$ values, probably due to the consumption of trees enriched in $\delta^{13}C$ or plants in a less humid (xeric) environment with high $\delta^{13}C$ (e.g. Cerling & Harris, 1999), although the mesowear scores indicate a browsing diet in red deer population from level 8 (Saravanan, 2024). Moreover, slightly elevated $\delta^{13}C_{carb}$ values can be observed in the winter phase from some layers [e.g. RPT-R7 (SU 5), RPT-R8 (SU 6), RPT-30 (SU 10c), RPT-35 (SU 13)] that can be due to an increasing contribution of grass-like plants, bushes, and xerophytes in the red deer diet. Conversely, several herbivores from all layers, except level 13, revealed lower $\delta^{13}C_{carb}$ values in summer (e.g. RPT-18-M3, RPT-23-M3, RPT-27-M2) suggesting the high consumption of woody plants such as ^{13}C-depleted shrubs and deciduous trees (e.g. Drucker et al., 2001; Drucker et al., 2011; Drucker et al., 2024; Ferrio et al., 2003). This seasonal change in the diet could explain the mesowear scores of the red deer for which no pure browsing signal was detected. In addition, this difference in $\delta^{13}C_{carb}$ values might indicate that, as a group of species living in the sparse forest on the plain and the valley bottom, red deer could occupy different ecosystems with different ^{13}C compositional plants at diverse altitudes (e.g. Bartolomei et al., 1982; Gazzoni et al., 2013; Ravazzi et al., 2007).

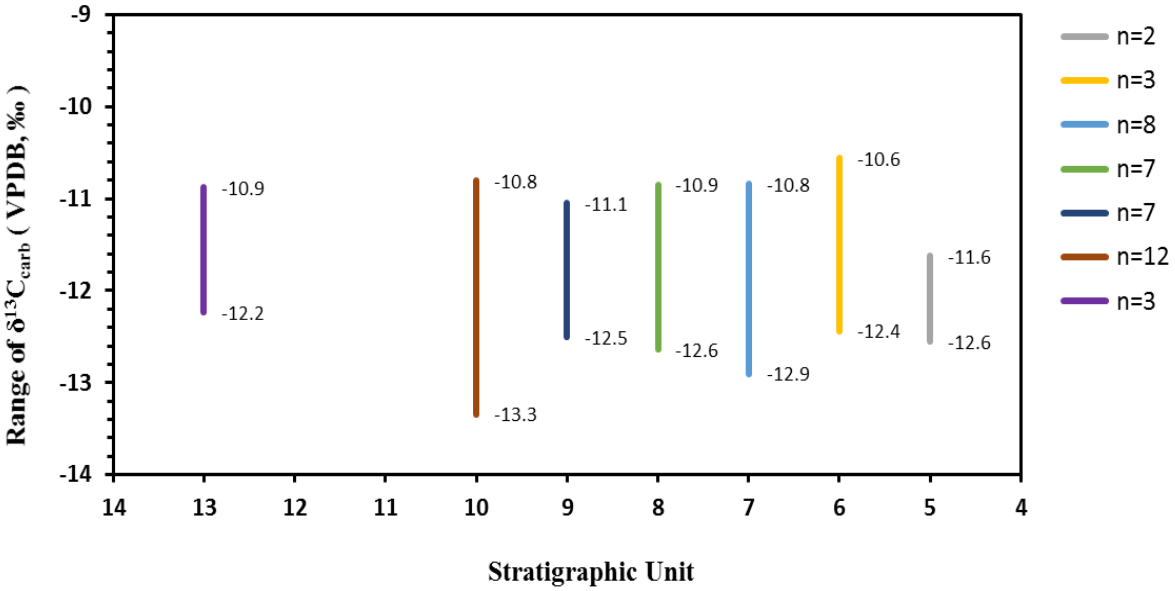

Fig. 20. Range of minimum and maximum $\delta^{13}C_{carb}$ values for each archaeological layer based on intra-tooth M2 and M3 isotopic values collectively
n = number of red deer teeth per stratigraphic unit.

5.2 Intra-tooth oxygen isotope variation in red deer tooth enamel and implications for paleoclimate in the Southern Alps between GS-2.1a and GI-1.

The red deer $\delta^{18}O_{carb}$ values revealed a record of the seasonal variations in more than half of the analysed specimens; that is mainly the winter phase in the third molars and summer in the second molars (e.g. Drucker et al., 2024; Stevens et al., 2011). Indeed, level 13 that was dated to the first part of the colder stage, Oldest Dryas (GS-2.1a) (Gazzoni et al., 2013), recorded the lowest $\delta^{18}O_{carb}$ value in winter with an estimated mean monthly degree of – 6.5 °C. This low $\delta^{18}O_{carb}$ value, in parallel with the above mentioned relatively higher $\delta^{13}C_{carb}$ values of red deer from this level, confirms a cooler, arid, and open grassland habitat in the site. Based on the data at hand, it is not able to give any description of the summer periods in this colder archaeological layer. Apparently, this carbonate isotopic study of the Late Epigravettian series at Riparo Tagliente rock-shelter is the first extensive one among the late Pleistocene sites in the region of northeast Italy. Thus derived mean monthly temperatures from $\delta^{18}O_{carb}$ values, which would need to be confirmed, cannot be compared with any related carbonate isotopic studies (***Table 4*** and ***Fig. 21***). However, there are regional and intra-site studies with other environmental proxies that testified the land and climate improvement during the late

Pleistocene and early Holocene period. As it was mentioned before, Gazzoni *et. al.* (2013) confirmed that the cold phase effects were detected from their bone collagen isotope analysis ($\delta^{13}C$ and $\delta^{15}N$) applied to herbivores from level 13 at the Tagliente shelter. Intra-site micro-mammals analysis (Berto et al., 2018) also testified that the surroundings were periglacial open landscape during layers 13-14 due to dominant cold species (e.g. *Microtus arvalis*). However, in this micro-mammal study, the temperatures (MAT, MTC, MTW) estimated using the "Bioclimatic model" described by (Hernández Fernández, 2001b; 2001a), were relatively higher, particularly in the mean temperatures of the warmest months, compared with our estimations. For instance, MTC (Mean Temperature of the Coldest month) is 0.6 °C and MAT (Mean Annual Temperature) is 8.7 °C for level 13, whereas our calculated mean monthly T_{air} (MMT) for level 13 can be as negative as – 6.5 °C and MAT is 3.6 °C in winter (***Table 4*** and ***Fig. 21***).

As we mentioned earlier, the reconstructed air temperatures (MAT and MMT) for short crowns of the red deer teeth, encompass no more than one or two (summer and/or winter) seasons recorded during the enamel formation of the red deer molars.

In our study, layer 10 can be considered as a significant layer in the sequence; however, we missed two more preceding layers (11 and 12) due to a lack of adequate specimens. The red deer population experienced much colder and milder winters (MMT rose from –8.9 °C to –3.0 °C in winter) as well as temperate warm summers in this Macrounit 10 that might suggest the ending of periglacial conditions and the onset of climate improvement during this phase (e.g. Bartolomei et al., 1982; Berto et al., 2018; Rocci Ris, 2006). The unit indeed attests to the transition between the end of Oldest Dryas (GS-2) and the beginning of Bølling–Allerød (GI-1) in the Southern Alps. Moreover, micro-mammal studies also well confirmed the beginning of GI-1 during level 10 with a slightly increased MTC of 1.7 °C. A similar interpretation was also observed in the intra-site malacofauna analysis that testified to the progressive climate improvement along the Epigravettian series 12-10 with a dominant xero-thermophilous species (Bartolomei et al., 1982). The intra-site micro-mammal assemblage starting from the following levels 9-8 and 7-5, testified an impact of the general milder climate warming registered during GI-1 (Björck et al., 1998; Rasmussen et al., 2014), to some extent confirming our seasonal estimates. Relatively much warmer seasonal contrast in $\delta^{18}O_{carb}$ values can be observed in levels 9 and 7 (***Fig. 18***). Again, the gradually decline temperature was recorded in units 6 and 5 (winter minimum of –3.1 °C and 0.1 °C, respectively) which might be likely the onset of another colder stage such as GS-1, but we are not able to confirm it now since we do not have a precisely dated chronology for these stratigraphic units. However, they were already associated with GI-1c2, a

colder sub-event of Bølling–Allerød, according to the large mammal studies that recorded the increasing of cold species in levels 7b-5 along the Late Epigravettian sequence (Berto et al., 2018; Fontana et al., 2009; Rocci Ris, 2006). Equivalent reconstructed paleotemperatures were inferred on a regional scale too. Chironomid assemblages testified the mean summer (sole July) temperature reaching the values of 10.5 – 10.8 °C in Northern Italy prior to the rapid warming of Late Glacial Interstadial at ca. 14,700 cal. BP and around 13.8 – 15.3 °C during Bølling-Allerød warming (Heiri et al., 2007).

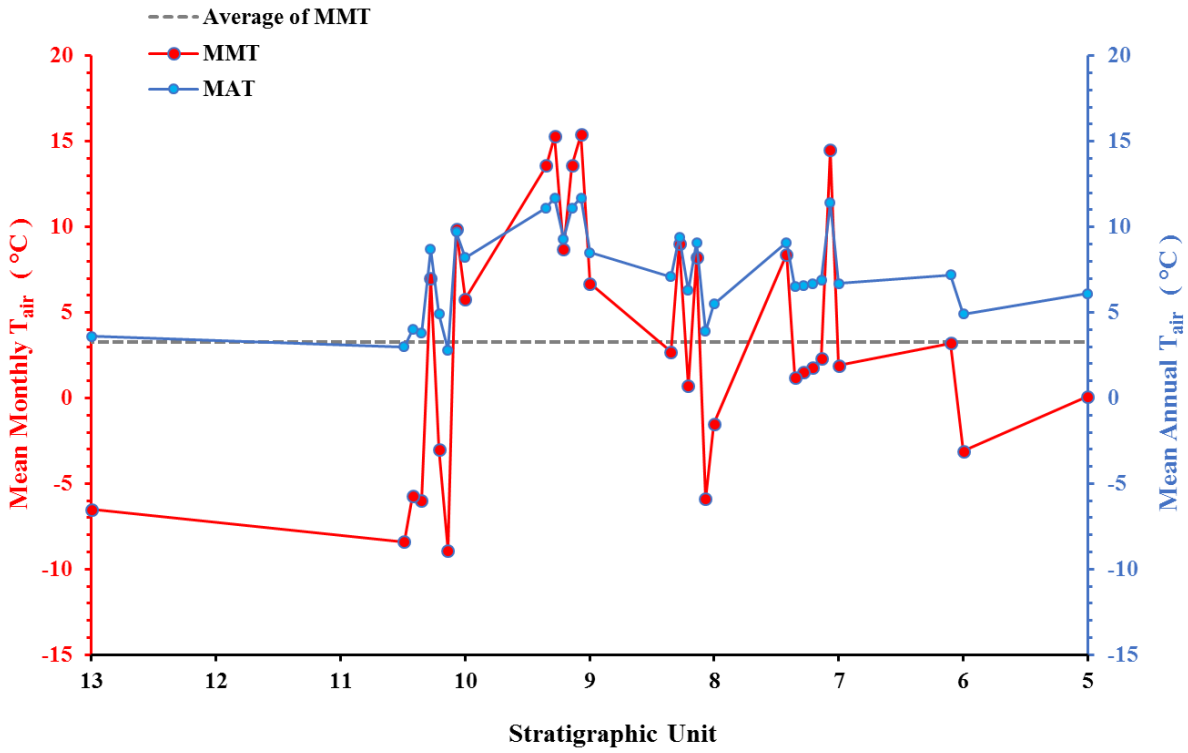

Fig. 21. The mean monthly (relative to Feletto Umberto GNIP station) and mean annual (related to the entire continent of Europe) air temperature indexes for the Late Epigravettian series at Riparo Tagliente**.** Average of MMT includes all stratigraphic levels: 5 – 13.

In this study, the second molars recorded slightly elevated $\delta^{18}O_{carb}$ values, particularly in level 9 (RPT-21, RPT-24), and consequently, the estimated MMT temperatures became relatively higher than in the third molars (***Fig. 18***). This $\delta^{18}O_{carb}$ elevation in second molar probably due to the slightly affection by the isotopic composition of breast milk consumed by infant deer (e.g. Chinique de Armas et al., 2022; Fuller et al., 2006; Kohn et al., 1998), since the second molar in red deer can start erupt prior to weaning (before 3 months) (Brown & Chapman, 1991a, 1991b). However, no significant changes in the corresponding $\delta^{13}C_{carb}$ values were detected to support this breastfeeding effect on M2.

Similar patterns of oxygen isotope variation across the second and third molars with similar absolute values of $\delta^{18}O_{carb}$ were detected in some stratigraphic units, which might suggest the seasonality within the same year or within five consecutive years with a slight change (no more than 1‰) in absolute values of $\delta^{18}O_{carb}$ (e.g. Stevens et al., 2011). It is worth pointing out that this interpretation about five-year period seasonality has been derived based on the recent study by (Stevens et al., 2011) who carried out the carbonate oxygen isotope analysis on modern red deer teeth from Isle of Rum, Scotland. For instance, RPT-11 and RPT-13 red deer from level 7 have resembling winter profiles in $\delta^{18}O_{carb}$ and absolute values that might indicate a winter phase of one identical year or any winters within a five-year period (**Fig. A.1 - 3**). A similar case was recorded in RPT-36 and RPT-37 specimens from level 10a, where analogous winter profiles and absolute values were exhibited (**Fig. A.1 - 6**). Both the second and third molars of two individuals (RPT-19 and RPT-20) from level 8 represented similarity in oxygen pattern as well as in the $\delta^{18}O_{carb}$ absolute values, which may indicate that red deer experienced winter and summer of the same five-year period (**Fig. A.1 - 4**). Furthermore, the similarity of the intra-tooth isotope variation for red deer suggests that the $\delta^{18}O$ of the drinking water ingested was similar for all individuals discovered in the same stratigraphic unit. On the contrary, the difference between intra-tooth isotope variation for deer could be due to the individuals inhabited different environments under different conditions (e.g. Stevens et al., 2011).

Some specimens recorded a more balanced, flat curve with high $\delta^{18}O_{carb}$ values (RPT-19, RPT-27, RPT-35) seemingly consistent with the values of the summer stage (**Fig. A.1 - 4**, **Fig. A.1 - 6**, **Fig. A.1 - 7**). This can be considered as an ecological signal, reflecting that red deer might spent the winter phases in a milder environment away from the rock-shelter area. In addition, this balanced $\delta^{18}O_{carb}$ values of red deer teeth enamel, on the one hand, could be induced by the altitudinal effects (e.g. Flaim et al., 2013; Kern et al., 2014), on the other hand, red deer might ingested water enriched in heavy ^{18}O isotopes during colder seasons. If to consider the geographical context of the archaeological site, then both these assumptions appear to be relevant. However, in our results, the intra-tooth carbon values of the corresponding deer did not record the expected elevation influences: an altitude-dependence increase in the ^{13}C isotopic composition of enamel (e.g. Männel et al., 2007). The presence of freshwater ecosystems in the area surrounding the Riparo Tagliente site, including the Progno River flowing in front of the shelter, the Garda Lake (ca. 22 km), and the Adige River (ca. 15 km) (Gazzoni et al., 2013), more support the hypothesis of drinking water enriched in the heavy oxygen. This may suggest, that during the summer/winter period, the ungulates might

consumed the river and/or lake water. Moreover, the lake water is relatively enriched in the heavy ^{18}O isotope than meteoric water (Gat, 1996), and the larger the body of fresh water from which terrestrial mammals drink, the less (or no) seasonal variation will be recorded in $\delta^{18}O$ values (Koch, 2007). In addition, the aquatic remains (e.g. fish bones, shellfish) were already documented in the late Epigravettian series at Riparo Tagliente (Fontana et al., 2009). This might suggest the Epigravettian groups indeed could have exploited the local freshwater habitats around the rock-shelter (e.g. Gazzoni et al., 2013). However, this still needs to be confirmed by further zooarchaeological and stable isotope analyses to reconstruct the possible mobility routes.

At the end of the discussion chapter, it should be noted once again that the entire $\delta^{13}C_{carb}$ values for the red deer enamel analyzed in this study are consistent with the presence of open canopy woodland in the region during the Late Glacial period (from GS-2.1a to GI-1) and testified the lack of dense forest cover in the habitat. Red deer from layer 13 dated to the first part of the Oldest Dryas (GS-2.1a), recorded relatively high $\delta^{13}C_{carb}$ and low $\delta^{18}O_{carb}$ values suggesting the open grassland and colder phase. Layer 10 can be considered as a turning point in the sequence when red deer individuals experienced the coldest and temperate warmer seasons. Starting from level 9 and further can be observed a relative warming phase, which can be correlated to the rapid warming recorded in the Bølling-Allerød Interstadial (GI-1). A slight temperature decrease was detected in the latter levels (6, 5), particularly in level 5. These data inferred from red deer teeth assemblages have been compared and supported by other studies on the regional scale, as well as with the intra-site proxies. The climate reconstruction based on the micro-mammals within the site and Chironomids from Northern Italy testified similar temperatures to some of our estimated mean monthly and mean annual temperatures for the Riparo Tagliente. Ultimately, the forthcoming section will be the final stage of this research study.

Chapter 6 – CONCLUSIONS AND FUTURE PERSPECTIVES

Multidisciplinary archaeological studies on the ecological and climatic variability of the southern pre-Alpine and Alpine regions during the Late Glacial are intensively carried out to gain insight into the environmental conditions inhabited by the Late Epigravettian hunter-gatherer groups. Of great importance is stable isotope analysis that allows exploring the diet, habitat, and seasonal climatic changes within the early lives of animals. This analysis has been applied to the teeth of red deer (*Cervus elaphus*), which played an important role in human subsistence at that time. The isotopic compositions of red deer teeth samples yield more detailed recordings on the fractions of C_3 biomass, and ratios of browsing and grazing in diets of red deer, seasonality changes in plant consumption of red deer, vegetation cover in habitat, as well as an amplitude of the winter and summer seasonal shifts.

Hitherto, there have been limited studies that exploit this biogeochemical analysis in the paleoecological context of the south-eastern Italian Alps, except for the stable isotope tracking of the paleoecology of the herbivore ungulates and the paleodiet of human individuals, which reveal the averaged record of diet and environment (Gazzoni et al., 2013; Manzella et al., 2024). To our knowledge, our isotopic study on red deer teeth collected through the Late Epigravettian sequence of Tagliente rock-shelter is the first extensive work that presents an intra-individual isotopic record of diet, habitat, and seasonal climate, for the Late Glacial period of the south-eastern pre-Alpine region of the Italian peninsula.

The analysis of stable isotopic values of red deer teeth enamel testifies to a lack of dense canopy forests in their habitat and suggests that the environment exploited by the Late Epigravettian hunter-gatherers of Riparo Tagliente was an open woodland forest during the colder phase GS-2.1a and the first part of the temperate period GI-1 (Bølling – Allerød). In addition, the mean value of stable carbon isotopic ratios of red deer teeth is consistent with the consumption of C_3 plants in an open environment. Fluctuating seasonal shifts are recorded in the oxygen ($\delta^{18}O_{carb}$) isotopic values of red deer teeth, which allows us to calculate seasonal temperatures based on the mean monthly temperature (MMT) and mean annual temperature (MAT) relationships for the habitats exploited by these species. These calculated MMT and MAT temperatures indicate warmer seasonal conditions during the first part of the Bølling–Allerød Interstadial.

The isotopic results confirm that the lower layer 13 (dated at GS-2.1a) was still relatively cold, arid, and dominated by wooded grassland due to the higher carbon ($\delta^{13}C_{carb}$) isotope values. Similar effects can be observed in the upper levels (6 – 5) where the $\delta^{13}C_{carb}$ values are increasing, suggesting a shift in plant consumption by the red deer group. Furthermore, the calculated mean monthly temperature testifies a colder winter season in this level 13 (MMT = – 6.5 °C). Layer 10 (dated to the end of GS-2.1a and beginning of GI-1e) can be considered as a turning point at which decisive climatic transitions occur, recording the coldest and little milder winter seasons, as well as warm summers (especially in MMT). The peak of the summer maximum is recorded in layers 9 and 7, reaching almost 15 °C in the MMT. Most of the third molars exhibit winter patterns and the second molars summer in the intra-tooth oxygen values, consistent with the principle – 'the second molars of red deer mainly record summer, the first season in red deer life, and third molars mostly reveal the winter of the year after' based on the time range of enamel growth (Brown & Chapman, 1991b) and an isotopic study on modern red deer (Stevens et al., 2011). Whereas some of the teeth samples recorded a flat profile with high oxygen values, suggesting that during winter or summer, some red deer individuals foraged in different ecosystems away from the Tagliente shelter.

The data inferred from the isotopic studies on the red deer teeth collection from Riparo Tagliente show that the Late Epigravettian hunter-gatherers survived the cold climatic conditions existed far before Bølling–Allerød Interstadial warming, and confirm a relative stability of the open environments in Valpantena valley, along the southern Alpine fringe. In the end, these reconstructed ecological and seasonal climatic conditions will serve as complementary information to further paleoenvironmental studies in the region.

In summary, it is worth noting that we reconstructed the seasonal temperatures for the lower (13) and upper (5, 6) layers based on only a few specimens that gave reliable data for isotopic interpretations. In addition, we lack adequate specimens from the lowermost layers that date back to the first part of the Late Glacial (GS-2.1a). As a future research suggestion, it will be helpful to carry out another biogeochemical analysis in these layers (below layer 10) of the Late Epigravettian, to reconstruct the environments and seasonal climate changes as a whole set for the Late Epigravettian occupation in the Late Glacial. Last but not the least, the mobility patterns of the red deer herbivores should be confirmed by further zooarchaeological or isotopic analyses

REFERENCES

Alessio, M., Bella, F., Improta, S., Belluomini, G., Cortesi, C., & Turi, B. (1970). University of Rome Carbon-14 Dates VIII. *Radiocarbon*, *12*(2), 599-616. https://doi.org/10.1017/S0033822200008304

Arnaud, J., Peretto, C., Panetta, D., Tripodi, M., Fontana, F., Arzarello, M.,…Benazzi, S. (2016). A reexamination of the Middle Paleolithic human remains from Riparo Tagliente, Italy. *Quaternary International*, *425*, 437-444. https://doi.org/https://doi.org/10.1016/j.quaint.2016.09.009

Aspes, A. (2002). Preistoria Veronese. Contributi e aggiornamenti. In (Vol. 5, pp. 1-251). Verona: Museo Civico di Storia Naturale di Verona.

Ayliffe, L. K., Chivas, A. R., & Leakey, M. G. (1994). The retention of primary oxygen isotope compositions of fossil elephant skeletal phosphate. *Geochimica et Cosmochimica Acta*, *58*(23), 5291-5298. https://doi.org/https://doi.org/10.1016/0016-7037(94)90312-3

Azorit, C., Analla, M., Carrasco, R., Calvo, J., & Muñoz-Cobo, J. (2002). Teeth eruption pattern in red deer (Cervus elaphus hispanicus) in southern Spain. *Anales de Biología*, *24*, 107-114.

Balasse, M. (2002). Reconstructing dietary and environmental history from enamel isotopic analysis: time resolution of intra-tooth sequential sampling. *International Journal of Osteoarchaeology*, *12*(3), 155-165. https://doi.org/https://doi.org/10.1002/oa.601

Balasse, M., Ambrose, S. H., Smith, A. B., & Price, T. D. (2002). The Seasonal Mobility Model for Prehistoric Herders in the South-western Cape of South Africa Assessed by Isotopic Analysis of Sheep Tooth Enamel. *Journal of Archaeological Science*, *29*(9), 917-932. https://doi.org/https://doi.org/10.1006/jasc.2001.0787

Balasse, M., Smith, A. B., Ambrose, S. H., & Leigh, S. R. (2003). Determining Sheep Birth Seasonality by Analysis of Tooth Enamel Oxygen Isotope Ratios: The Late Stone Age Site of Kasteelberg (South Africa). *Journal of Archaeological Science*, *30*(2), 205-215. https://doi.org/https://doi.org/10.1006/jasc.2002.0833

Bartolomei, G., Broglio, A., Cattani, L., Cremaschi, M., Guerreschi, A., Mantovani, E.,…Sala, B. (1982). I depositi Wurmiani del Riparo Tagliente. *Annali dell'Università di Ferrara (N.S.) sez. 15*, *III*(4), 61-105.

Bender, M. M. (1968). Mass Spectrometric Studies of Carbon 13 Variations in Corn and Other Grasses. *Radiocarbon*, *10*(2), 468-472. https://doi.org/10.1017/S0033822200011103

Berto, C. (2013). *Distribuzione ed evoluzione delle associazioni a piccoli mammiferi della penisola italiana durante il Pleistocene superiore* (PhD Thesis). Università degli Studi di Ferrara. p. 158].

Berto, C., Luzi, E., Canini, G. M., Guerreschi, A., & Fontana, F. (2018). Climate and landscape in Italy during Late Epigravettian. The Late Glacial small mammal sequence of Riparo Tagliente (Stallavena di Grezzana, Verona, Italy). *Quaternary Science Reviews*, *184*, 132-142. https://doi.org/https://doi.org/10.1016/j.quascirev.2017.07.022

Bertola, S., Broglio, A., Cassoli, P., Cilli, C., Cusinato, A., Dalmeri, G.,…ZIGGIOTTI, S. (2007). L'Epigravettiano recente nell'area prealpina e alpina orientale. *In Martini F. (a cura di) L'Italia tra 15.000 e 10.000 anni fa. Cosmopolitismo e regionalità nel Tardoglaciale. Millenni, Studi di Archeologia Preistorica*(5), 39-94.

Bertola, S., Fontana, F., & Visentin, D. (2018). Lithic raw material circulation and settlement dynamics in the Upper Palaeolithic of the Venetian Prealps (NE Italy). A key-role for palaeoclimatic and landscape changes across the LGM?

Björck, S., Walker, M. J. C., Cwynar, L. C., Johnsen, S., Knudsen, K.-L., Lowe, J. J.,…INTIMATE Members. (1998). An event stratigraphy for the Last Termination in the North Atlantic region based on the Greenland ice-core record: a proposal by the INTIMATE group. *Journal of Quaternary Science*, *13*(4), 283-292. https://doi.org/https://doi.org/10.1002/(SICI)1099-1417(199807/08)13:4<283::AID-JQS386>3.0.CO;2-A

Bocherens, H., & Drucker, D. G. (2007). CARBONATE STABLE ISOTOPES | Terrestrial Teeth and Bones. In S. A. Elias (Ed.), *Encyclopedia of Quaternary Science* (pp. 309-317). Elsevier. https://doi.org/https://doi.org/10.1016/B0-44-452747-8/00353-7

Bocherens, H., Fogel, M. L., Tuross, N., & Zeder, M. (1995). Trophic Structure and Climatic Information From Isotopic Signatures in Pleistocene Cave Fauna of Southern England. *Journal of Archaeological Science*, *22*(2), 327-340. https://doi.org/https://doi.org/10.1006/jasc.1995.0035

Bocherens, H., Koch, P. L., Mariotti, A., Geraads, D., & Jaeger, J.-J. (1996). Isotopic biogeochemistry (13 C, 18 O) of mammalian enamel from African Pleistocene hominid sites. *PALAIOS*, *11*(4), 306-318. https://doi.org/10.2307/3515241

Bocherens, H., & Mariotti, A. (1992). Biogéochimie isotopique du carbone dans les os et les dents de mammifères actuels et fossiles de zones froides et tempérées. *Comptes Rendus de l'Academie des Sciences, Paris*, *315*, 1147-1153.

Bond, G., Broecker, W., Johnsen, S., McManus, J., Labeyrie, L., Jouzel, J., & Bonani, G. (1993). Correlations between climate records from North Atlantic sediments and Greenland ice. *Nature*, *365*(6442), 143-147. https://doi.org/10.1038/365143a0

Bond, G., Showers, W., Cheseby, M., Lotti, R., Almasi, P., deMenocal, P.,…Bonani, G. (1997). A Pervasive Millennial-Scale Cycle in North Atlantic Holocene and Glacial Climates. *Science*, *278*(5341), 1257-1266. https://doi.org/doi:10.1126/science.278.5341.1257

Brown, W. A. B., & Chapman, N. G. (1991a). The dentition of red deer (Cervus elaphus): a scoring scheme to assess age from wear of the permanent molariform teeth. *Journal of Zoology*, *224*, 519-536.

Brown, W. A. B., & Chapman, N. G. (1991b). Age assessment of red deer (Cervus elaphus): from a scoring scheme based on radiographs of developing permanent molariform teeth. *Journal of Zoology*, *225*(1), 85-97. https://doi.org/https://doi.org/10.1111/j.1469-7998.1991.tb03803.x

Béres, S., Cserpák, F., Moskal-del Hoyo, M., Repiszky, T., Sázelová, S., Wilczyński, J., & Lengyel, G. (2021). Zöld Cave and the Late Epigravettian in Eastern Central Europe. *Quaternary International*, *587-588*, 158-171. https://doi.org/https://doi.org/10.1016/j.quaint.2020.09.050

Cancellieri, E. (2018). An overview of early Epigravettian techno-economic behavior in northern and western Adriatic area. In B. Valentina & C. Emanuela (Eds.), *Palaeolithic Italy. Advanced studies on early human adaptations in the Apennine peninsula* (pp. 265-285). Sidestone Press Academics, Leiden.

Cavallo, G., Fontana, F., Gonzato, F., Guerreschi, A., Riccardi, M. P., Sardelli, G., & Zorzin, R. (2017). Sourcing and processing of ochre during the late upper Palaeolithic at Tagliente rock-shelter (NE Italy) based on conventional X-ray powder diffraction analysis. *Archaeological and Anthropological Sciences*, *9*(5), 763-775. https://doi.org/10.1007/s12520-015-0299-3

Cerling, T. E., & Harris, J. M. (1999). Carbon isotope fractionation between diet and bioapatite in ungulate mammals and implications for ecological and paleoecological studies. *Oecologia*, *120*(3), 347-363. https://doi.org/10.1007/s004420050868

Cerling, T. E., Harris, J. M., Ambrose, S. H., Leakey, M. G., & Solounias, N. (1997). Dietary and environmental reconstruction with stable isotope analyses of herbivore tooth enamel from the Miocene locality of Fort Ternan, Kenya. *Journal of Human Evolution*, *33*(6), 635-650. https://doi.org/https://doi.org/10.1006/jhev.1997.0151

Cerling, T. E., & Sharp, Z. D. (1996). Stable carbon and oxygen isotope analysis of fossil tooth enamel using laser ablation. *Palaeogeography, Palaeoclimatology, Palaeoecology*, *126*(1), 173-186. https://doi.org/https://doi.org/10.1016/S0031-0182(96)00078-8

Chinique de Armas, Y., Mavridou, A.-M., Garcell Domínguez, J., Hanson, K., & Laffoon, J. (2022). Tracking breastfeeding and weaning practices in ancient populations by combining carbon, nitrogen and oxygen stable isotopes from multiple non-adult tissues. *PLOS ONE*, *17*(2), e0262435. https://doi.org/10.1371/journal.pone.0262435

Cilli, C., Giacobini, G., Guerreschi, A., & Gurioli, F. (2006). L'industria e gli oggetti ornamentali in materia dura animale dell'Epigravettiano di Riparo Tagliente, Verona. In *Atti della XXXIX Riunione scientifica : materie prime e scambi nella preistoria italiana : nel cinquantenario della fondazione dell'Istituto italiano di preistoria e protostoria : Firenze, 25-27 novembre 2004 : vol. I-II-III* (pp. 843-854). Istituto italiano di preistoria e protostoria.

Cohen, K. M., Finney, S. C., Gibbard, P. L., & Fan, J. X. (2013). The ICS International Chronostratigraphic Chart. *International Union of Geological Sciences*, *36*(3), 199-204. https://doi.org/10.18814/epiiugs/2013/v36i3/002

Cohen, K. M., & Gibbard, P. L. (2019). Global chronostratigraphical correlation table for the last 2.7 million years, version 2019 QI-500. *Quaternary International*, *500*, 20-31. https://doi.org/https://doi.org/10.1016/j.quaint.2019.03.009

Coplen, T. B. (1988). Normalization of oxygen and hydrogen isotope data. *Chemical Geology: Isotope Geoscience section*, *72*(4), 293-297. https://doi.org/https://doi.org/10.1016/0168-9622(88)90042-5

DeNiro, M. J., & Epstein, S. (1978). Influence of diet on the distribution of carbon isotopes in animals. *Geochimica et Cosmochimica Acta*, *42*(5), 495-506. https://doi.org/https://doi.org/10.1016/0016-7037(78)90199-0

Dettman, D. L., Kohn, M. J., Quade, J., Ryerson, F. J., Ojha, T. P., & Hamidullah, S. (2001). Seasonal stable isotope evidence for a strong Asian monsoon throughout the past 10.7 m.y. *Geology*, *29*(1), 31-34. https://doi.org/10.1130/0091-7613(2001)029<0031:ssiefa>2.0.co;2

Drucker, D., Amanova, M., & Fontana, F. (2024b). Isotopic tracking of the ecology of red deer during the Late Glacial in the south-eastern Alps: evidence from Riparo Tagliente (Verona, Italy). In (eds), P. Wojtal, J. Wilczyński, & N. Kowalik, 4 th Conference World of Gravettain Hunters, ISEA PAS, Kraków.

Drucker, D., Bocherens, H., Bridault, A., & Billiou, D. (2003). Carbon and nitrogen isotopic composition of red deer (Cervus elaphus) collagen as a tool for tracking palaeoenvironmental change during the Late-Glacial and Early Holocene in the northern Jura (France). *Palaeogeography, Palaeoclimatology, Palaeoecology*, *195*(3), 375-388. https://doi.org/https://doi.org/10.1016/S0031-0182(03)00366-3

Drucker, D., Bocherens, H., Pike-Tay, A., & Mariotti, A. (2001). Isotopic tracking of seasonal dietary change in dentine collagen: preliminary data from modern caribou. *Comptes Rendus de*

l'Académie des Sciences - Series IIA - Earth and Planetary Science, *333*(5), 303-309. https://doi.org/https://doi.org/10.1016/S1251-8050(01)01640-8

Drucker, D., Bridault, A., Cupillard, C., Hujic, A., & Bocherens, H. (2011). Evolution of habitat and environment of red deer (Cervus elaphus) during the Late-glacial and early Holocene in eastern France (French Jura and the western Alps) using multi-isotope analysis (δ 13C, δ 15N, δ 18O, δ 34S) of archaeological remains. *Quaternary International - QUATERN INT*, *245*, 268-278. https://doi.org/10.1016/j.quaint.2011.07.019

Drucker, D., Bridault, A., Hobson, K., Szuma, E., & Bocherens, H. (2008). Can Carbon-13 in large herbivores reflect the canopy effect in temperate and boreal ecosystems? Evidence from modern and ancient ungulates. *Palaeogeography, Palaeoclimatology, Palaeoecology*, *266*, 69-82. https://doi.org/10.1016/j.palaeo.2008.03.020

Drucker, D. G., Rivals, F., Nadal, J., Rufí, I., Soler, J., Soler, N., & Maroto, J. (2024). Ecology of large ungulates in the northeastern Iberian Peninsula during the Upper Palaeolithic through stable isotopes and tooth wear analysis. *Quaternary Environments and Humans*, *2*(4), 100011. https://doi.org/https://doi.org/10.1016/j.qeh.2024.100011

Ferrio, J. P., Voltas, J., & Araus, J. L. (2003). Use of carbon isotope composition in monitoring environmental changes. *Management of Environmental Quality: An International Journal*, *14*(1), 82-98. https://doi.org/10.1108/14777830310460405

Filippi, M. L., Heiri, O., Arpenti, E., Angeli, N., Bortolotti, M., Lotter, A., & van der Borg, K. (2007). Evoluzione paleoambientale dal Tardoglaciale a oggi ricostruita attraverso lo studio dei sedimenti del Lago di Lavarone (Altopiano di Folgaria e Lavarone, Trentino). *Studi Trentini di Scienze Naturali Acta Geologica, 82*.

Fiore, I., Gala, M., Dalmeri, G., Duches, R., & Tagliacozzo, A. (2022). Bird exploitation from the epigravettian site of Riparo Dalmeri (Trento, Italy). *Quaternary International*, *626-627*, 33-42. https://doi.org/https://doi.org/10.1016/j.quaint.2020.11.026

Flaim, G., Camin, F., Tonon, A., & Obertegger, U. (2013). Stable isotopes of lakes and precipitation along an altitudinal gradient in the Eastern Alps. *Biogeochemistry*, *116*(1), 187-198. https://doi.org/10.1007/s10533-013-9855-z

Fontana, F., Cilli, C., Cremona, M. G., Giacomo, G., Fabio, G., Jeremie, L.,…Antonio, G. (2009). Recent data on the Late Epigravettian occupation at Riparo Tagliente, Monti Lessini (Grezzana, Verona): a multidisciplinary perspective. *Preistoria Alpina, 44*, pp. 51-60.

Fontana, F., Falceri, L., Gajardo, A., Bertola, S., Cremona, M. G., Cavulli, F.,…Visentin, D. (2018). Re-colonising the Southern Alpine fringe. Diachronic data on the use of sheltered space in the Late Epigravettian site of Riparo Tagliente (Verona, Italy).

Fontana, F., Guerreschi, A., Bertola, S., Cremona, M. G., Cavulli, F., Falceri, L.,…Visentin, D. (2015). *I livelli più antichi della serie epigravettiana "interna" di Riparo Tagliente: sfruttamento delle risorse litiche e sistemi tecnici* (Vol. XXVIII).

Frisia, S., Borsato, A., Spötl, C., Villa, I., & Cucchi, F. (2005). Climate variability in the SE Alps of Italy over the past 17 000 years reconstructed from a stalagmite record. *Boreas*, *34*, 445-455. https://doi.org/10.1080/03009480500231336

Fuller, B. T., Fuller, J. L., Harris, D. A., & Hedges, R. E. M. (2006). Detection of breastfeeding and weaning in modern human infants with carbon and nitrogen stable isotope ratios. *American Journal of Physical Anthropology*, *129*(2), 279-293. https://doi.org/https://doi.org/10.1002/ajpa.20249

Gasparik, M., Major, I., Lisztes-Szabó, Z., Magyari, E., Szabó, B., Pandolfi, L.,…Markó, A. (2023). Multi-disciplinary study of a late Pleistocene woolly rhinoceros found in the Pannonian Basin and implications for the contemporaneous palaeoenvironment. *Journal of Quaternary Science*, *38*(7), 1159-1170. https://doi.org/https://doi.org/10.1002/jqs.3533

Gat, J. R. (1996). OXYGEN AND HYDROGEN ISOTOPES IN THE HYDROLOGIC CYCLE. *Annual Review of Earth and Planetary Sciences*, *24*(1), 225-262. https://doi.org/https://doi.org/10.1146/annurev.earth.24.1.225

Gazzoni, V., Goude, G., Herrscher, E., Guerreschi, A., Antonioli, F., & Fontana, F. (2013). Late Upper Palaeolithic human diet: First stable isotope evidence from Riparo Tagliente (Verona, Italy). *Bulletins et mémoires de la Société d'anthropologie de Paris*, *25*. https://doi.org/10.1007/s13219-012-0079-x

Gifford-Gonzalez, D. (2018). *An Introduction to Zooarchaeology*. Springer International Publishing AG part of Springer Nature. https://doi.org/10.1007/978-3-319-65682-3

Godawa, J. (1989). Age determination in the red deer (Cervus elaphus). In (Vol. 34, pp. 381-384). Białowieża.

Heaton, T. H. E. (1999). Spatial, Species, and Temporal Variations in the13C/12C Ratios of C3Plants: Implications for Palaeodiet Studies. *Journal of Archaeological Science*, *26*(6), 637-649. https://doi.org/https://doi.org/10.1006/jasc.1998.0381

Heinrich, H. (1988). Origin and consequences of cyclic ice rafting in the Northeast Atlantic Ocean during the past 130,000 years. *Quaternary Research*, *29*(2), 142-152. https://doi.org/https://doi.org/10.1016/0033-5894(88)90057-9

Heiri, O., Filippi, M. L., & Lotter, A. F. (2007). Lateglacial summer temperature in the Trentino area (Northern Italy) as reconstructed by fossil chironomid assemblages in Lago di Lavarone (1100 m a.s.l.). *Studi Trentini Sci. Nat., Acta Geol. 82, Studi Trentini Sci. Nat., Acta Geol. 82*(Studi Trentini Sci. Nat., Acta Geol. 82), 299-308.

Heptner, V. G., Nasimovich, A. A., & Bannikov, A. G. (1989). *Mammals of the Soviet Union* (Vol. 1: Ungulates). E. J. Brill, Leiden.

Hernández Fernández, M. (2001b). Bioclimatic discriminant capacity of terrestrial mammal faunas. *Global Ecology and Biogeography*, *10*(2), 189-204. https://doi.org/https://doi.org/10.1046/j.1466-822x.2001.00218.x

Hernández Fernández, M. (2001a). Análisis Paleoecológico y Paleoclimático de las Sucesiones de Mamíferos del Plio-Pleistoceno Ibérico. *Universidad Complutense de Madrid*

Hillson, S. (2005). *Teeth* (2 ed.). Cambridge University Press.

Hughes, P. D., & Gibbard, P. L. (2015). A stratigraphical basis for the Last Glacial Maximum (LGM). *Quaternary International*, *383*, 174-185. https://doi.org/https://doi.org/10.1016/j.quaint.2014.06.006

Iacumin, P., Bocherens, H., Mariotti, A., & Longinelli, A. (1996). Oxygen isotope analyses of co-existing carbonate and phosphate in biogenic apatite: a way to monitor diagenetic alteration of bone phosphate? *Earth and Planetary Science Letters*, *142*(1), 1-6. https://doi.org/https://doi.org/10.1016/0012-821X(96)00093-3

IAEA/WMO. (2024). *Global Network of Isotopes in Precipitation.* The GNIP Database. Accessible at: https://nucleus.iaea.org/wiser.

Kern, Z., Kohán, B., & Leuenberger, M. (2014). Precipitation isoscape of high reliefs: interpolation scheme designed and tested for monthly resolved precipitation oxygen isotope records of an Alpine domain. *Atmos. Chem. Phys.*, *14*(4), 1897-1907. https://doi.org/10.5194/acp-14-1897-2014

Koch, P., Tuross, N., & Fogel, M. (1997). The Effects of Sample Treatment and Diagenesis on the Isotopic Integrity of Carbonate in Biogenic Hydroxylapatite. *J. Archaeol. Sci.*, *24*, 417-429. https://doi.org/10.1006/jasc.1996.0126

Koch, P. L. (2007). Isotopic Study of the Biology of Modern and Fossil Vertebrates. In *Stable Isotopes in Ecology and Environmental Science* (pp. 99-154). https://doi.org/https://doi.org/10.1002/9780470691854.ch5

Koch, P. L., Fisher, D. C., & Dettman, D. (1989). Oxygen isotope variation in the tusks of extinct proboscideans: A measure of season of death and seasonality. *Geology*, *17*(6), 515-519. https://doi.org/10.1130/0091-7613(1989)017<0515:oivitt>2.3.co;2

Kohn, M., & Cerling, T. (2002). Stable Isotope Compositions of Biological Apatite. In M. J. Kohn, Rakovan, J. and Hughes, J.M. (Ed.), *Reviews in Mineralogy and Geochemistry. Phosphates. Geochemical, Geobiological, and Materials Importance* (Vol. 48, pp. 455-488). Mineralogical Society of America, Washington, D.C. https://doi.org/10.2138/rmg.2002.48.12

Kohn, M. J., Schoeninger, M. J., & Valley, J. W. (1998). Variability in oxygen isotope compositions of herbivore teeth: reflections of seasonality or developmental physiology? *Chemical Geology*, *152*(1), 97-112. https://doi.org/https://doi.org/10.1016/S0009-2541(98)00099-0

Kukla, G. J., Bender, M. L., de Beaulieu, J.-L., Bond, G., Broecker, W. S., Cleveringa, P.,…Winograd, I. J. (2002). Last Interglacial Climates. *Quaternary Research*, *58*(1), 2-13. https://doi.org/https://doi.org/10.1006/qres.2001.2316

Lee-Thorp, J. A., Sealy, J. C., & van der Merwe, N. J. (1989). Stable carbon isotope ratio differences between bone collagen and bone apatite, and their relationship to diet. *Journal of Archaeological Science*, *16*(6), 585-599. https://doi.org/https://doi.org/10.1016/0305-4403(89)90024-1

Leroy, S. A. G., Giralt, S., Francus, P., & Seret, G. (1996). The high sensitivity of the palynological record in the Vico maar lacustrine sequence (Latium, Italy) highlights the climatic gradient through Europe for the last 90 ka. *Quaternary Science Reviews*, *15*(2), 189-201. https://doi.org/https://doi.org/10.1016/0277-3791(95)00023-2

Lisiecki, L. E., & Raymo, M. E. (2005). A Pliocene-Pleistocene stack of 57 globally distributed benthic δ18O records. *Paleoceanography*, *20*(1). https://doi.org/https://doi.org/10.1029/2004PA001071

Lüttge, U. (2004). Ecophysiology of Crassulacean Acid Metabolism (CAM). *Annals of Botany*, *93*(6), 629-652. https://doi.org/10.1093/aob/mch087

Magny, M., Aalbersberg, G., Bégeot, C., Benoit-Ruffaldi, P., Bossuet, G., Disnar, J.-R.,…Walter-Simonnet, A.-V. (2006). Environmental and climatic changes in the Jura mountains (eastern France) during the Lateglacial–Holocene transition: a multi-proxy record from Lake Lautrey. *Quaternary Science Reviews*, *25*(5), 414-445. https://doi.org/https://doi.org/10.1016/j.quascirev.2005.02.005

Magyari, E. K., Kuneš, P., Jakab, G., Sümegi, P., Pelánková, B., Schäbitz, F.,…Chytrý, M. (2014). Late Pleniglacial vegetation in eastern-central Europe: are there modern analogues in Siberia? *Quaternary Science Reviews*, *95*, 60-79. https://doi.org/https://doi.org/10.1016/j.quascirev.2014.04.020

Makarewicz, C. A., & Pederzani, S. (2017). Oxygen (δ18O) and carbon (δ13C) isotopic distinction in sequentially sampled tooth enamel of co-localized wild and domesticated caprines: Complications to establishing seasonality and mobility in herbivores. *Palaeogeography, Palaeoclimatology, Palaeoecology*, *485*, 1-15. https://doi.org/https://doi.org/10.1016/j.palaeo.2017.01.010

Mangerud, J., ANDERSEN, S. T., BERGLUND, B. E., & DONNER, J. J. (1974). Quaternary stratigraphy of Norden, a proposal for terminology and classification. *Boreas*, *3*(3), 109-126. https://doi.org/https://doi.org/10.1111/j.1502-3885.1974.tb00669.x

Manzella, G., Fontana, A., Marín-Arroyo, A. B., Agudo Pérez, L., Peresani, M., & Duches, R. (2024). Paleoecology of mid-mountain Alps (Trentino, Italy) between Greenland interstadial 1 and Early Holocene. Carbon and nitrogen stable isotope analysis of ibex and red deer. *Quaternary Science Reviews*, *328*, 108549. https://doi.org/https://doi.org/10.1016/j.quascirev.2024.108549

Martin, C., Bentaleb, I., Kaandorp, R., Iacumin, P., & Chatri, K. (2008). Intra-tooth study of modern rhinoceros enamel δ18O: Is the difference between phosphate and carbonate δ18O a sound diagenetic test? *Palaeogeography, Palaeoclimatology, Palaeoecology*, *266*(3), 183-189. https://doi.org/https://doi.org/10.1016/j.palaeo.2008.03.039

Monegato, G., Ravazzi, C., Culiberg, M., Pini, R., Bavec, M., Calderoni, G.,…Perego, R. (2015). Sedimentary evolution and persistence of open forests between the south-eastern Alpine fringe and the Northern Dinarides during the Last Glacial Maximum. *Palaeogeography, Palaeoclimatology, Palaeoecology*, *436*, 23-40. https://doi.org/https://doi.org/10.1016/j.palaeo.2015.06.025

Monegato, G., Scardia, G., Hajdas, I., Rizzini, F., & Piccin, A. (2017). The Alpine LGM in the boreal ice-sheets game. *Scientific Reports*, *7*(1), 2078. https://doi.org/10.1038/s41598-017-02148-7

Männel, T., Auerswald, K., & Schnyder, H. (2007). Altitude gradients of grassland carbon and nitrogen isotope composition are recorded in hair of grazers. *Global Ecology and Biogeography*, *16*, 583-592. https://doi.org/10.1111/j.1466-8238.2007.00322.x

O'Leary, M. H. (1988). Carbon isotopes in photosynthesis. *Bioscience*, *38*(5), 328-336.

Oxilia, G., Bortolini, E., Badino, F., Bernardini, F., Gazzoni, V., Lugli, F.,…Cristiani, E. (2021). Exploring late Paleolithic and Mesolithic diet in the Eastern Alpine region of Italy through multiple proxies. *Am J Phys Anthropol*, *174*(2), 232-253. https://doi.org/10.1002/ajpa.24128

Peresani, M. (2006). Cultures et traditions du Paléolithique supérieur dans les régions nord-méditerranéennes. In J. L. Sanchidrianan Torti, A. M. Marquez Alcantara, J. M. Fullola, & Pericot (Eds.), *La Cuenca Mediterránea durante el Paleolítico Superior (38.000-10.000 años)* (pp. 408-429). Nerja: Fundación Cueva de Nerja.

Peresani, M., Monegato, G., Ravazzi, C., Bertola, S., Margaritora, D., Breda, M.,…Zerboni, A. (2021). Hunter-gatherers across the great Adriatic-Po region during the Last Glacial Maximum: Environmental and cultural dynamics. *Quaternary International*, *581-582*, 128-163. https://doi.org/https://doi.org/10.1016/j.quaint.2020.10.007

Peretto, C., Biagi, P., Boschian, G., Broglio, A., De Stefani, M., Fasani, L.,…Tozzi, C. (2004). Living-floors and structures from the Lower Paleolithic to the Bronze Age in Italy. *Coll Antropol*, *28*(1), 63-88.

Pini, R., Ravazzi, C., & Reimer, P. J. (2010). The vegetation and climate history of the last glacial cycle in a new pollen record from Lake Fimon (southern Alpine foreland, N-Italy). *Quaternary Science Reviews*, *29*(23), 3115-3137. https://doi.org/https://doi.org/10.1016/j.quascirev.2010.06.040

Quade, J., Cerling, T. E., Barry, J. C., Morgan, M. E., Pilbeam, D. R., Chivas, A. R.,…van der Merwe, N. J. (1992). A 16-Ma record of paleodiet using carbon and oxygen isotopes in fossil teeth from Pakistan. *Chemical Geology*, *94*(3), 183-192. https://doi.org/https://doi.org/10.1016/S0009-2541(10)80003-8

Rasmussen, S. O., Andersen, K. K., Svensson, A. M., Steffensen, J. P., Vinther, B. M., Clausen, H. B.,…Ruth, U. (2006). A new Greenland ice core chronology for the last glacial termination. *Journal of Geophysical Research: Atmospheres*, *111*(D6). https://doi.org/https://doi.org/10.1029/2005JD006079

Rasmussen, S. O., Bigler, M., Blockley, S. P., Blunier, T., Buchardt, S. L., Clausen, H. B.,…Winstrup, M. (2014). A stratigraphic framework for abrupt climatic changes during the Last Glacial period based on three synchronized Greenland ice-core records: refining and extending the INTIMATE event stratigraphy. *Quaternary Science Reviews*, *106*, 14-28. https://doi.org/https://doi.org/10.1016/j.quascirev.2014.09.007

Ravazzi, C., Peresani, M., Pini, R., & Vescovi, E. (2007). Il Tardoglaciale nelle Alpi italiane e in Pianura Padana. Evoluzione stratigrafica, storia della vegetazione e del popolamento antropico. *Il Quaternario*, *20*, 163–184.

Ravazzi, C., Pini, R., Badino, F., De Amicis, M., Londeix, L., & Reimer, P. J. (2014). The latest LGM culmination of the Garda Glacier (Italian Alps) and the onset of glacial termination. Age of glacial collapse and vegetation chronosequence. *Quaternary Science Reviews*, *105*, 26-47. https://doi.org/https://doi.org/10.1016/j.quascirev.2014.09.014

Rey, C., Renugopalakrishnan, V., Shimizu, M., Collins, B., & Glimcher, M. J. (1991). A resolution-enhanced Fourier transform infrared spectroscopic study of the environment of the CO3(2-) ion in the mineral phase of enamel during its formation and maturation. *Calcif Tissue Int*, *49*(4), 259-268. https://doi.org/10.1007/bf02556215

Rink, W. J., & Schwarcz, H. P. (1995). Tests for Diagenesis in Tooth Enamel: ESR Dating Signals and Carbonate Contents. *Journal of Archaeological Science*, *22*(2), 251-255. https://doi.org/https://doi.org/10.1006/jasc.1995.0026

Rocci Ris, A. (2006). *I macromammiferi di Riparo Tagliente. Archeozoologia e tafonomia dei livelli epigravettiani.* PhD Thesis, Dottorato di ricerca in Scienze Antropologiche, Ciclo XVIII, Dipartimento di Anatomia, Farmacologia e medicina Legale, Università degli Studi di Torino. p.535].

Saravanan, S. (2024). *Decoding diets: Microwear and Mesowear insights into red deer teeth from the Late Epigravettian at Riparo Tagliente (Italy)* University of Ferrara]. (Unpublished Master's thesis).

Skrzypek, G., Wiśniewski, A., & Grierson, P. F. (2011). How cold was it for Neanderthals moving to Central Europe during warm phases of the last glaciation? *Quaternary Science Reviews*, *30*(5), 481-487. https://doi.org/https://doi.org/10.1016/j.quascirev.2010.12.018

Smith, B. N., & Epstein, S. (1971). Two Categories of 13C/12C Ratios for Higher Plants. *Plant Physiology*, *47*(3), 380-384. https://doi.org/10.1104/pp.47.3.380

Stevens, R. E., Balasse, M., & O'Connell, T. C. (2011). Intra-tooth oxygen isotope variation in a known population of red deer: Implications for past climate and seasonality reconstructions. *Palaeogeography, Palaeoclimatology, Palaeoecology*, *301*(1), 64-74. https://doi.org/https://doi.org/10.1016/j.palaeo.2010.12.021

Stuiver, M., & Reimer, P. J. (1993). Extended 14C Data Base and Revised CALIB 3.0 14C Age Calibration Program. *Radiocarbon*, *35*(1), pp. 215-230. https://doi.org/10.1017/S0033822200013904

Suggate, R. P. (1965). The Definition of "Interglacial". *The Journal of Geology*, *73*(4), 619-626.

Tieszen, L. L. (1991). Natural variations in the carbon isotope values of plants: Implications for archaeology, ecology, and paleoecology. *Journal of Archaeological Science*, *18*(3), 227-248. https://doi.org/https://doi.org/10.1016/0305-4403(91)90063-U

Tsutaya, T., & Yoneda, M. (2015). Reconstruction of breastfeeding and weaning practices using stable isotope and trace element analyses: A review. *Am J Phys Anthropol*, *156 Suppl 59*, 2-21. https://doi.org/10.1002/ajpa.22657

Tütken, T., Furrer, H., & Walter Vennemann, T. (2007). Stable isotope compositions of mammoth teeth from Niederweningen, Switzerland: Implications for the Late Pleistocene climate, environment, and diet. *Quaternary International*, *164-165*, 139-150. https://doi.org/https://doi.org/10.1016/j.quaint.2006.09.004

Uno, K. T., Rivals, F., Bibi, F., Pante, M., Njau, J., & de la Torre, I. (2018). Large mammal diets and paleoecology across the Oldowan–Acheulean transition at Olduvai Gorge, Tanzania from stable isotope and tooth wear analyses. *Journal of Human Evolution*, *120*, 76-91. https://doi.org/https://doi.org/10.1016/j.jhevol.2018.01.002

van der Merwe, N. J., & Medina, E. (1989). Photosynthesis and 13C12C ratios in Amazonian rain forests. *Geochimica et Cosmochimica Acta*, *53*(5), 1091-1094. https://doi.org/https://doi.org/10.1016/0016-7037(89)90213-5

van der Merwe, N. J., & Medina, E. (1991). The canopy effect, carbon isotope ratios and foodwebs in amazonia. *Journal of Archaeological Science*, *18*(3), 249-259. https://doi.org/https://doi.org/10.1016/0305-4403(91)90064-V

Wang, Y., & Cerling, T. E. (1994). A model of fossil tooth and bone diagenesis: implications for paleodiet reconstruction from stable isotopes. *Palaeogeography, Palaeoclimatology, Palaeoecology*, *107*(3), 281-289. https://doi.org/https://doi.org/10.1016/0031-0182(94)90100-7

Wiedemann, F. B., Bocherens, H., Mariotti, A., Driesch, A. v. d., & Grupe, G. (1999). Methodological and Archaeological Implications of Intra-tooth Isotopic Variations (δ13C, δ18O) in Herbivores from Ain Ghazal (Jordan, Neolithic). *Journal of Archaeological Science*, *26*(6), 697-704. https://doi.org/https://doi.org/10.1006/jasc.1998.0392

Willis, K. J., Rudner, E., & Sümegi, P. (2000). The Full-Glacial Forests of Central and Southeastern Europe. *Quaternary Research*, *53*(2), 203-213. https://doi.org/https://doi.org/10.1006/qres.1999.2119

Wright, L. E., & Schwarcz, H. P. (1998). Stable carbon and oxygen isotopes in human tooth enamel: identifying breastfeeding and weaning in prehistory. *Am J Phys Anthropol*, *106*(1), 1-18. https://doi.org/10.1002/(sici)1096-8644(199805)106:1<1::aid-ajpa1>3.0.co;2-w

Wright, L. E., & Schwarcz, H. P. (1999). Correspondence Between Stable Carbon, Oxygen and Nitrogen Isotopes in Human Tooth Enamel and Dentine: Infant Diets at Kaminaljuyú. *Journal of Archaeological Science*, *26*(9), 1159-1170. https://doi.org/https://doi.org/10.1006/jasc.1998.0351

Zazzo, A., Balasse, M., & Patterson, W. P. (2005). High-resolution δ13C intratooth profiles in bovine enamel: Implications for mineralization pattern and isotopic attenuation. *Geochimica et Cosmochimica Acta*, *69*(14), 3631-3642. https://doi.org/https://doi.org/10.1016/j.gca.2005.02.031

Zazzo, A., Balasse, M., & Patterson, W. P. (2006). The reconstruction of mammal individual history: refining high-resolution isotope record in bovine tooth dentine. *Journal of Archaeological Science*, *33*(8), 1177-1187. https://doi.org/https://doi.org/10.1016/j.jas.2005.12.006

Zorzi, F., & Mezzana, F. (1962). Provincia di Verona. *Grezzana,. Riv di Sci Preist*, *17*, 284-285.

APPENDIX

Table A. 1. Results of the carbonate isotopic analysis (δ^{13}C and δ^{18}O) for Riparo Tagliente red deer *(Cervus elaphus*) teeth

Δ – intra-tooth ranges in weight percent carbonate (without excluding samples); SU – stratigraphic unit; R – right side; L – left side; Isotopic values in ***[brackets]*** and ***(parentheses)*** are not considered for further interpretation.

Tooth	SU	Excavation ID	Tissue	Lab ID	Crown height (mm)	Distance from ERJ (mm)	Distance from the lowest crown part (mm)	$CaCO_3$ (%)	$\delta^{13}C_{carb}$ (‰ VPDB)	$\delta^{18}O_{carb}$ (‰ VPDB)	$\delta^{18}O_{carb}$ (‰ VSMOW)	Δ $CaCO_3$ (%)
M3 L	5	RT81 Q3519 #9138	Enamel	RPT-R6a	23.5	21.02		3.6	-12.0	-5.6	25.2	0.6
			Enamel	RPT-R6b		18.3		3.4	-11.9	-5.6	25.1	
			Enamel	RPT-R6c		15.0		3.4	-12.1	-6.7	24.0	
			Enamel	RPT-R6d		12.5		3.3	-11.9	-6.7	24.0	
			Enamel	RPT-R6e		8.9		3.1	-11.8	-7.6	23.1	
			Enamel	RPT-R6f		6.3		3.5	-11.8	-8.0	22.6	
			Enamel	RPT-R6g		4.1		3.0	-12.0	-7.8	22.9	
			Dentine	RPT-R6den		-		4.6	-12.3	-6.6	24.1	
M3 L	5	RT q20/4 #6574	Enamel	RPT-R7a	17.6		14.8	3.9	-12.6	-4.4	26.4	1.2
			Enamel	RPT-R7b			11.6	2.7	-12.5	-4.2	26.6	
			Enamel	RPT-R7c			8.9	3.4	-11.8	-5.4	25.4	
			Enamel	RPT-R7d			6.1	3.2	-11.6	-5.3	25.4	
			Enamel	RPT-R7e			3.9	2.8	-12.1	-5.4	25.3	
			Dentine	RPT-R7den			-	4.9	-11.6	-6.3	24.4	
M3 R	6	RT q631 #6757	Enamel	RPT-R8a	21.1	19.9		2.8	-11.4	-6.2	24.5	1.2

Tooth	SU	Excavation ID	Tissue	Lab ID	Crown height (mm)	Distance from ERJ (mm)	Distance from the lowest crown part (mm)	$CaCO_3$ (%)	$\delta^{13}C_{carb}$ (‰ VPDB)	$\delta^{18}O_{carb}$ (‰ VPDB)	$\delta^{18}O_{carb}$ (‰ VSMOW)	Δ $CaCO_3$ (%)
			Enamel	RPT-R8b		17.4		2.5	-11.6	-6.9	23.9	
			Enamel	RPT-R8c		15.2		2.7	-11.5	-7.2	23.5	
			Enamel	RPT-R8d		13.0		2.8	-11.4	-7.9	22.8	
			Enamel	RPT-R8e		10.3		2.9	-11.4	-8.6	22.0	
			Enamel	RPT-R8f		8.2		3.0	-11.3	-8.8	21.8	
			Enamel	RPT-R8g		5.5		2.7	-10.7	-8.7	22.0	
			Enamel	RPT-R8h		3.1		3.7	-10.6	-8.0	22.7	
			Dentine	RPT-R8den		-		4.5	-12.4	-5.8	25.0	
M3 L	6	RT81 q5015 #9488	Enamel	RPT-R9a	18.0		15.1	[2.9]	(-12.4)	(-6.1)	(24.6)	1.1
			Enamel	RPT-R9b			13.3	[2.8]	(-12.2)	(-6.8)	(23.9)	
			Enamel	RPT-R9c			11.5	3.6	-12.4	-6.2	24.5	
			Enamel	RPT-R9d			9.8	3.6	-12.4	-7.0	23.7	
			Enamel	RPT-R9e			7.5	3.4	-12.2	-7.2	23.5	
			Enamel	RPT-R9f			5.3	3.9	-12.2	-7.2	23.5	
			Enamel	RPT-R9g			3.3	3.7	-12.1	-7.4	23.3	
			Dentine	RPT-R9den			-	4.7	-11.0	-5.9	24.8	
M3 L	6	RT81 q5016 #9475	Enamel	RPT-R10a	16.6	14.6		[2.8]	(-11.4)	(-5.6)	(25.1)	1.3
			Enamel	RPT-R10b		11.9		3.7	-11.2	-5.5	25.3	
			Enamel	RPT-R10c		10.1		3.9	-11.1	-5.9	24.8	
			Enamel	RPT-R10d		7.5		3.5	-11.1	-7.2	23.4	
			Enamel	RPT-R10e		5.8		4.0	-11.2	-6.5	24.2	
			Enamel	RPT-R10f		3.4		4.1	-11.2	-6.2	24.6	
			Dentine	RPT-R10den		-		5.0	-9.7	-6.1	24.7	

Tooth	SU	Excavation ID	Tissue	Lab ID	Crown height (mm)	Distance from ERJ (mm)	Distance from the lowest crown part (mm)	$CaCO_3$ (%)	$\delta^{13}C_{carb}$ (‰ VPDB)	$\delta^{18}O_{carb}$ (‰ VPDB)	$\delta^{18}O_{carb}$ (‰ VSMOW)	Δ $CaCO_3$ (%)
M3 R	7b	RT q23 #7001	Enamel	RPT-R11a	23.2	20.8		3.4	-11.3	-4.7	26.1	0.6
			Enamel	RPT-R11b		18.6		3.8	-11.3	-4.9	25.9	
			Enamel	RPT-R11c		16.5		3.5	-11.7	-5.6	25.1	
			Enamel	RPT-R11d		15.3		[3.2]	(-11.9)	(-8.1)	(22.5)	
			Enamel	RPT-R11e		12.3		3.2	-11.8	-6.2	24.5	
			Enamel	RPT-R11f		10.3		3.4	-11.8	-7.3	23.4	
			Enamel	RPT-R11g		8.0		3.5	-11.7	-7.6	23.1	
			Enamel	RPT-R11h		5.8		3.5	-11.7	-7.5	23.2	
			Enamel	RPT-R11i		3.1		3.6	-11.7	-7.0	23.7	
			Dentine	RPT-R11den		-		5.5	-11.1	-6.4	24.3	
M3 R	7	RT q9 #6920	Enamel	RPT-R12a	24.0	20.6		3.3	-12.4	-7.1	23.6	1.1
			Enamel	RPT-R12b		19.1		[2.9]	(-11.7)	(-7.4)	(23.3)	
			Enamel	RPT-R12c		17.8		3.3	-12.1	-6.8	23.9	
			Enamel	RPT-R12d		15.8		3.3	-12.0	-7.7	23.0	
			Enamel	RPT-R12e		13.1		3.6	-11.3	-7.3	23.4	
			Enamel	RPT-R12f		11.1		[2.9]	(-10.8)	(-7.5)	(23.2)	
			Enamel	RPT-R12g		8.3		3.4	-11.1	-7.6	23.0	
			Enamel	RPT-R12h		6.2		3.2	-11.3	-7.5	23.2	
			Enamel	RPT-R12i		4.1		[2.5]	(-11.7)	(-7.7)	(23.0)	
			Enamel	RPT-R12j		2.6		3.6	-11.8	-6.6	24.1	
			Dentine	RPT-R12den		-		5.5	-12.3	-5.5	25.2	
M2 R	7	RT81 q21/8	Enamel	RPT-R13a	15.5	12.5		3.3	-11.2	-7.2	23.5	1.0
			Enamel	RPT-R13ab		11.3		3.5	-11.3	-6.2	24.5	
			Enamel	RPT-R13b		9.1		3.6	-10.9	-4.9	25.9	

Tooth	SU	Excavation ID	Tissue	Lab ID	Crown height (mm)	Distance from ERJ (mm)	Distance from the lowest crown part (mm)	$CaCO_3$ (%)	$\delta^{13}C_{carb}$ (‰ VPDB)	$\delta^{18}O_{carb}$ (‰ VPDB)	$\delta^{18}O_{carb}$ (‰ VSMOW)	Δ $CaCO_3$ (%)
			Enamel	RPT-R13bb		7.7		3.7	-11.4	-4.6	26.2	
			Enamel	RPT-R13c		6.3		3.5	-11.1	-4.4	26.3	
			Enamel	RPT-R13cb		4.8		4.2	-11.6	-4.4	26.4	
			Enamel	RPT-R13d		3.2		3.2	-11.3	-4.7	26.0	
			Enamel	RPT-R13db		1.7		3.4	-11.2	-5.1	25.6	
			Dentine	RPT-R13den1		-		4.9	-10.7	-7.1	23.6	
M3 R	7	RT81 q21/8	Enamel	RPT-R13e	19.1	16.5		3.4	-11.7	-5.5	25.3	0.5
			Enamel	RPT-R13f		15.2		3.3	-11.3	-6.0	24.7	
			Enamel	RPT-R13g		12.8		3.4	-11.6	-6.6	24.1	
			Enamel	RPT-R13h		10.9		3.4	-11.7	-6.8	23.8	
			Enamel	RPT-R13i		8.6		3.2	-11.8	-7.1	23.6	
			Enamel	RPT-R13j		6.8		3.4	-11.7	-7.5	23.2	
			Enamel	RPT-R13k		4.9		3.3	-11.9	-7.2	23.5	
			Enamel	RPT-R13l		2.4		2.9	-12.0	-6.5	24.2	
			Dentine	RPT-R13den2		-		4.5	-11.3	-6.9	23.8	
M3 R	7	RT q6 #6839	Enamel	RPT-R14a	18.6	16.4		3.7	-12.5	-5.8	24.9	1.3
			Enamel	RPT-R14b		14.6		3.5	-12.5	-5.8	24.9	
			Enamel	RPT-R14c		12.7		3.3	-12.4	-6.0	24.7	
			Enamel	RPT-R14d		10.7		2.5	-12.6	-7.0	23.7	
			Enamel	RPT-R14e		7.8		3.3	-12.7	-7.1	23.6	
			Enamel	RPT-R14f		6.0		2.5	-12.5	-7.6	23.1	
			Enamel	RPT-R14g		3.5		3.5	-12.2	-7.1	23.6	
			Dentine	RPT-R14den		-		4.4	-11.9	-6.8	23.9	

Tooth	SU	Excavation ID	Tissue	Lab ID	Crown height (mm)	Distance from ERJ (mm)	Distance from the lowest crown part (mm)	$CaCO_3$ (%)	$\delta^{13}C_{carb}$ (‰ VPDB)	$\delta^{18}O_{carb}$ (‰ VPDB)	$\delta^{18}O_{carb}$ (‰ VSMOW)	Δ $CaCO_3$ (%)
M3 R	7	RT81 q35/7 #7002	Enamel	RPT-R15a	19.3	17.3		3.0	-11.6	-6.0	24.7	1.6
			Enamel	RPT-R15b		15.5		[2.9]	(-11.6)	(-6.2)	(24.5)	
			Enamel	RPT-R15c		13.1		3.2	-11.8	-6.9	23.7	
			Enamel	RPT-R15d		11.0		3.9	-11.8	-7.2	23.5	
			Enamel	RPT-R15e		9.5		[2.9]	(-11.7)	(-8.1)	(22.6)	
			Enamel	RPT-R15f		7.9		3.6	-11.7	-7.7	23.0	
			Enamel	RPT-R15g		4.8		3.8	-11.6	-7.5	23.2	
			Enamel	RPT-R15h		3.1		[4.5]	(-11.7)	(-7.6)	(23.1)	
			Dentine	RPT-R15den		-		3.9	-11.6	-7.3	23.3	
M2 R	7	RT q6 #6850	Enamel	RPT-R16a	12.7		11.1	4.0	-12.7	-7.7	22.9	0.7
			Enamel	RPT-R16b			9.8	[3.3]	(-12.6)	(-7.9)	(22.8)	
			Enamel	RPT-R16c			7.2	4.0	-12.4	-6.6	24.1	
			Enamel	RPT-R16d			5.8	4.0	-12.1	-6.1	24.7	
			Enamel	RPT-R16e			3.2	3.7	-12.3	-5.4	25.3	
			Dentine	RPT-R16den1			-	1.8	-11.2	-7.5	23.2	
M3 R	7	RT q6 #6850	Enamel	RPT-R16f	13.0		13.0	3.5	-12.2	-6.5	24.2	1.0
			Enamel	RPT-R16g			10.4	3.6	-11.7	-5.9	24.8	
			Enamel	RPT-R16h			8.1	2.9	-12.1	-6.7	24.0	
			Enamel	RPT-R16i			6.1	2.8	-12.3	-7.1	23.6	
			Enamel	RPT-R16j			4.3	2.5	-12.9	-7.7	22.9	
			Enamel	RPT-R16k			2.6	2.8	-11.9	-7.3	23.4	
			Dentine	RPT-R16den2			-	1.5	-11.2	-8.3	22.4	
M3 R	8	RT62 Q20/7 #7636	Enamel	RPT-17a	20.7	18.5		3.5	-11.6	-5.5	25.2	0.7

Tooth	SU	Excavation ID	Tissue	Lab ID	Crown height (mm)	Distance from ERJ (mm)	Distance from the lowest crown part (mm)	$CaCO_3$ (%)	$\delta^{13}C_{carb}$ (‰ VPDB)	$\delta^{18}O_{carb}$ (‰ VPDB)	$\delta^{18}O_{carb}$ (‰ VSMOW)	Δ $CaCO_3$ (%)
			Enamel	RPT-17b		16.3		3.5	-11.2	-5.9	24.8	
			Enamel	RPT-17c		14.3		3.0	-11.3	-6.7	24.0	
			Enamel	RPT-17d		12.2		3.0	-11.0	-7.1	23.6	
			Enamel	RPT-17e		9.8		3.3	-11.0	-6.8	23.9	
			Enamel	RPT-17f		7.7		3.1	-11.1	-8.1	22.5	
			Enamel	RPT-17g		4.5		2.9	-11.1	-8.4	22.2	
			Enamel	RPT-17h		1.4		2.9	-10.8	-8.2	22.5	
			Dentine	RPT-17den		-		5.2	-9.7	-6.1	24.6	
M2 R	8	RT8 q6 #7628	Enamel	RPT-18a	17.3		15.6	[2.3]	(-11.4)	(-9.8)	(20.8)	1.8
			Enamel	RPT-18b			14.4	3.5	-11.5	-9.3	21.3	
			Enamel	RPT-18c			13.2	3.8	-11.6	-9.5	21.1	
			Enamel	RPT-18d			12.0	3.8	-11.5	-9.5	21.1	
			Enamel	RPT-18e			10.8	[3.9]	(-11.4)	(-8.3)	(22.4)	
			Enamel	RPT-18f			8.9	[3.5]	(-11.0)	(-8.4)	(22.2)	
			Enamel	RPT-18g			7.5	4.1	-11.6	-8.7	21.9	
			Enamel	RPT-18h			4.5	3.9	-11.5	-7.4	23.2	
			Enamel	RPT-18i			2.0	3.9	-11.6	-6.1	24.6	
M3 R	8	RT8 q6 #7628	Enamel	RPT-18j	21.1	19.2		3.3	-12.6	-6.2	24.5	0.6
			Enamel	RPT-18k		17.2		3.3	-12.4	-6.5	24.3	
			Enamel	RPT-18l		15.3		3.6	-12.1	-5.9	24.7	
			Enamel	RPT-18m		12.9		3.5	-12.3	-6.5	24.2	
			Enamel	RPT-18n		10.1		3.6	-11.8	-6.2	24.5	
			Enamel	RPT-18o		7.3		3.4	-11.9	-7.1	23.5	
			Enamel	RPT-18p		5.2		[3.0]	(-11.5)	(-7.4)	(23.3)	

Tooth	SU	Excavation ID	Tissue	Lab ID	Crown height (mm)	Distance from ERJ (mm)	Distance from the lowest crown part (mm)	$CaCO_3$ (%)	$\delta^{13}C_{carb}$ (‰ VPDB)	$\delta^{18}O_{carb}$ (‰ VPDB)	$\delta^{18}O_{carb}$ (‰ VSMOW)	Δ $CaCO_3$ (%)
			Enamel	RPT-18q		2.7		3.3	-11.5	-7.6	23.1	
			Dentine	RPT-18den		-		4.4	-12.1	-6.5	24.2	
M2 R	8	RT Q3613 #7643	Enamel	RPT-19a	16.6	13.8		3.5	-12.5	-7.5	23.2	0.4
			Enamel	RPT-19b		10.9		3.8	-12.2	-7.6	23.0	
			Enamel	RPT-19c		8.7		3.9	-12.6	-7.9	22.8	
			Enamel	RPT-19d		6.5		3.5	-12.6	-7.2	23.5	
			Enamel	RPT-19e		4.1		3.6	-12.5	-5.9	24.8	
			Enamel	RPT-19f		1.7		3.8	-12.1	-5.9	24.9	
M3 R	8	RT Q3613 #7643	Enamel	RPT-19g	18.6	16.5		3.6	-12.4	-5.9	24.8	0.7
			Enamel	RPT-19h		13.8		3.4	-12.1	-6.2	24.5	
			Enamel	RPT-19i		11.9		3.5	-12.0	-6.5	24.2	
			Enamel	RPT-19j		9.2		3.7	-11.8	-6.6	24.2	
			Enamel	RPT-19k		6.7		[4.1]	(-11.9)	(-6.6)	(24.1)	
			Enamel	RPT-19l		3.9		3.6	-11.5	-6.7	24.0	
			Dentine	RPT-19den		-		3.9	-11.0	-6.8	23.9	
M2 R	8	RT Q6 #7556	Enamel	RPT-20a	14.0	12.5		3.6	-11.7	-7.2	23.5	0.8
			Enamel	RPT-20b		10.3		3.8	-11.9	-6.8	23.9	
			Enamel	RPT-20c		7.2		3.3	-12.0	-6.0	24.7	
			Enamel	RPT-20d		5.1		4.1	-12.3	-5.8	24.9	
			Enamel	RPT-20e		2.3		4.1	-12.1	-6.1	24.6	
M3 R	8	RT Q6 #7556	Enamel	RPT-20f	15.8	13.4		3.4	-12.3	-6.1	24.6	0.7
			Enamel	RPT-20g		11.8		3.4	-12.1	-6.8	23.9	
			Enamel	RPT-20h		9.4		3.7	-12.1	-6.5	24.2	

Tooth	SU	Excavation ID	Tissue	Lab ID	Crown height (mm)	Distance from ERJ (mm)	Distance from the lowest crown part (mm)	$CaCO_3$ (%)	$\delta^{13}C_{carb}$ (‰ VPDB)	$\delta^{18}O_{carb}$ (‰ VPDB)	$\delta^{18}O_{carb}$ (‰ VSMOW)	Δ $CaCO_3$ (%)
			Enamel	RPT-20i		7.2		3.4	-12.0	-6.9	23.8	
			Enamel	RPT-20j		5.7		[4.1]	(-12.2)	(-6.6)	(24.1)	
			Enamel	RPT-20k		3.9		3.8	-11.8	-7.4	23.3	
			Enamel	RPT-20l		1.8		3.7	-11.9	-6.9	23.8	
			Dentine	RPT-20den		-		4.2	-12.1	-7.0	23.7	
M2 R	9	RT Q80/9 #9727	Enamel	RPT-21a	14.1	12.0		3.9	-11.9	-6.3	24.4	0.1
			Enamel	RPT-21b		9.9		3.8	-12.0	-6.4	24.4	
			Enamel	RPT-21c		7.4		3.9	-12.1	-5.5	25.2	
			Enamel	RPT-21d		5.5		3.9	-11.9	-4.2	26.6	
			Enamel	RPT-21e		3.5		3.8	-11.8	-5.0	25.8	
M3 R	9	RT Q80/9 #9727	Enamel	RPT-21f	13.0	11.1		3.6	-11.8	-5.8	24.9	0.6
			Enamel	RPT-21g		9.7		3.4	-11.9	-6.6	24.1	
			Enamel	RPT-21h		7.6		3.5	-11.7	-6.9	23.8	
			Enamel	RPT-21i		4.8		3.6	-11.8	-7.5	23.2	
			Enamel	RPT-21j		2.6		3.5	-12.0	-8.4	22.2	
			Enamel	RPT-21k		1.1		[4.0]	(-11.4)	(-7.6)	(23.1)	
			Dentine	RPT-21den		-		2.8	-11.2	-7.9	22.8	
M2 R	9	RT Q23 #8512	Enamel	RPT-22a	13.7	11.1		4.3	-12.5	-8.4	22.3	0.7
			Enamel	RPT-22b		9.4		4.2	-12.2	-7.1	23.6	
			Enamel	RPT-22c		7.3		[3.6]	(-11.9)	(-6.9)	(23.7)	
			Enamel	RPT-22d		4.5		3.9	-11.9	-5.5	25.2	
			Enamel	RPT-22e		2.5		3.9	-11.5	-5.1	25.7	

Tooth	SU	Excavation ID	Tissue	Lab ID	Crown height (mm)	Distance from ERJ (mm)	Distance from the lowest crown part (mm)	$CaCO_3$ (%)	$\delta^{13}C_{carb}$ (‰ VPDB)	$\delta^{18}O_{carb}$ (‰ VPDB)	$\delta^{18}O_{carb}$ (‰ VSMOW)	Δ $CaCO_3$ (%)
M3 R	9	RT Q23 #8512	Enamel	RPT-22f	14.7	12.3		[4.1]	(-11.9)	(-5.1)	(25.7)	1.2
			Enamel	RPT-22g		10.6		3.7	-11.4	-6.0	24.7	
			Enamel	RPT-22h		9.0		3.8	-11.4	-6.1	24.6	
			Enamel	RPT-22i		7.3		3.7	-11.1	-6.3	24.4	
			Enamel	RPT-22j		4.1		[2.9]	(-11.2)	(-6.9)	(23.8)	
			Enamel	RPT-22k		2.3		3.9	-11.1	-7.4	23.2	
M3 R	9	RT Q64/5-8 #8536	Enamel	RPT-23a	21.5	19.4		3.8	-12.2	-5.3	25.4	0.5
			Enamel	RPT-23b		17.6		4.0	-12.0	-4.9	25.8	
			Enamel	RPT-23c		15.8		3.4	-12.0	-5.5	25.3	
			Enamel	RPT-23d		13.9		3.9	-11.7	-4.6	26.1	
			Enamel	RPT-23e		12.1		3.7	-11.8	-5.3	25.5	
			Enamel	RPT-23f		9.9		3.5	-11.6	-5.8	24.9	
			Enamel	RPT-23g		7.8		3.9	-11.4	-5.8	25.0	
			Enamel	RPT-23h		5.8		3.4	-11.4	-7.7	23.0	
			Enamel	RPT-23i		3.9		3.7	-11.1	-7.6	23.0	
			Dentine	RPT-23den		-		6.4	-11.1	-7.0	23.7	
M2 R	9	RT Q6 #9536	Enamel	RPT-24a	19.0	17.1		[3.0]	(-11.8)	(-6.6)	(24.1)	0.9
			Enamel	RPT-24b		14.9		[3.3]	(-12.0)	(-6.2)	(24.6)	
			Enamel	RPT-24c		12.5		[3.1]	(-12.1)	(-5.7)	(25.0)	
			Enamel	RPT-24d		10.4		3.6	-12.0	-5.8	24.9	
			Enamel	RPT-24e		8.7		3.8	-12.1	-5.9	24.9	
			Enamel	RPT-24f		6.9		3.8	-12.0	-5.6	25.2	
			Enamel	RPT-24g		5.3		3.6	-12.2	-4.8	26.0	

Tooth	SU	Excavation ID	Tissue	Lab ID	Crown height (mm)	Distance from ERJ (mm)	Distance from the lowest crown part (mm)	$CaCO_3$ (%)	$\delta^{13}C_{carb}$ (‰ VPDB)	$\delta^{18}O_{carb}$ (‰ VPDB)	$\delta^{18}O_{carb}$ (‰ VSMOW)	Δ $CaCO_3$ (%)
			Enamel	RPT-24h		3.7		3.9	-12.1	-4.2	26.6	
			Enamel	RPT-24i		1.4		3.7	-11.8	-5.6	25.1	
M3 R	9	RT Q6 #9536	Enamel	RPT-24j	18.9	16.9		3.4	-12.3	-5.0	25.7	0.7
			Enamel	RPT-24k		14.8		4.1	-12.3	-4.6	26.2	
			Enamel	RPT-24l		12.3		3.8	-12.1	-5.1	25.6	
			Enamel	RPT-24m		9.6		3.7	-12.1	-5.9	24.9	
			Enamel	RPT-24n		6.9		3.9	-12.2	-5.6	25.1	
			Enamel	RPT-24o		5.1		3.8	-12.3	-6.3	24.4	
			Enamel	RPT-24p		3.0		3.9	-12.3	-7.2	23.5	
			Enamel	RPT-24q		1.3		3.9	-12.4	-7.4	23.2	
			Dentine	RPT-24den		-		4.4	-10.5	-7.5	23.2	
M3 L	10a	RT Q19/4 #1181	Enamel	RPT-25a	16.7	14.6		[3.8]	(-11.8)	(-6.3)	(24.4)	0.6
			Enamel	RPT-25b		12.3		3.6	-11.7	-6.7	24.1	
			Enamel	RPT-25c		9.3		3.4	-12.0	-6.6	24.1	
			Enamel	RPT-25d		7.1		3.5	-12.1	-7.0	23.7	
			Enamel	RPT-25e		5.0		3.6	-12.1	-7.4	23.2	
			Enamel	RPT-25f		3.2		3.5	-11.9	-8.3	22.3	
			Enamel	RPT-25g		1.3		[4.0]	(-12.0)	(-9.4)	(21.2)	
			Dentine	RPT-25den		-		4.0	-11.2	-9.2	21.4	
M3 R	10a	RT Q35/6 #1176	Enamel	RPT-26a	17.5	14.6		4.3	-12.4	-5.7	25.1	0.7
			Enamel	RPT-26b		11.8		4.2	-12.2	-5.5	25.2	
			Enamel	RPT-26c		9.8		3.6	-12.1	-6.0	24.8	
			Enamel	RPT-26d		7.4		3.9	-12.0	-7.2	23.5	

Tooth	SU	Excavation ID	Tissue	Lab ID	Crown height (mm)	Distance from ERJ (mm)	Distance from the lowest crown part (mm)	$CaCO_3$ (%)	$\delta^{13}C_{carb}$ (‰ VPDB)	$\delta^{18}O_{carb}$ (‰ VPDB)	$\delta^{18}O_{carb}$ (‰ VSMOW)	Δ $CaCO_3$ (%)
			Enamel	RPT-26e		5.2		3.9	-12.0	-7.7	230	
			Enamel	RPT-26f		2.9		4.1	-11.9	-8.7	22.0	
			Dentine	RPT-26den		-		[23.5]	(-21.4)	(-5.9)	(24.8)	
M2 R	10a	RT Q22	Enamel	RPT-27a	15.5	11.2		3.7	-12.1	-8.1	22.6	1.0
			Enamel	RPT-27b		9.9		3.8	-12.0	-7.1	23.6	
			Enamel	RPT-27c		7.8		3.7	-12.2	-6.9	23.8	
			Enamel	RPT-27d		5.9		[2.9]	(-12.3)	(-6.1)	(24.6)	
			Enamel	RPT-27e		4.7		3.9	-12.5	-6.1	24.6	
			Enamel	RPT-27f		2.5		3.8	-12.6	-6.0	24.8	
M3 R	10a	RT Q22	Enamel	RPT-27g	17.9	15.8		4.0	-11.6	-6.7	24.0	0.5
			Enamel	RPT-27h		13.3		3.4	-11.4	-7.0	23.7	
			Enamel	RPT-27i		11.4		3.9	-11.5	-6.8	23.9	
			Enamel	RPT-27j		9.9		3.7	-11.6	-7.0	23.7	
			Enamel	RPT-27k		7.3		3.5	-11.6	-6.9	23.8	
			Enamel	RPT-27l		5.1		3.9	-11.0	-6.7	24.0	
			Enamel	RPT-27m		3.2		3.4	-11.1	-6.3	24.4	
			Dentine	RPT-27den		-		4.3	-11.4	-5.7	25.1	
M3 R	10b	RT Q38/6 #1198	Enamel	RPT-28a	17.5	15.0		3.7	-11.2	-5.2	25.5	0.8
			Enamel	RPT-28b		13.1		3.0	-11.0	-6.2	24.5	
			Enamel	RPT-28c		10.3		3.3	-11.1	-6.4	24.3	
			Enamel	RPT-28d		8.3		3.1	-11.2	-6.5	24.2	
			Enamel	RPT-28e		6.3		3.6	-11.3	-6.7	24.0	
			Enamel	RPT-28f		4.6		3.8	-11.3	-7.0	23.7	

Tooth	SU	Excavation ID	Tissue	Lab ID	Crown height (mm)	Distance from ERJ (mm)	Distance from the lowest crown part (mm)	$CaCO_3$ (%)	$\delta^{13}C_{carb}$ (‰ VPDB)	$\delta^{18}O_{carb}$ (‰ VPDB)	$\delta^{18}O_{carb}$ (‰ VSMOW)	Δ $CaCO_3$ (%)
			Enamel	RPT-28g		3.2		3.8	-11.1	-6.1	24.6	
			Dentine	RPT-28den		-		4.3	-11.5	-6.7	24.0	
M3 R	10b	RT Q80/7 #1237	Enamel	RPT-29a	22.3	19.8		3.6	-13.1	-8.1	22.6	0.4
			Enamel	RPT-29b		18.4		3.9	-13.2	-8.4	22.2	
			Enamel	RPT-29c		17.5		4.0	-13.3	-9.2	21.4	
			Enamel	RPT-29d		16.2		4.0	-13.1	-9.2	21.4	
			Enamel	RPT-29e		14.6		3.8	-13.0	-9.8	20.8	
			Enamel	RPT-29f		12.8		3.6	-12.8	-10.1	20.5	
			Enamel	RPT-29g		11.3		3.7	-12.8	-9.9	20.7	
			Enamel	RPT-29h		10.0		3.8	-12.8	-10.3	20.3	
			Enamel	RPT-29i		8.6		3.8	-12.5	-9.6	21.0	
			Enamel	RPT-29j		7.1		3.9	-12.3	-9.7	20.9	
			Enamel	RPT-29k		5.6		3.7	-12.3	-9.8	20.8	
M3 R	10c	RT Q37/6 #1166bis	Enamel	RPT-30a	23.2	21.1		3.5	-11.7	-6.5	24.2	1.0
			Enamel	RPT-30b		18.5		3.5	-11.6	-6.3	24.4	
			Enamel	RPT-30c		15.6		3.6	-11.9	-7.0	23.7	
			Enamel	RPT-30d		13.5		3.3	-11.6	-7.6	23.1	
			Enamel	RPT-30e		11.1		3.4	-11.6	-8.1	22.6	
			Enamel	RPT-30f		8.6		3.8	-11.3	-8.8	21.8	
			Enamel	RPT-30g		5.4		3.6	-11.1	-8.4	22.2	
			Enamel	RPT-30h		3.3		4.3	-11.3	-8.1	22.5	
			Dentine	RPT-30den		-		5.2	-10.7	-8.0	22.6	
M3 R	10d	RT Q50 #1229	Enamel	RPT-31a	22.8	20.5		4.1	-11.7	-6.8	23.9	0.9

Tooth	SU	Excavation ID	Tissue	Lab ID	Crown height (mm)	Distance from ERJ (mm)	Distance from the lowest crown part (mm)	$CaCO_3$ (%)	$\delta^{13}C_{carb}$ (‰ VPDB)	$\delta^{18}O_{carb}$ (‰ VPDB)	$\delta^{18}O_{carb}$ (‰ VSMOW)	Δ $CaCO_3$ (%)
			Enamel	RPT-31b		17.6		3.8	-11.4	-8.0	22.7	
			Enamel	RPT-31c		15.2		4.3	-11.6	-6.8	23.9	
			Enamel	RPT-31d		12.9		3.8	-11.5	-7.9	22.8	
			Enamel	RPT-31e		10.5		4.1	-11.3	-7.6	23.1	
			Enamel	RPT-31f		8.3		[4.6]	(-11.4)	(-7.7)	(23.0)	
			Enamel	RPT-31g		5.2		[3.6]	(-10.8)	(-8.5)	(22.2)	
			Enamel	RPT-31h		3.3		4.3	-11.0	-8.2	22.5	
			Dentine	RPT-31den		-		6.1	-11.3	-6.9	23.8	
M3 R	10d	RT Q79/9 #1239	Enamel	RPT-32a	19.1	16.8		3.8	-11.8	-7.5	23.1	0.8
			Enamel	RPT-32b		15.8		3.8	-12.0	-7.8	22.9	
			Enamel	RPT-32c		13.8		4.2	-11.9	-8.5	22.2	
			Enamel	RPT-32d		12.0		3.9	-12.2	-9.3	21.3	
			Enamel	RPT-32e		10.1		3.7	-12.1	-9.6	21.0	
			Enamel	RPT-32f		7.6		3.8	-12.1	-9.5	21.1	
			Enamel	RPT-32g		5.5		4.0	-12.0	-9.1	21.5	
			Enamel	RPT-32h		3.5		4.5	-12.2	-9.2	21.5	
			Dentine	RPT-32den		-		4.5	-12.2	-8.0	22.6	
M3 L	13	RT Q15 #4727	Enamel	RPT-33a	23.7	21.0		4.2	-11.7	-6.6	24.1	0.5
			Enamel	RPT-33b		19.6		3.8	-11.5	-7.2	23.4	
			Enamel	RPT-33c		16.4		3.8	-11.5	-7.8	22.8	
			Enamel	RPT-33d		13.6		4.0	-11.4	-7.5	23.2	
			Enamel	RPT-33e		11.5		3.8	-11.8	-8.5	22.2	
			Enamel	RPT-33f		9.1		3.8	-11.5	-8.4	22.3	

Tooth	SU	Excavation ID	Tissue	Lab ID	Crown height (mm)	Distance from ERJ (mm)	Distance from the lowest crown part (mm)	$CaCO_3$ (%)	$\delta^{13}C_{carb}$ (‰ VPDB)	$\delta^{18}O_{carb}$ (‰ VPDB)	$\delta^{18}O_{carb}$ (‰ VSMOW)	Δ $CaCO_3$ (%)
			Enamel	RPT-33g		6.6		3.8	-11.2	-9.0	21.6	
			Enamel	RPT-33h		3.3		3.6	-11.0	-9.1	21.5	
			Dentine	RPT-33den		-		4.0	-11.4	-6.3	24.4	
M3 L	13	RT Q511-7 #4118	Enamel	RPT-34a	21.1	17.5		4.1	-11.5	-7.9	22.8	0.8
			Enamel	RPT-34b		14.9		4.0	-11.6	-8.2	22.4	
			Enamel	RPT-34c		12.5		3.7	-11.3	-8.4	22.2	
			Enamel	RPT-34d		10.1		3.8	-11.0	-8.0	22.6	
			Enamel	RPT-34e		8.0		3.3	-10.9	-8.7	21.9	
			Enamel	RPT-34f		5.2		3.5	-10.9	-9.7	20.9	
			Enamel	RPT-34g		2.7		3.3	-11.0	-9.5	21.1	
			Dentine	RPT-34den		-		6.3	-12.0	-6.3	24.4	
M3 L	13	RT Q15 #4695	Enamel	RPT-35a	18.2	16.5		3.2	-12.0	-7.3	23.4	0.6
			Enamel	RPT-35b		14.8		3.6	-12.1	-7.4	23.2	
			Enamel	RPT-35c		12.4		3.7	-12.1	-7.8	22.9	
			Enamel	RPT-35d		11.1		3.5	-12.2	-7.7	22.9	
			Enamel	RPT-35e		9.9		3.3	-11.8	-7.3	23.4	
			Enamel	RPT-35f		8.7		3.5	-11.8	-7.6	23.1	
			Enamel	RPT-35g		4.5		3.3	-11.1	-7.5	23.2	
			Enamel	RPT-35h		2.3		3.8	-11.6	-7.2	23.5	
			Dentine	RPT-35den		-		5.3	(-9.5)	-7.3	23.4	
M3 R	10a	RT Q22 #3055	Enamel	RPT-36a	21.2	15.8		4.2	-11.7	-7.1	23.6	0.6
			Enamel	RPT-36b		12.7		4.4	-11.6	-8.5	22.1	
			Enamel	RPT-36c		10.6		4.5	-11.5	-9.2	21.4	

Tooth	SU	Excavation ID	Tissue	Lab ID	Crown height (mm)	Distance from ERJ (mm)	Distance from the lowest crown part (mm)	$CaCO_3$ (%)	$\delta^{13}C_{carb}$ (‰ VPDB)	$\delta^{18}O_{carb}$ (‰ VPDB)	$\delta^{18}O_{carb}$ (‰ VSMOW)	Δ $CaCO_3$ (%)
			Enamel	RPT-36d		8.4		4.4	-11.5	-9.5	21.1	
			Enamel	RPT-36e		6.1		4.8	-11.5	-9.5	21.1	
			Enamel	RPT-36f		3.8		4.9	-11.6	-9.0	21.6	
			Dentine	RPT-36den		-		-	-	-	-	
M3 R	10a	RT Q54 #1302	Enamel	RPT-37a	27.6	22.8		4.0	-11.4	-6.9	23.8	0.4
			Enamel	RPT-37b		20.3		4.0	-11.5	-7.6	23.1	
			Enamel	RPT-37c		18.4		4.1	-11.5	-8.2	22.5	
			Enamel	RPT-37d		15.9		4.1	-11.5	-8.8	21.8	
			Enamel	RPT-37e		13.2		4.2	-11.5	-9.4	21.2	
			Enamel	RPT-37f		11.1		4.0	-11.3	-9.8	20.8	
			Enamel	RPT-37g		8.2		4.3	-11.7	-10.2	20.4	
			Enamel	RPT-37h		5.7		4.4	-11.8	-9.7	20.9	
			Enamel	RPT-37i		2.6		4.3	-12.0	-8.5	22.2	
			Dentine	RPT-37den		-		-	-	-	-	
M3 R	10a	RT Q9519 #1191	Enamel	RPT-38a	18.9	15.1		4.1	-12.6	-6.9	23.8	0.3
			Enamel	RPT-38b		12.9		4.1	-12.4	-7.7	23.0	
			Enamel	RPT-38c		10.7		4.4	-12.2	-8.4	22.2	
			Enamel	RPT-38d		8.3		4.3	-12.0	-8.9	21.7	
			Enamel	RPT-38e		6.2		4.4	-11.9	-9.5	21.1	
			Enamel	RPT-38f		3.3		4.3	-11.6	-10.1	20.5	
			Dentine	RPT-38den		-		-	-	-	-	

Figure A. 1. Incremental plots of red deer teeth

Fig. A.1 - 1

Layer – 5

Red deer (*Cervus elaphus*) teeth – Riparo Tagliente (Late Epigravettian).

Lower M3 L

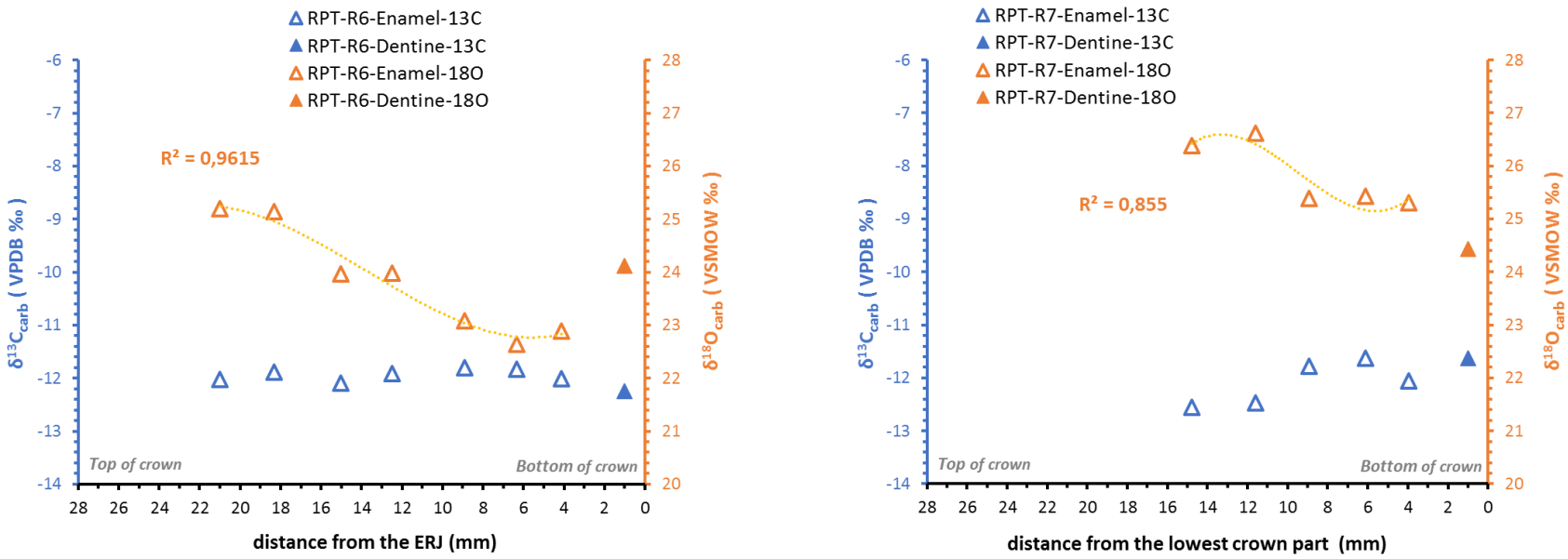

Fig. A.1 - 2

Layer – 6

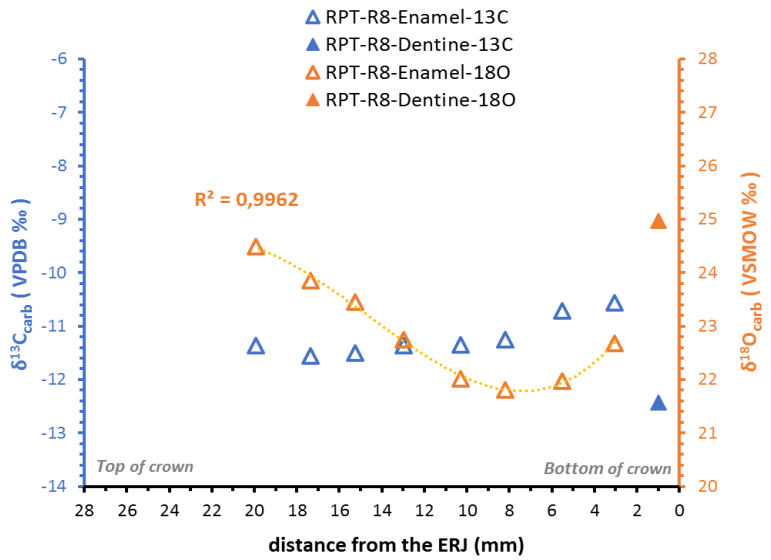

Lower M3 L

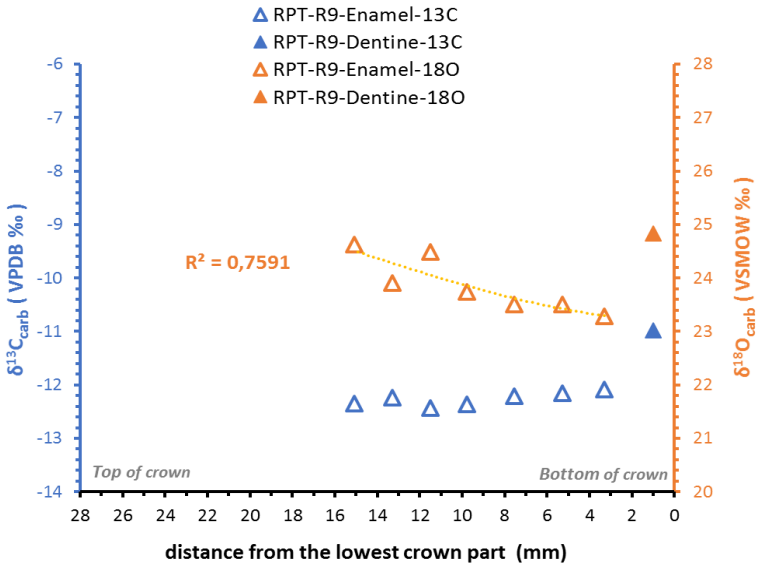

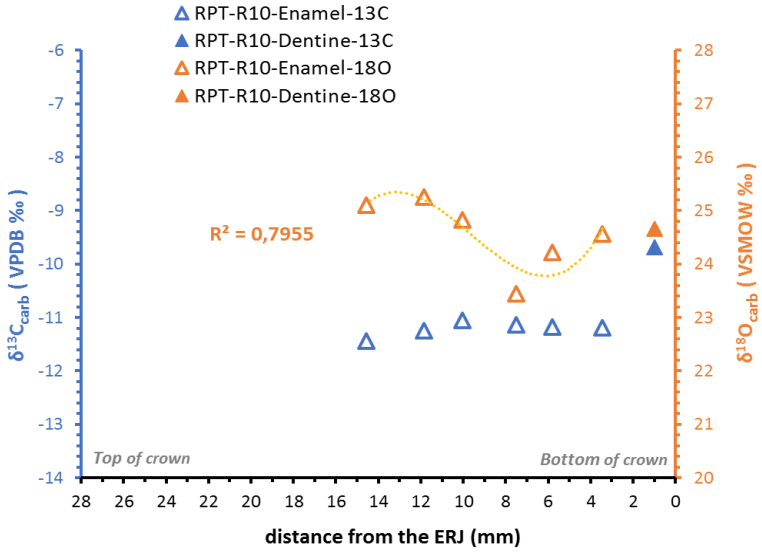

Fig. A.1 - 3

Layer – 7

Lower M3 R (7b)

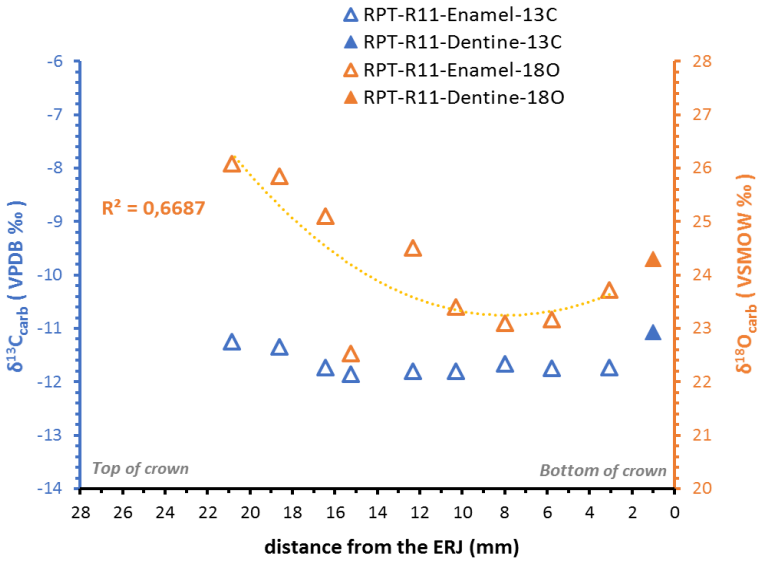

Lower M3 R

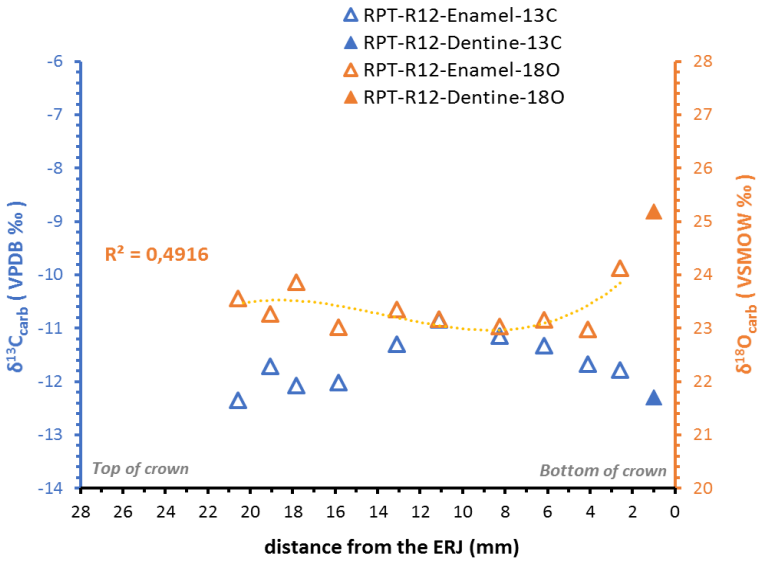

Lower M2 R and M3 R

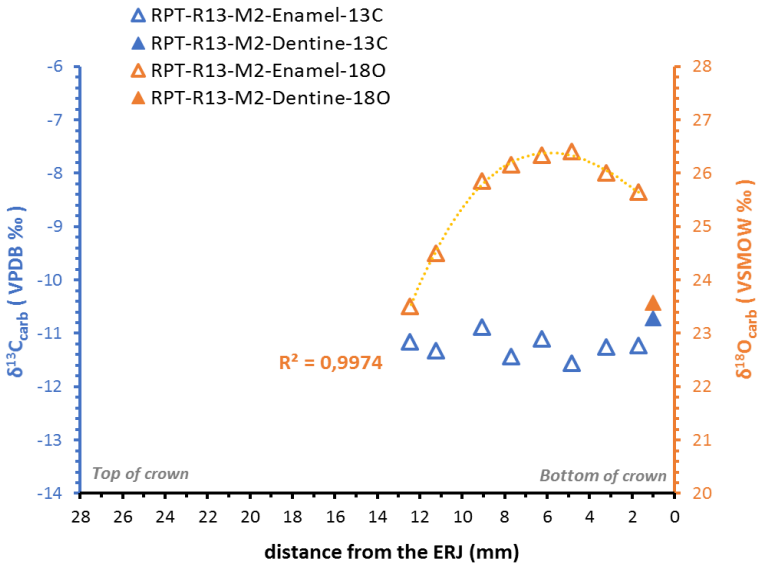

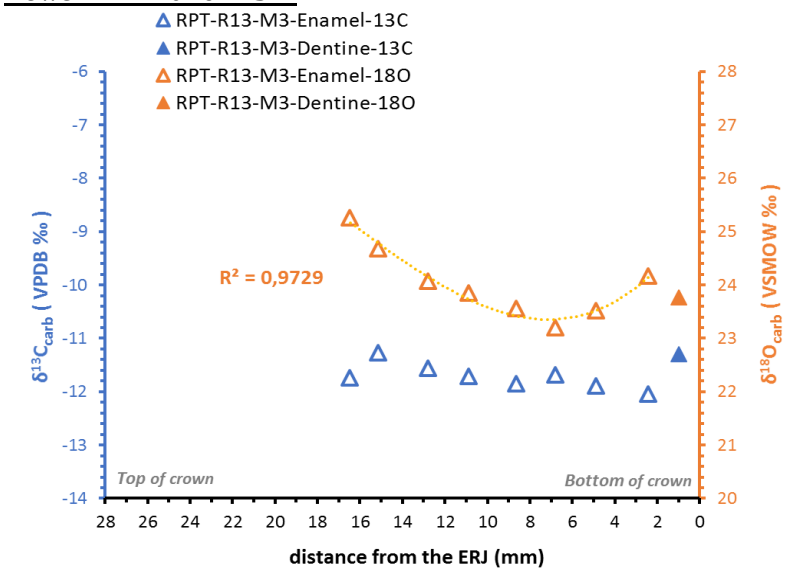

Fig. A.1 – 3 **Layer – 7**

Lower M3 R

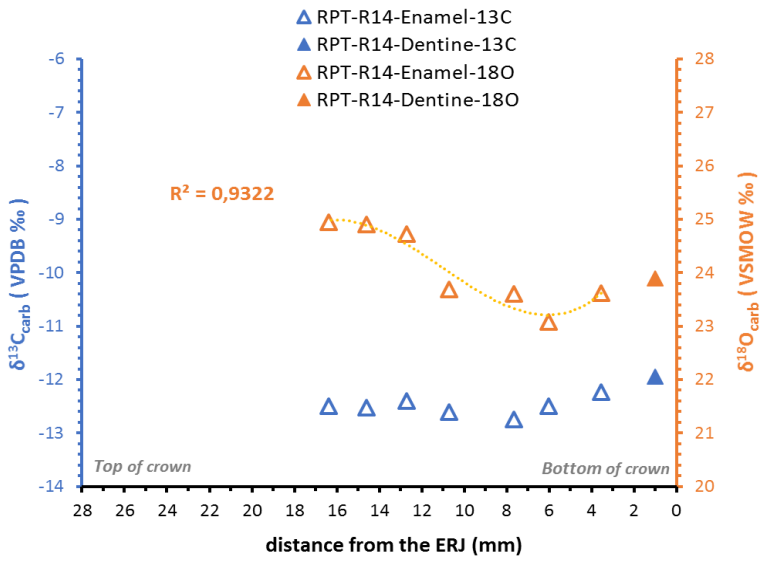

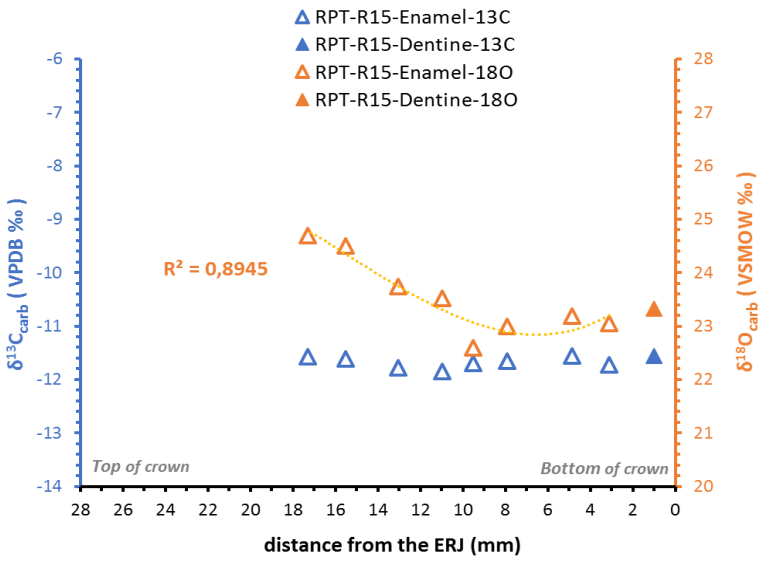

Lower M2 R and M3 R

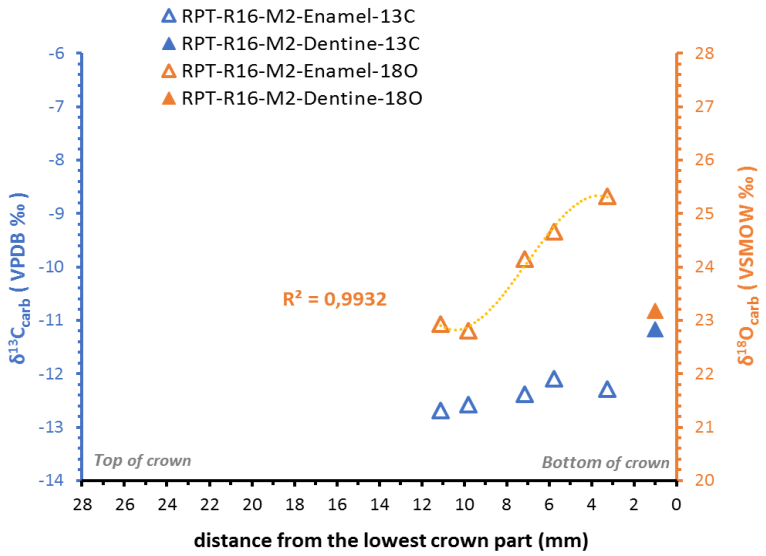

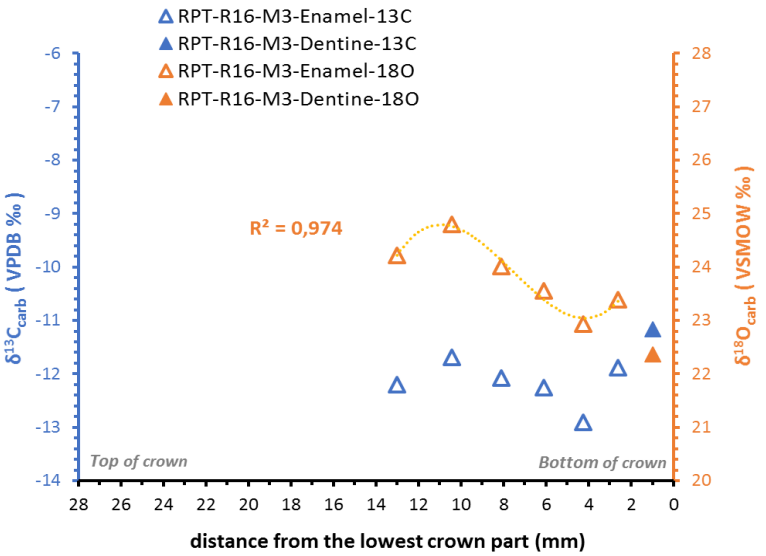

Fig. A.1 - 4

Layer – 8

Lower M3 R

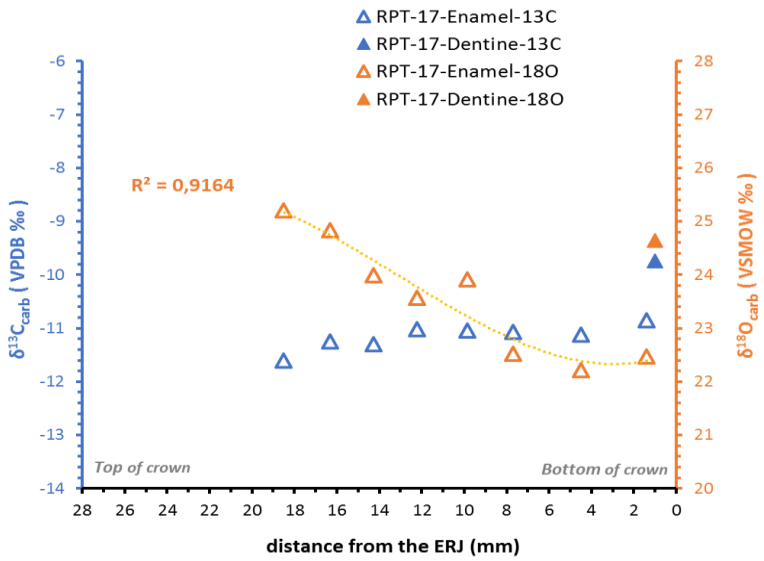

Lower M2 R and M3 R

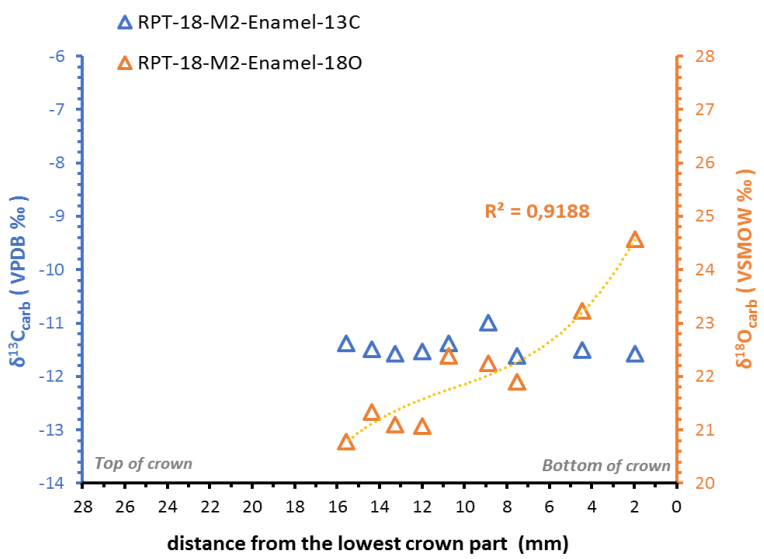

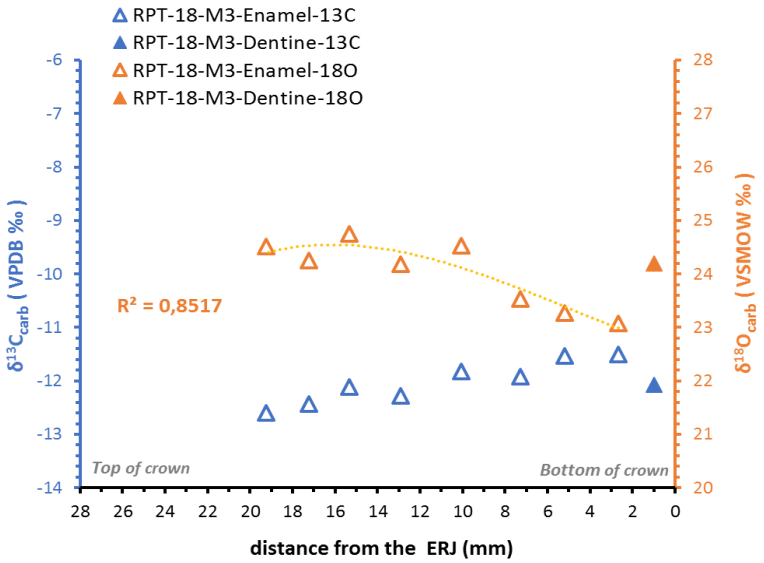

Fig. A.1 – 4

Layer – 8

Lower M2 R and M3 R

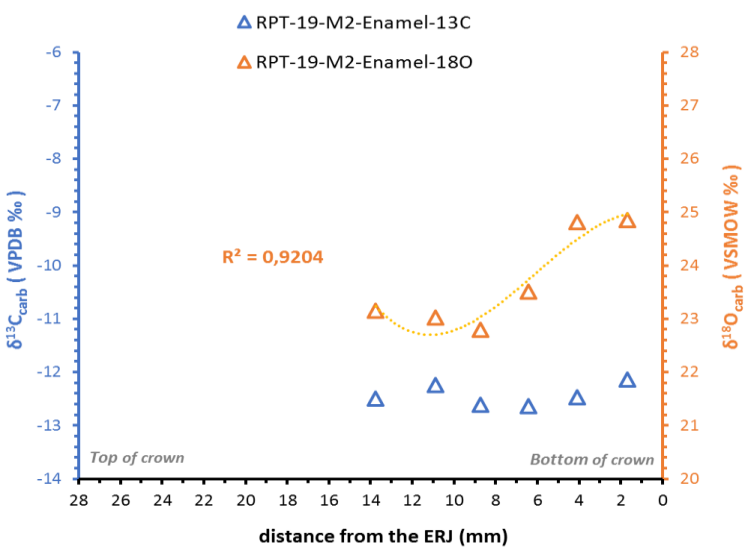

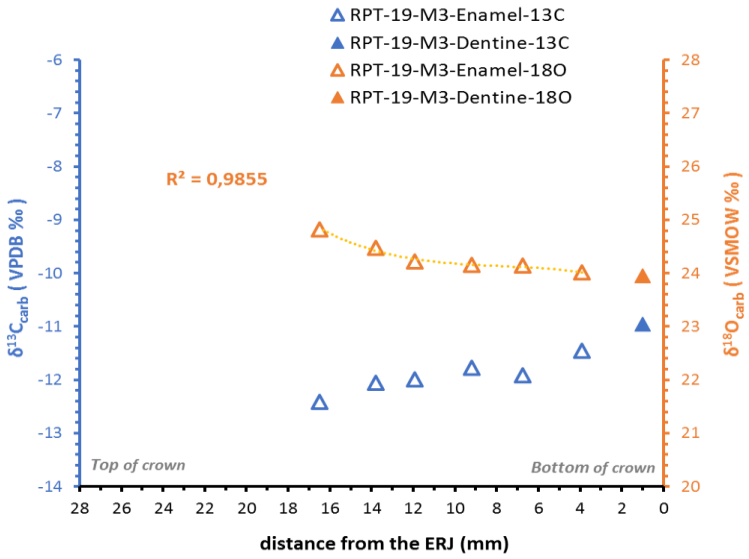

Lower M2 R and M3 R

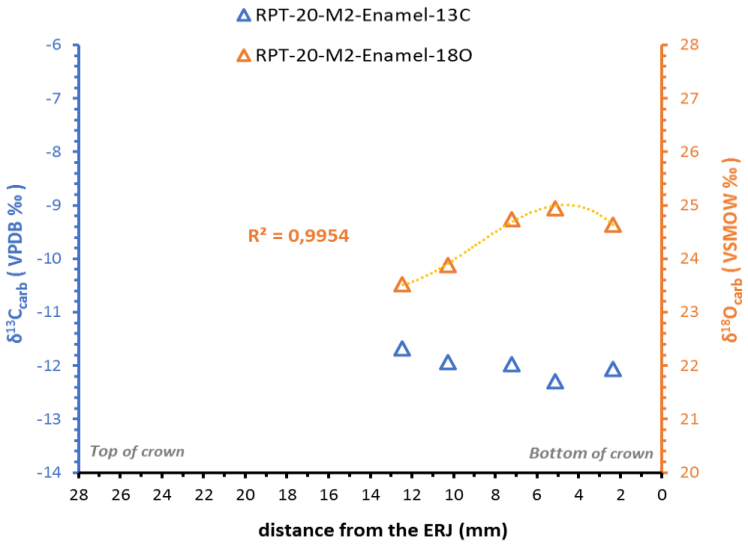

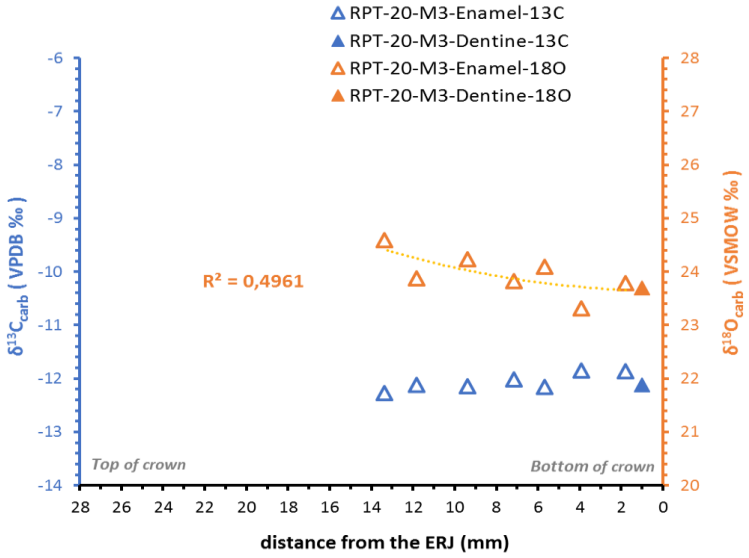

Fig. A.1 - 5

Layer – 9

Lower M2 R and M3 R

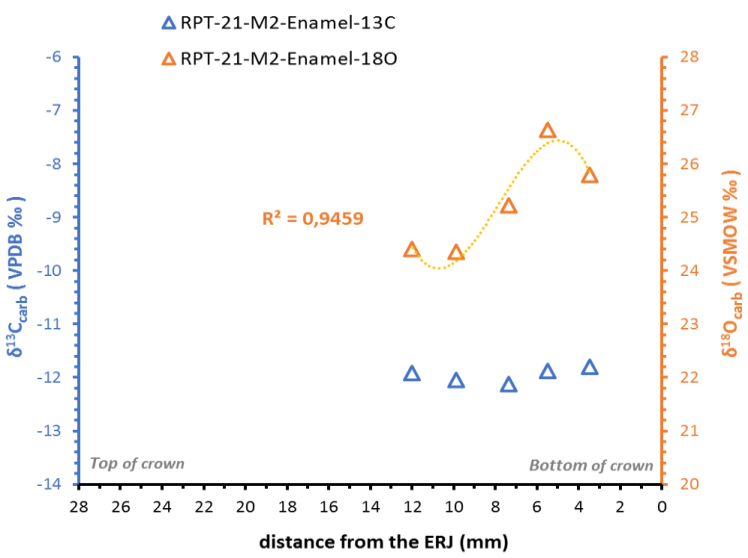

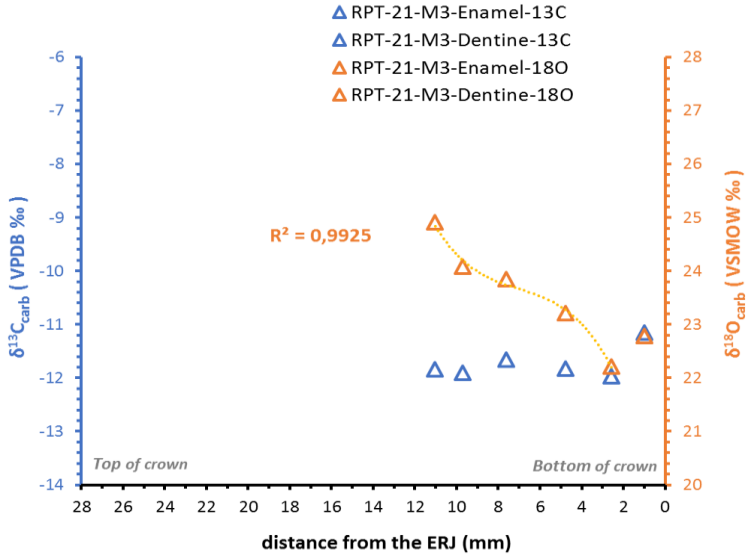

Lower M2 R and M3 R

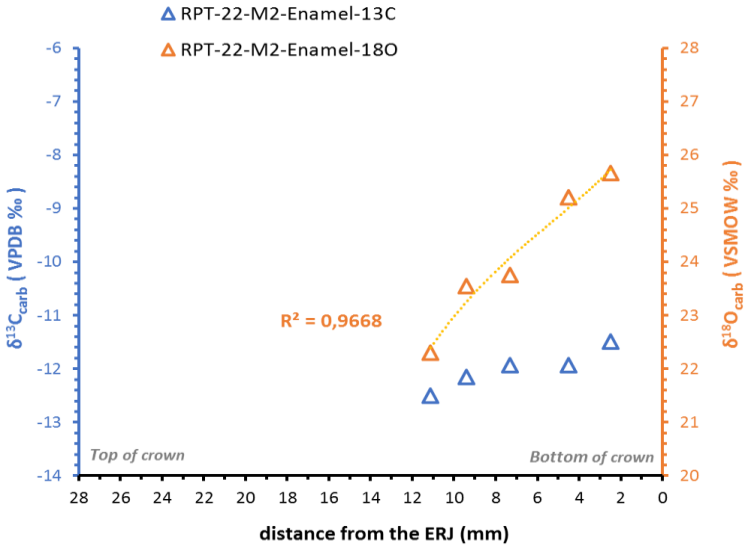

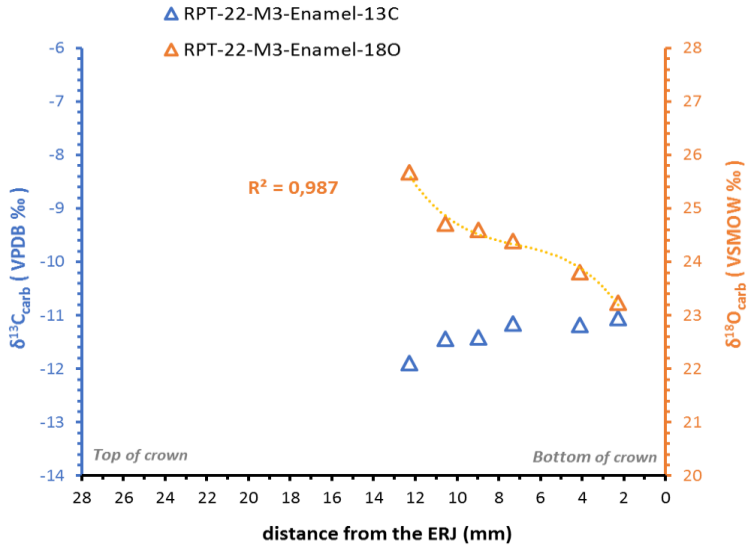

Fig. A.1 – 5

Layer – 9

Lower M3 R

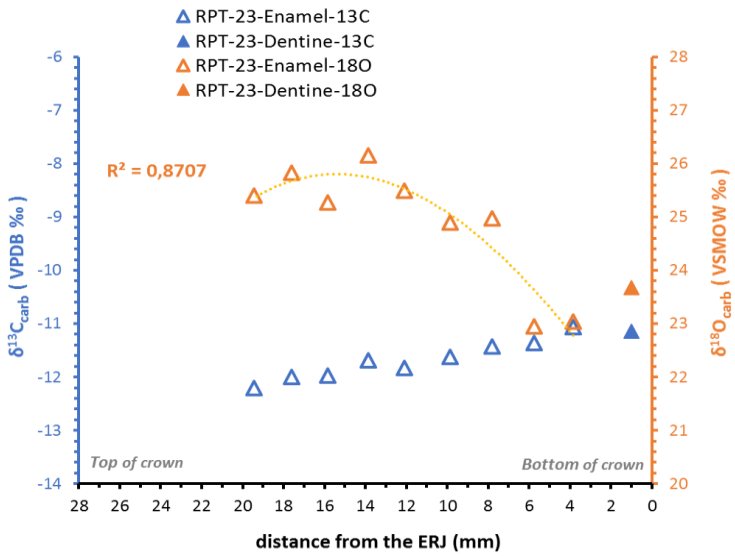

Lower M2 R and M3 R

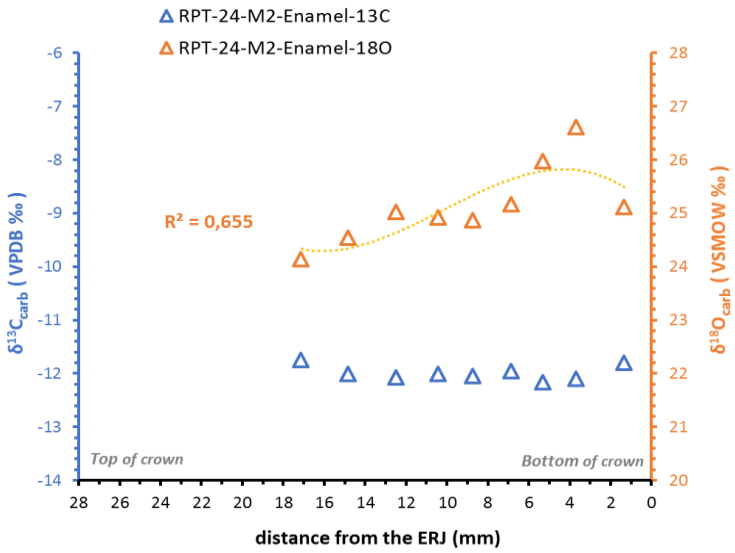

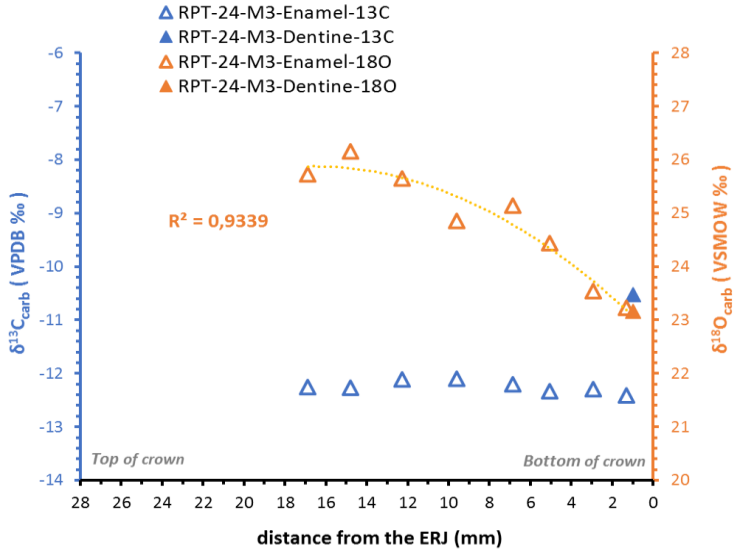

Fig. A.1 - 6

Layer – 10a

Lower M3 L

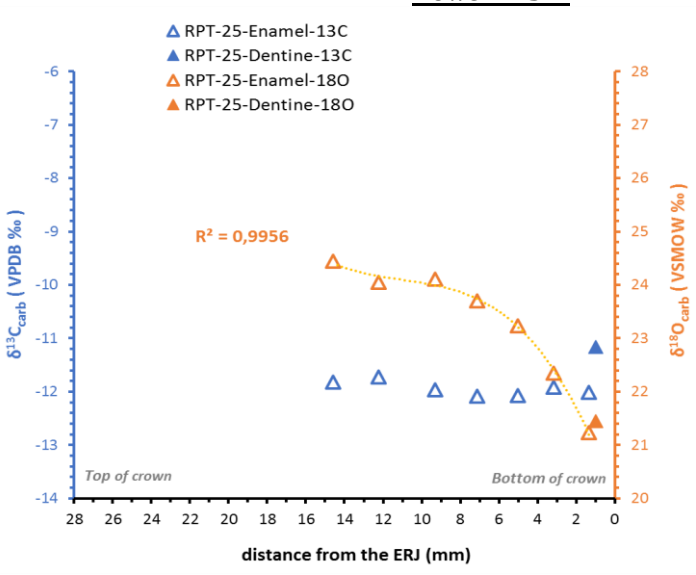

Lower M3 R

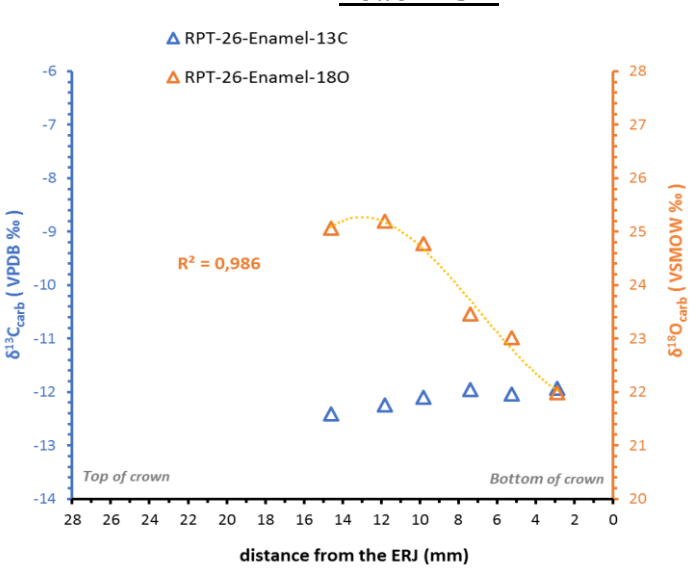

Lower M2R and M3 R

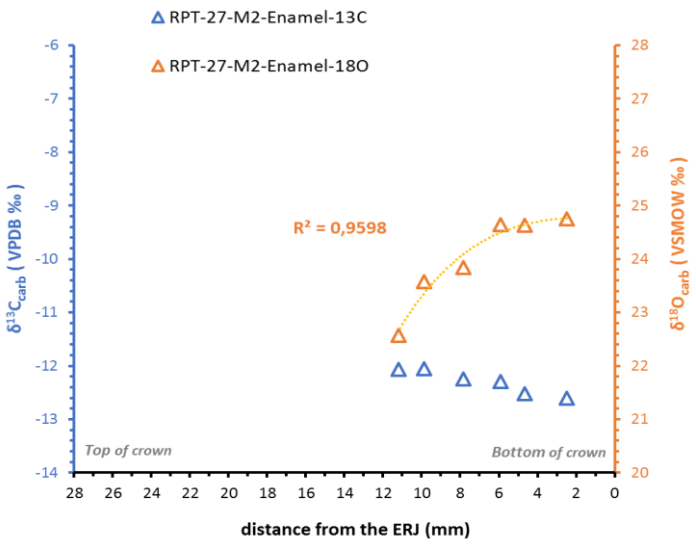

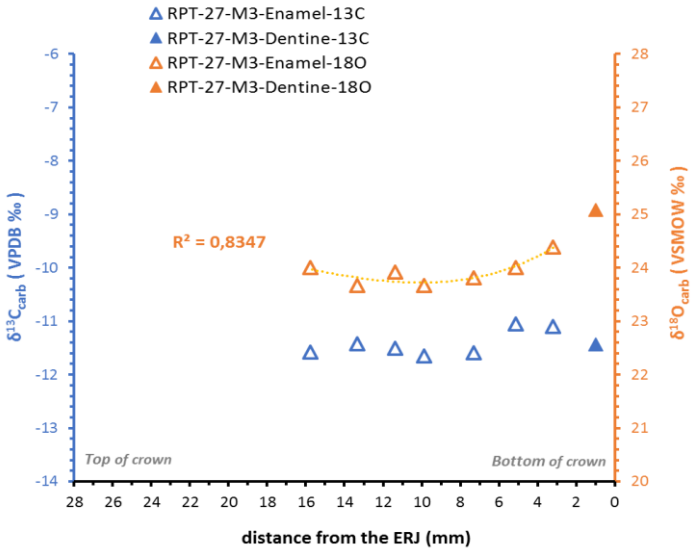

Fig. A.1 – 6

Layer – 10a

Lower M3 R

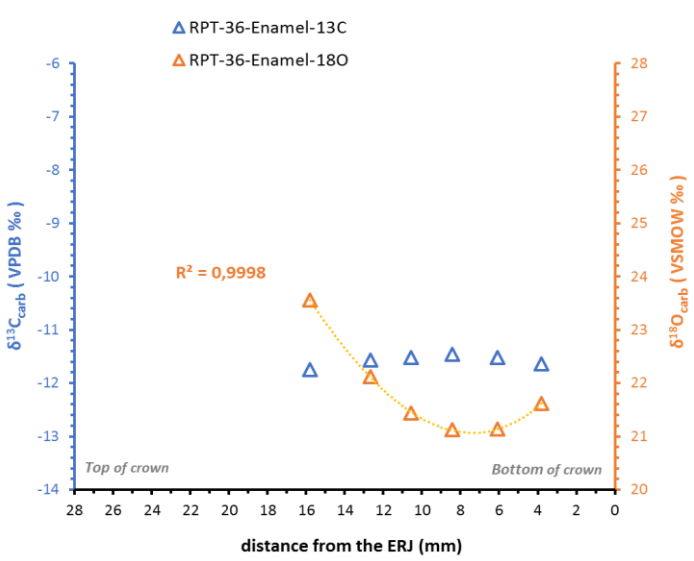

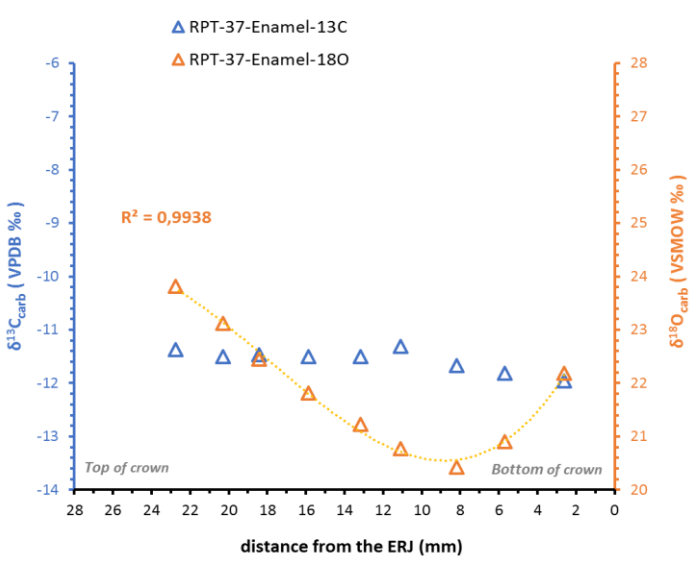

Lower M3 R

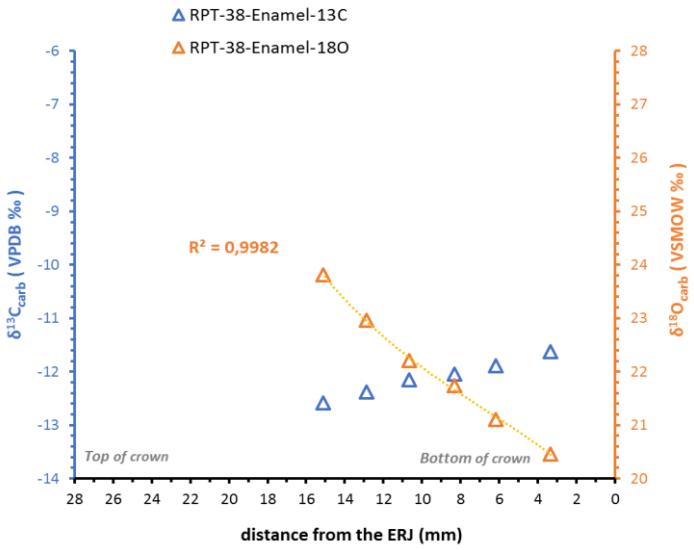

Fig. A.1 – 6

Layer – 10b, 10c

Lower M3 R (10b)

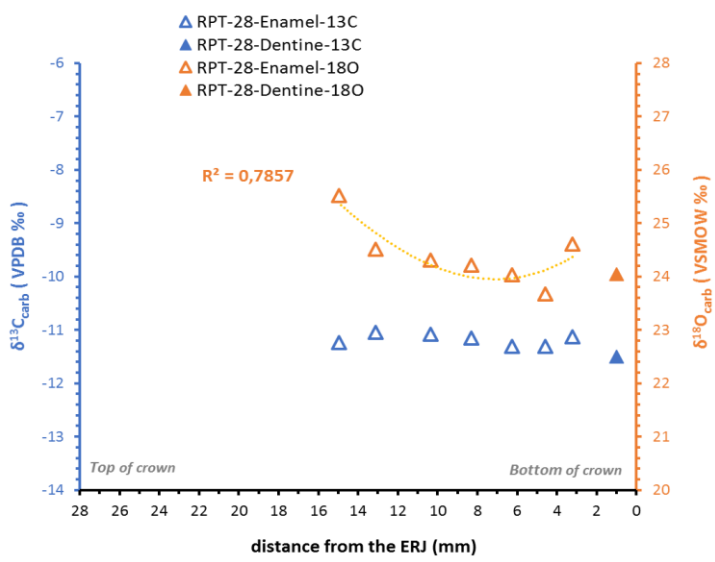

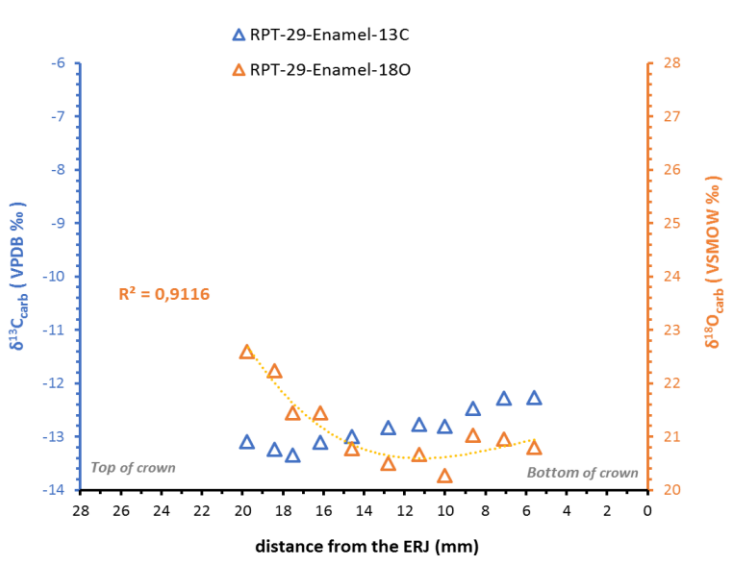

Lower M3 R (10c)

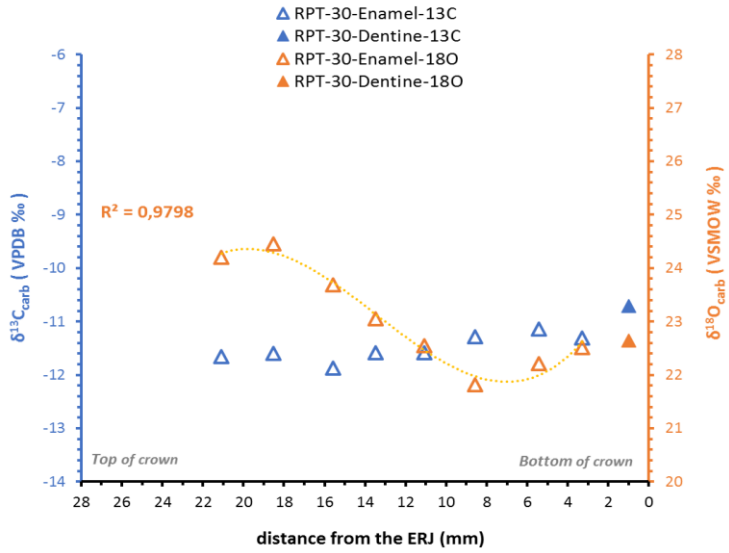

Fig. A.1 – 6

Layer – 10d

Lower M3 R

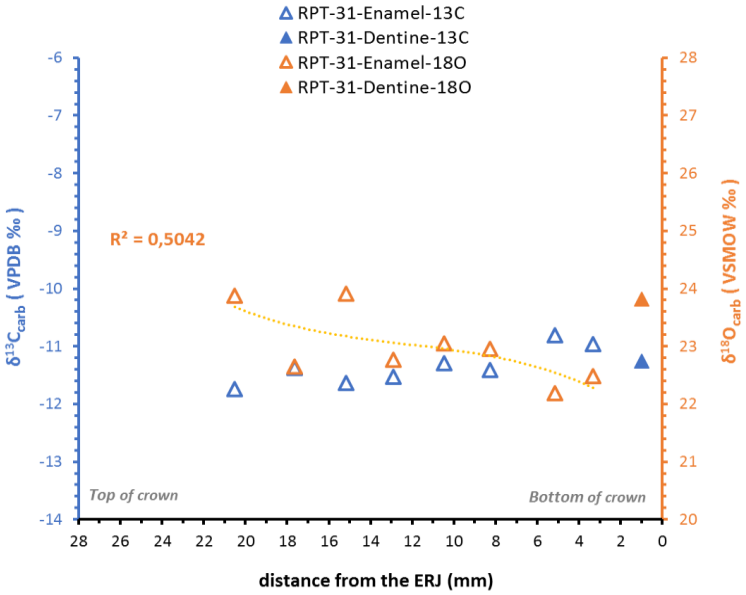

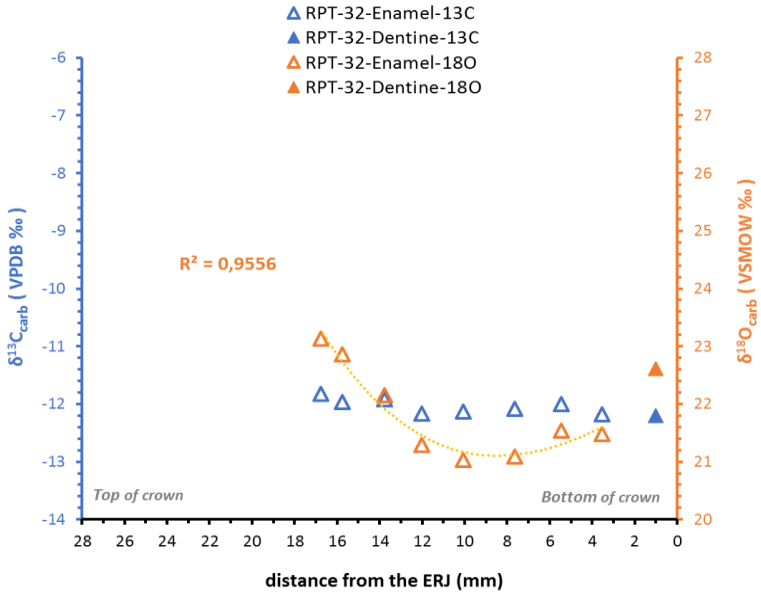

Fig. A.1 - 7

Layer – 13

Lower M3 L

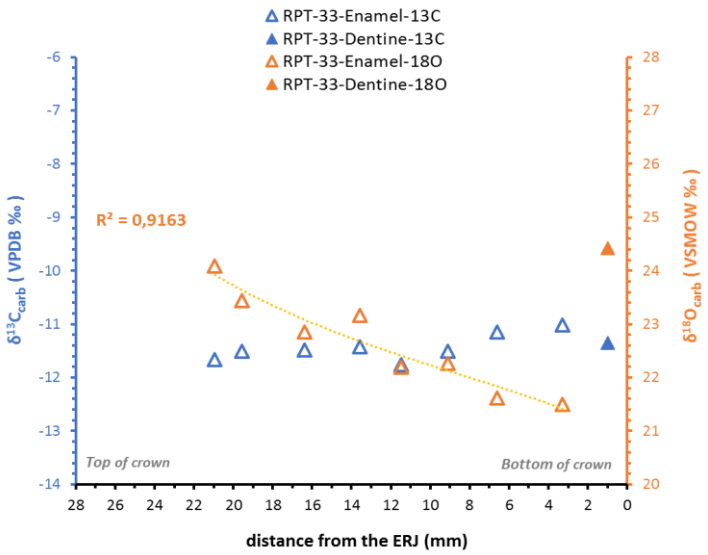

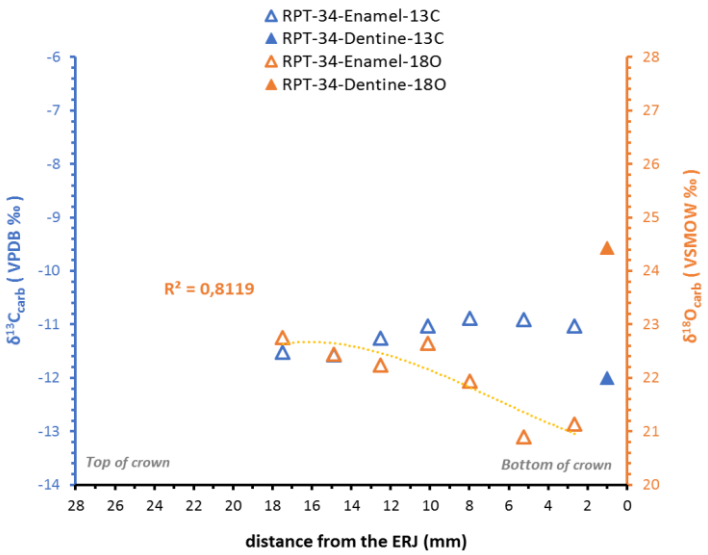

Lower M3 L